Spring 5-31-1997

An investigation into the feasibility of utilizing pneumatic ultrasonic devices coupled with pneumatic fracturing in enhancing removal of volatile organic compounds from soils

Hugo J. Fernandez
New Jersey Institute of Technology

Copyright Warning & Restrictions

The copyright law of the United States (Title 17, United States Code) governs the making of photocopies or other reproductions of copyrighted material.

Under certain conditions specified in the law, libraries and archives are authorized to furnish a photocopy or other reproduction. One of these specified conditions is that the photocopy or reproduction is not to be "used for any purpose other than private study, scholarship, or research." If a, user makes a request for, or later uses, a photocopy or reproduction for purposes in excess of "fair use" that user may be liable for copyright infringement,

This institution reserves the right to refuse to accept a copying order if, in its judgment, fulfillment of the order would involve violation of copyright law.

Please Note: The author retains the copyright while the New Jersey Institute of Technology reserves the right to distribute this thesis or dissertation

Printing note: If you do not wish to print this page, then select "Pages from: first page # to: last page #" on the print dialog screen

ABSTRACT

AN INVESTIGATION INTO THE FEASIBILITY OF UTILIZING PNEUMATIC ULTRASONIC DEVICES COUPLED WITH PNEUMATIC FRACTURING IN ENHANCING REMOVAL OF VOLATILE ORGANIC COMPOUNDS FROM SOILS

A bench scale investigation was conducted in a Plexiglass™ Test cell 1 foot square by 2 feet in height, packed with 400 mesh sand to a density of 100 lb. /ft^3. The sand was contaminated with a mixture of 10% ethanol and 90% water by weight having a total weight of 11.1 pounds, before it was packed in the test cell. A geotextile 1/2 inch thick was used as a simulated fracture and was placed 3 inches from the bottom of the tank. A siren and a whistle were tested in this fracture.

The data were divided into a transient, two phase flow region, and a falling rate region similar to drying theory analysis. Free moisture versus time data showed a 39.1% improvement for the siren and a 412.4% improvement for the whistle in the transient region, and a 69% improvement for the siren and a 455 % improvement for the whistle in the falling rate region. Concentration of ethanol versus time data showed a 62.9% improvement for the siren in the transient region and no comparison was established for the whistle. A 192.0% improvement for the siren and a 931.4 % improvement for the whistle were measured in the falling rate region.

The average time to reach asymptotic value of 0.01 free moisture with the siren was reduced by 37% and greater than 74.3% with the whistle. The average time to reach an ethanol concentration of 1 ppmv was reduced by greater than 41.3% with the siren and by greater than 74% with the whistle.

AN INVESTIGATION INTO THE FEASIBILITY OF UTILIZING PNEUMATIC ULTRASONIC DEVICES COUPLED WITH PNEUMATIC FRACTURING IN ENHANCING REMOVAL OF VOLATILE ORGANIC COMPOUNDS FROM SOILS

by
Hugo J. Fernandez

A Thesis
Submitted to the Faculty of
New Jersey Institute of Technology
in Partial Fulfillment of the Requirements for the Degree of
Master of Science in Chemical Engineering

Department of Chemical Engineering, Chemistry and Environmental Science

May 1997

APPROVAL PAGE

AN INVESTIGATION INTO THE FEASIBILITY OF UTILIZING PNEUMATIC ULTRASONIC DEVICES COUPLED WITH PNEUMATIC FRACTURING IN ENHANCING REMOVAL OF VOLATILE ORGANIC COMPOUNDS FROM SOILS

Hugo J. Fernandez

Dr. Deran Hanesian, Thesis Advisor — Date
Professor of Chemical Engineering Chemistry and Environmental Science

Dr. Angelo J. Perna, Committee Member — Date
Professor of Chemical Engineering Chemistry and Environmental Engineering

Dr. John R. Schuring, Committee Member — Date
Professor of Civil and Environmental Engineering

BIOGRAPHICAL INFORMATION

Author: Hugo J. Fernandez

Degree: Master of Science

Date: May 1997

Undergraduate and Graduate Education

- Master of Science in Chemical Engineering
  New Jersey Institute of Technology, Newark, New Jersey, 1997

- Bachelor of Science in Chemical Engineering
  New Jersey Institute of Technology, Newark, New Jersey, 1995

Major: Chemical Engineering

Presentations and Publications:

Fernandez, H.J., Hanesian, D., Perna, A.J. and Schuring, J.R..1995. Ultrasonic Enhancement for In Situ Remediation of Contaminated Soil. *Sixth Annual Minitech. Student Conference*, Stevens Institute of Technology, Hoboken NJ.

Fernandez, H.J., Hanesian, D., Perna, A.J. and Schuring, J.R..1996. Ultrasonic Enhancement for In Situ Remediation of Contaminated Soil. *HSRC / WERC Joint Conference on the Environment*, Albuquerque, NM.

Fernandez, H.J., Hanesian, D., Perna, A.J. and Schuring, J.R..1997. Ultrasonic Enhancement of Soil Fracturing Technologies for In Situ Detoxifiction of Contaminated Soil. *1997 Spring National Meeting of the American Institute of Chemical Engineers* Houston, TX.

Fernandez, H.J., Hanesian, D., Perna, A.J. and Schuring, J.R..1997. Ultrasonic Enhancement for In Situ Remediation of Contaminated Soil. *Seventh Annual Minitech. Student Conference*, Bridgewater, NJ.

Fernandez, H.J., Hanesian, D., Perna, A.J. and Schuring, J.R..1997 Remediation of Volatile Organic Compounds for Low Permeable Soils by Coupling Pneumatic Fracturing and Ultrasound in the Vadose Zone. *HSRC / WERC Joint Conference on the Environment*, Albuquerque, NM.

Awards

Fernandez, H.J., Hanesian, D., Perna, A.J. and Schuring, J.R..1996. Ultrasonic Enhancement for In Situ Remediation of Contaminated Soil. *HSRC / WERC Joint Conference on the Environment*, Albuquerque, NM - **Received Honorable Mention**

Fernandez, H.J., Hanesian, D., Perna, A.J. and Schuring, J.R..1997 Remediation of Volatile Organic Compounds for Low Permeable Soils by Coupling Pneumatic Fracturing and Ultrasound in the Vadose Zone. *HSRC / WERC Joint Conference on the Environment*, Albuquerque, NM. - **Received Third Place**

This thesis is dedicated to my future wife
Maricela Changano and my parents
Yolanda and Hugo G. Fernandez
for their unconditional support, love and encouragement

In Memory of Mima (Grandma)

ACKNOWLEDGMENT

I would like to start by thanking my advisors, Dr. Deran Hanesian for his time, patience and wisdom in preparing this thesis and during the course of this research work , Dr. Angelo Perna for his common sense, ideas and insights into this research, and Dr. John Schuring for his inspirational, as well as, technical support throughout the course of this research work, because without them, none of this would have been realized.

I also would like to thank all the members of the Pneumatic Fracturing Team because they played a key part in the making of this research including Brian Sielski, Heather Hall, Jenny Lin, Chamiris Carrion, Mike Galbraith, Mike Canino, Vincent De Biasi, Joseph Gomez, Tom Boland, Sean Simeon, Verdane Simeon, Joe DiBernardo, Laurence Thoraval and Suresh Puppala.

I finally like to acknowledge the technical support as well as the help of Clint Brockway, John Eimess, William Guzy, William Forster and John Griscavage.

TABLE OF CONTENTS

TABLE OF CONTENTS
(Continued)

Chapter **Page**

TABLE OF CONTENTS
(Continued)

TABLE OF CONTENTS
(Continued)

LIST OF TABLES

LIST OF FIGURES

Figure Page

LIST OF FIGURES
(Continued)

Figure **Page**

LIST OF FIGURES
(Continued)

Figure **Page**

LIST OF FIGURES
(Continued)

Figure | Page

LIST OF SYMBOLS

a_i	=	Incident Coefficient (Dimensionless)
a_r	=	Reflection Coefficient (Dimensionless)
a_t	=	Transmission Coefficient (Dimensionless)
A	=	Area (ft^2)
A_p	=	Amplitude of Sound Wave (ft)
B	=	Bulk Modulus of Air (ft^3 psi /f t^3)
c	=	Speed of Sound (ft / h)
c_1	=	Speed of Sound in Medium 1 (ft / h)
c_2	=	Speed of Sound in Medium 2 (ft / h)
D_L	=	Diffusivity of Liquids (ft^2 / h)
D_o	=	Whistle Nozzle Orifice Diameter (ft)
D	=	Outlet Diameter of Vortex Whistle (ft)
f	=	Frequency (1 / h)
G	=	Mass Flow Rate of Air per Surface Area(lb_m / ft^2-h)
h	=	Heat Transfer Coefficient (Btu / h-ft^2-°F)
H	=	Slab Thickness (ft)
I	=	Intensity (Btu / h / ft^2)
I_o	=	Intensity at the Source (Btu / h / ft^2)
k	=	Pore Distribution Coefficient (Dimensionless)
k_m	=	Total Mass Transfer Coefficient (lb mole / h / ft^2 / mol frac)
k_y	=	Mass Transfer Coefficient of Vapor (lb-mole / h / ft^2 / mol frac)

LIST OF SYMBOLS
(Continued)

k_v	=	Vapor Mass Transfer Coefficient (lb mole / h / ft^2 / mol-frac)
k_w	=	Mass Transfer Coefficient of Liquids (lb-mol/h-ft^2-mol frac)
k_∞	=	Fraction of Vapor Arriving at the Surface of the Solid (lb_m / lb_m)
K	=	Total Kinetic Energy (Btu)
K_1	=	Constant 1 for Whistle Frequency Calculation (Dimensionless)
K_2	=	Constant 2 for Whistle Frequency Calculation (Dimensionless)
K'	=	Proportionality Constant for the Stem Jet Whistle Dependent on the Whistle Shape (Btu / h / psi)
L	=	Length of the Vibrating Body (ft)
M_A	=	Molecular Weight of Component A (lb_m / lb-mol)
n	=	Number of Droplets (Dimensionless)
N_A	=	Rate of Molar Transport of Component A (lb-mole / h-ft^2)
O	=	Opening of the Resonator Cavity (cm)
p	=	Pressure (psi)
P_A	=	Atmospheric Pressure (kg / cm^2)
P_R	=	Reservoir Pressure (kg / cm^2)
P_1	=	Gas Pressure Entering the Vortex Whistle (psi)
P_2	=	Gas Pressure Leaving the Vortex Whistle (psi)
q	=	Rate of Heat Flux (Btu / h)
r	=	Radius of Penetration (ft)
r_c	=	Critical Ratio of Atmospheric Pressure to Reservoir (psi / psi)

LIST OF SYMBOLS
(Continued)

r_r	=	Ratio of Atmospheric Pressure to Reservoir (psi / psi)
R	=	Removal Rate (lb_m H_2O/ h / ft^2)
R_c	=	Removal Rate at the End of the Constant Rate Period (lb_m H_2O/ h-ft^2)
s	=	Distance Traveled by a Moisture Particle Under in a Sound Field (ft)
S	=	String Tension (lb_m-ft / h^2), (lb_f)
S_2	=	Total Surface Area of Siren Ports (ft^2)
t	=	Time (h)
T	=	Temperature (°F)
T_s	=	Temperature of Solids (°F)
V	=	Volume (ft^3)
V_o	=	Initial Volume (ft^3)
w	=	Acoustic Impedance (lb_m / ft^2-h^2)
w_A	=	Acoustic Impedance of Medium A (lb_m / ft^2-h^2)
w_B	=	Acoustic Impedance of Medium B (lb_m / ft^2-h^2)
W	=	Mass of Dry Solids and Mass of Moisture (lb_m)
W_P	=	Acoustic Power (Btu / h)
W_s	=	Mass of Solids Dry (lb_m)
x	=	Displacement of Particle from Equilibrium (ft)
X_P	=	Distance Traveled by the Moisture Droplet (ft)
x_1	=	Depth of the Bed (ft)
X	=	Mass of Moisture per Mass of Dry Solids (lb_m / lb_m)

LIST OF SYMBOLS
(Continued)

X_c	=	Mass of Moisture per Mass of Dry Solids at the End of the Constant Rate Region (lb_m / lb_m)
X_D	=	Mass of Free Moisture per Mass of Dry Solids at the End of First Falling Rate Period (lb_m / lb_m)
X_t	=	Mass of Free Moisture per Mass of Dry Solids (lb_m / lb_m)
X_0	=	Initial Mass of Free Moisture per Mass of Dry Solids (lb_m / lb_m)
X_1	=	Mass of Free Moisture per Mass of Dry Solids at Point 1 (lb_m / lb_m)
X_2	=	Mass of Free Moisture per Mass of Dry Solids at Point 2 (lb_m / lb_m)
X^*	=	Equilibrium Mass of Moisture per Mass of Dry Solids (lb_m / lb_m)
y	=	Mole Fraction of Vapor (mol frac.)
y_w	=	Mole Fraction of Water Vapor (mol frac.)
Y	=	Young's Modulus of Elasticity (psi-ft / ft)
α	=	Constant for Vortex Whistle (Dimensionless)
α_p	=	Attenuation Coefficient (1 / ft)
β	=	Sound Level (Dimensionless)
δ	=	Linear Density (lb_m / ft)
γ	=	Heat Capacities at Constant Pressure to Constant Volume (Dimensionless)
φ	=	Angle of Moisture Particle movement (Dimensionless)
λ	=	Wavelength (ft)
λ_A	=	Latent Heat of Vaporization of Component A (Btu / lb_m)
λ_o	=	Wavelength at the Source (ft)

LIST OF SYMBOLS
(Continued)

λ_w = Latent Heat of Vaporization of Water (Btu / lb)

μ = Viscosity (lb_m / ft-h)

θ = Angular Velocity of Siren (Dimensionless)

θ_c = Critical Angle (Dimensionless)

θ_i = Angle of Incidence (Dimensionless)

θ_r = Angle of Reflection (Dimensionless)

ρ = Density of air (lb / ft^3)

ρ_2 = Density of Air at the Outlet of the Siren (lb_m / ft^3)

σ = Surface Tension (lb_m-ft/ h^2-ft), (lb_f / ft)

υ = Droplet Velocity (ft / h)

ω = Total Air Mass Flow Through a Siren (lb_m / h)

ω_o = Average Air Mass Flow Through a Siren (lb_m / h)

CHAPTER 1

1. INTRODUCTION

1.1 Overview

The contamination of soil in the United States due to industrial activities has become a major concern (EPA/540/2-90/002). The dumping of chemicals, known as hazardous waste which poses a danger to humans, animals, and the environment, was common practice before 1976. As a result, the federal government intervened with a series of laws over the course of the past 21 years. These laws are the Resource Conservation and Recovery Act of 1976 (RCRA), the Comprehensive Environmental Response Compensation and Liability Act (CERCLA) of 1980, and the Superfund Amendments and Reauthorization Act (SARA) of 1986.

The first effort by the federal government to deal with hazardous waste and hazardous waste sites, which are fields where hazardous waste was dumped, was RCRA. RCRA regulated industries engaged in creating, transporting, treating and disposing of hazardous waste. This law also prohibited the use of open areas for the purpose of dumping hazardous waste. Unfortunately by 1976, many hazardous waste sites already existed. These sites contained unknown quantities of unknown waste and hence posed a potential environmental as well as a health problem. In response to this environmental and health threat, CERCLA was passed by the US Congress in 1980. The act provided a fund of 1.2 billion dollars from 1980 to 1985 to cleanup these sites. This law was enforced by the Environmental Protection Agency (EPA) and it entailed identification of the hazardous sites, feasibility studies and remedial action. In addition, the EPA was

authorized to identify the potentially responsible parties and required them to take remedial action. In 1986, Superfund was reauthorized under SARA for an additional 8 billion dollars for the period of 1986 to 1990, and with the act came new laws which were meant to protect all workers engaged in hazardous waste operation.

Despite the implementation of these hazardous waste cleanup laws, there are numerous hazardous sites throughout the US which pose a potential problem and/or are already causing problems by polluting the ground water table. The problem begins when hazardous waste, specifically organic waste in the liquid phase, comes in contact with soil. This results in the migration of these organic liquids through the soil and eventually into the underground water table. The time in which this event takes place can vary greatly according to the permeability of the soil, the depth of the ground water table and the viscosity of the hazardous waste in question.

A new revolutionary method to treat hazardous waste sites is Pneumatic Fracturing. Developed in the Hazardous Substance Management Research Center's (HSMRC) Laboratories at the New Jersey Institute of Technology (NJIT), Pneumatic Fracturing consists of fracturing tightly packed soils with the purpose of increasing air flow through the formation so that volatile organic waste can be removed efficiently (Shah 1991). Presently Pneumatic Fracturing followed by air injection and vapor extraction techniques has reduced the remedial time of an industrial site located in Highland Park, New Jersey, contaminated with trichloroethylene (TCE) in a tight mudstone, from 10 years to 2 years. This significant improvement in remediation time

constitutes to a considerable cost reduction and savings in cleaning hazardous sites that contain volatile organic waste.

A two year clean-up plan can be an expensive endeavor with the average cost for a two year operation running well into the millions of dollars (Highland Park). The technology that is presented in this thesis was designed to address the issue of cost by further reducing the remediation time. The technology consists of introducing a highly focused air-coupled sound field into an artificial or natural underground fracture with the purpose of increasing the mobility of volatile organic compounds (VOCs) out of tight soils and into the fracture in were it can volatilize and be carried away by conventional vapor extraction methods. Thus far, the technology presented in this thesis has been demonstrated in laboratory bench scale tests. The studies show that a high powered sound field in a fractured tight soil enhances the removal of volatile compounds in that tight soil, thus cutting down remediation time and henceforth making it more efficient to clean the soil.

1.2 Research Objective

The objective of the research presented in this document is to successfully couple the benefits of sonic enhanced mass transfer with soil fracturing to further enhance the removal rate of volatile organic compounds (VOCs) from low permeability soil. The study began by undertaking an extensive literature search of current sonic drying theory, sonic drying technologies and sonic generators that are used in sonic drying. Sound levels were studied in these devices in order to determine which sound generators produced the highest sound energy in order to maximize mass transfer. Based upon this study, two

pneumatic sound generators were selected, a siren type generator and a whistle type generator. Bench scale tests were conducted with each of the selected sonic generators to determined their respective degree of enhancement inside a fracture, and these results were compared to control runs with no sonic energy. This study will culminate in a field test of the technology at a contaminated site in Hillsborough, New Jersey.

CHAPTER 2

2. BACKGROUND OF THE STUDY

2.1 Overview of Current *In Situ* Remediation Technologies

There are many *in situ* technologies being employed today to remove and treat hazardous waste from soil (EPA/600/D-91/285). These technologies can be divided into two categories and these are: (1) *in situ* treatment technologies; and (2) *in situ* delivery and recovery technologies. *In situ* treatment technologies are technologies that treat contaminants on site without ever having to remove the soil from the earth. *In situ* recovery and delivery technologies are technologies that mobilize the contaminants from subsurface soils and into a treatment facility on site or off site. Some of the current *in situ* technologies that are being employed today are: soil flushing, solidification, stabilization, degradation, volatilization and chemical treatment.

2.1.1 Soil Flushing

Soil flushing is a recovery technology applied to permeable soils contaminated with solid and liquid waste. Usually, the site is treated with a solution that is able to dissolve the contaminants in the soil. The solvent travels through the contaminated subsurface soil into the ground water where it is pumped to the surface through extraction wells, treated and redistributed on the site again. Some of the advantages of this technology are the ability to remediate the site permanently, if successful, and the moderate cost of implementing this technology. Some of the disadvantages are the potential for the solvent to leak out of the treatment area and the possibility that all of the contaminants will not be removed because of permeability changes which trap the solvent and the contaminant in the soil.

2.1.2 Solidification and Stabilization

Solidification and stabilization are *in situ* treatment technologies designed to address the mobilization and toxicity of the contaminants. Solidification involves the encasing of semiliquid or liquid waste into large solid blocks where they are immobilized. Usually, this is accomplish by injecting solidifying agents around the contaminant.

Stabilization technologies involve changing the contaminant, not necessarily physically, so that the contaminant is in its least soluble or least mobile and/or least toxic state. Potentially, this technology can decrease leaching of contaminants into the water table. Furthermore, the contaminants need little or no further treatment if the process is successful. Potential disadvantages of this technology include possible volatilization of contaminants during soil mixing and also difficulty in properly mixing the soil with stabilization agents.

2.1.3 Degradation

Degradation is a very attractive technology for *in situ* treatment of contaminated soils because the hazardous waste is never removed from the formation, it is simply transformed into other substances which are not hazardous. Degradation of contaminants can be accomplished in many different ways. In chemical degradation, an oxidation agent is injected into the soil matrix which then causes a loss of electrons in the hazardous waste. This is called an oxidation reaction and this type of reaction is capable of changing the hazardous waste into a less toxic substances.

One extremely attractive degradation technology is biological degradation. This technology entails the injection of microorganisms to degrade the hazardous waste into harmless by-products such as biomass methane and carbon dioxide. In some cases the

microorganisms already exist in the soil and are actively degrading the contaminants. This process can be enhanced by adding more organisms and possibly adjusting the soil properties such as pH and temperature to promote growth of the microorganisms.

2.1.4 Technologies for Remediation of Volatile Waste

One of the most often used technologies for removal of volatile organic waste from subsurface soil is vapor extraction. Vapor extraction employs a system of bore holes in which some bore holes are used to extract and create a vacuum while the rest of the bore holes remain open to provide air into the soil matrix. This process helps the volatile organic compounds volatilize faster by reducing the air pressure in the soil matrix.

2.1.5 Ultrasonic Remediation Technologies

Remediation of subsurface soils using ultrasound is currently under development as an *in situ* technology (US Patent 5,198,122 1993 and US Patent 5,098,538). Potential applications of ultrasound identified thus far are the use of ultrasound to disperse tightly packed clays in wells, the use of ultrasound to enhance chemical reactions in soil and the use of ultrasonic energy to eliminate microbes that can potentially clog pore spaces in soils (Johnson 1970). United States Patent Number 5,198,122 describes a method by which contaminants trapped in tight clays are mobilized by a direct current electric field and a low frequency acoustic field. The method claims to mobilize the hazardous waste trapped in clays toward positive or negatively charged electrodes buried in the subsurface soil. This movement is enhanced by a low frequency sound field which shakes the clay particles. In US Patent Number 5,198,122 a method is described where ultrasonic energy is used in the presence of chemical reagents to transform the hazardous waste into less

toxic substances. The ultrasonic energy is said to enhance the chemical reaction by the acoustic related phenomenon known as cavitation.

Although this technology is still in its infancy, thus far laboratory tests have shown that ultrasonic energy in the form of an acoustic field is capable of increasing the hydraulic conductivities in clay and silts and thus facilitating the mobilization of hazardous waste (Reddi 1993). This technology can potentially be used as an enhancement technology when combined with soil washing techniques (Cleaveland 1993).

2.2 *In Situ* Remediation Enhancement Technologies

One of the most often used enhancement technologies that is currently in use to remediate tight soil is soil fracturing. Soil fracturing is performed by administering a fluid which is at a higher pressure than the consolidation pressure of the geologic formation to open up a fracture radially or vertically with respect to the formation. This is followed by injection of a granular material to keep the fracture open. There are currently three types of fracturing in use for *in situ* remediation and these are hydraulic fracturing, explosive fracturing, and pneumatic fracturing (Marks 1994).

2.2.1 Hydraulic Fracturing

Hydraulic fracturing technology was first employed in the petroleum industry. It is used to enhance the recovery of petroleum that is trapped in low permeable soil and also to enhance the injection of fluids that are used for displacing the oil. A new application of hydraulic fracturing has emerged where hydraulic fracturing is used to create fractures in low permeable soil to facilitate contaminant removal. This new application entails the injection of a liquid mainly water to create horizontal and vertical fractures in the saturated zone of the formation. The liquid is injected through a bore hole with the liquid

surpassing the consolidation pressure of the formation. Once the fracture has been created, contaminated liquids can be extracted easier (EPA/600/D-91/285).

2.2.2 Explosive Fracturing

Explosive fracturing was developed to treat low permeable soil contaminated with volatile or semi volatile compounds. Typically, a borehole is made and explosive charges are placed inside the borehole. The borehole is then covered up and the explosive are detonated. The explosion causes horizontal and vertical fractures in the low permeable formation which facilitates the movement of compounds trapped in the formation. (EPA/600/D-91/285).

2.2.3 Pneumatic Fracturing

Pneumatic Fracturing is a technology developed to treat contaminants that are trapped in low permeable geologic formations and it is mainly used in the vadose zone. It is considered a versatile technology because it opens spaces in tightly packed geologic formations so that conventional *in situ* treatment such as air injection and vapor extraction are more effective. Furthermore, the injection of granular materials can be made to maintain the fracture open and in some cases, biological organisms can also be injected for bioremediation (US Patent 5,032,042).

2.3 Basic Drying Theory as a Model for Vapor Extraction in Fractures

A fracture is a void in a tightly packed geologic formation. This void can be created artificially by pneumatically fracturing the formation or it can exist naturally. When air is injected into the formation, it will travel through the path of least resistance which is the fracture. As the air passes through the fracture, any moisture on the top or bottom part of the fracture will evaporate into that air stream due to concentration gradients, and if the

air stream is at high velocity, the moisture will be swept away. In essence the ground is being dried by a tangential air flow that is flowing parallel with the soil along the fracture and this lends itself for analysis using classical drying theory.

According to classical drying theory, the removal of liquids from solid material can be divided into 4 regions (Geankopolis 1993 and McCabe 1993). The first region of drying is a short transient region where the system is driving toward the constant drying rate region. This behavior is observed because the wet soil to be dried is at some initial equilibrium temperature and pressure before drying begins. So when drying begins, the condition of the wet material changes and the system begins to drive toward the new equilibrium.

The second drying region is the constant drying region where the liquid evaporates from the surface of the fracture at constant rate. In this region, the surface of the fracture is completely covered by the liquid and the liquid behaves as if the solid were not present. In this region, the removal rate of volatile organic compounds is bulk film diffusion controlled. This means that the resistance to mass transfer is mainly by diffusion of volatile organic compounds in the vapor film between the particles' surfaces at the fracture and the bulk air flow stream.

The third drying region is known as the first falling rate region where the evaporation rate is a function of time. In this region of falling rate, there is insufficient liquid present to maintain a continuous film of liquid at the solid surface. Hence the liquid at the fracture surface is being evaporated faster than liquid can be transferred to the surface of the fracture. At this point, internal diffusion in the soil takes control of the drying process and the drying process is said to be diffusion limited. The diffusion of the

liquid from within the soil toward the fracture depends upon the total pressure difference between the fracture and the soil interior, the concentration difference in the contaminant between the fracture and the soil interior, and the temperature difference between the bulk air temperature in the fracture and the liquid temperature at the surface of the fracture.

The fourth drying region is referred to as the second falling rate region. In this region of drying, the moisture that arrives at the surface of the fracture is strictly controlled by the diffusion rate of the liquid through the pores of the soil and out toward the fracture. Liquids that are trapped in the pores of the soil must first evaporate or diffuse out of the pores and then diffuses toward the fracture as vapor. Since the moisture is held in the pores of the soil by Van der Waals Forces, the process is time consuming and energy intensive.

Normally, drying data are collected in a simple laboratory experiment where the solid to be dried is mixed with a known amount of liquid and then it is weighed while it dries. The data are then converted into a drying rate curve. Two types of drying curve are generated from the data collected. The first plot is a plot of free moisture fraction versus time. The free moisture fraction is the fractional total moisture minus the fractional equilibrium moisture. The formula to calculate the fractional total moisture is given as follows:

$$X_t = \frac{W - W_s}{W_s} \tag{2.1}$$

In Equation 2.1, the variable X_t is the fractional total moisture of the solid to be dried which is a function of time. The variable W is the weight of the solids plus the moisture at any given time, and W_s is the weight of the dry solids. The fractional free moisture is

obtained by subtracting the equilibrium moisture content of the material in question from the fractional total moisture. The relationship is given by the following equation:

$$X = X_t - X^* \tag{2.2}$$

In Equation 2.2, X is the fractional free moisture available for drying and X^* is the fractional equilibrium moisture content of the material which is constant for a given temperature and relative humidity. **Figure 2.1** shows the fractional free moisture versus time.

Figure 2.2 is obtained by taking the derivative of **Figure 2.1**, dX/dt, multiplying it by the weight of the dry solids, W_s, and dividing it by the surface area, A, available for drying. The equation is as follows:

$$R = -\frac{W_s}{A}\frac{dX}{dt} \tag{2.3}$$

In Equation 2.3, the R, the drying rate, has units of mass of moisture per unit area per unit time, W_s, the weight of the dry solids has units of mass of dry solids, A, the surface area of the fracture has units of surface area and the term dX/dt, the infinitesimal change of the fractional free moisture with respect to time has units of fractional moisture per unit time **(See Figures 2.1 and 2.2)**.

2.3.1 Theoretical Prediction of Drying Rate Curves in the Constant Drying Rate Region.

In **Figure 2.1 and 2.2**, the constant drying rate region is shown by the length of the curve labeled BC in both plots. In this region, the solid is saturated with liquid so when an air stream passes parallel with the surface of the material, the liquid evaporates as if the solid

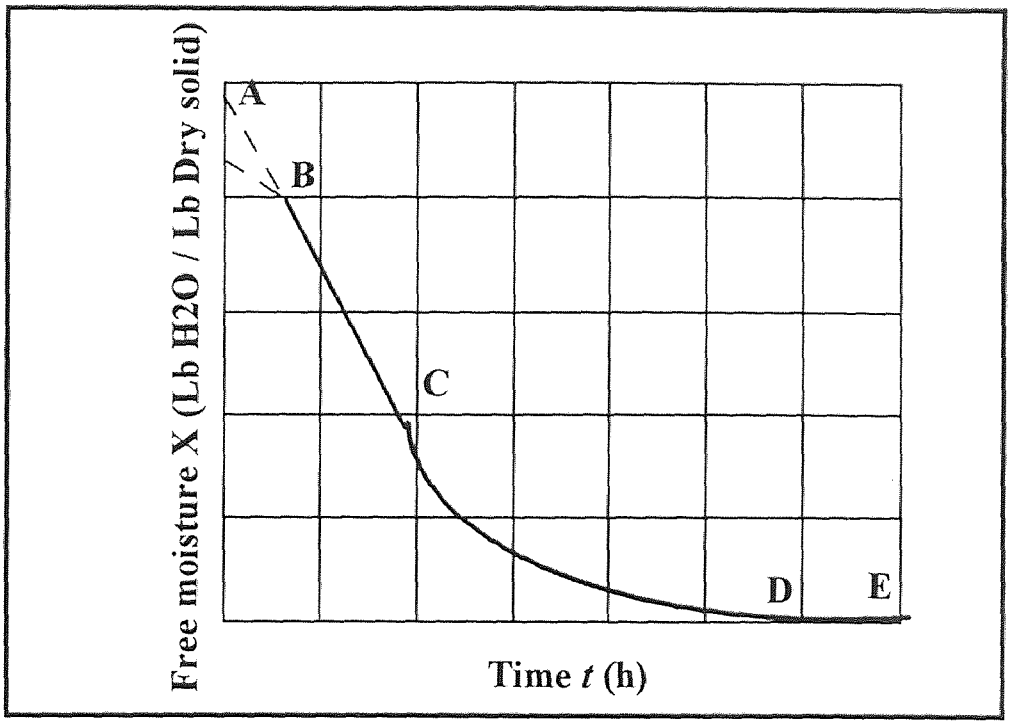

Figure 2.1* Typical Drying Curve for a Granulated Solid Showing the Four Regions of Drying: The Transient Region AB, The Constant Rate Region BC the First Falling Rate Region CD and the Second Falling Rate Region DE.

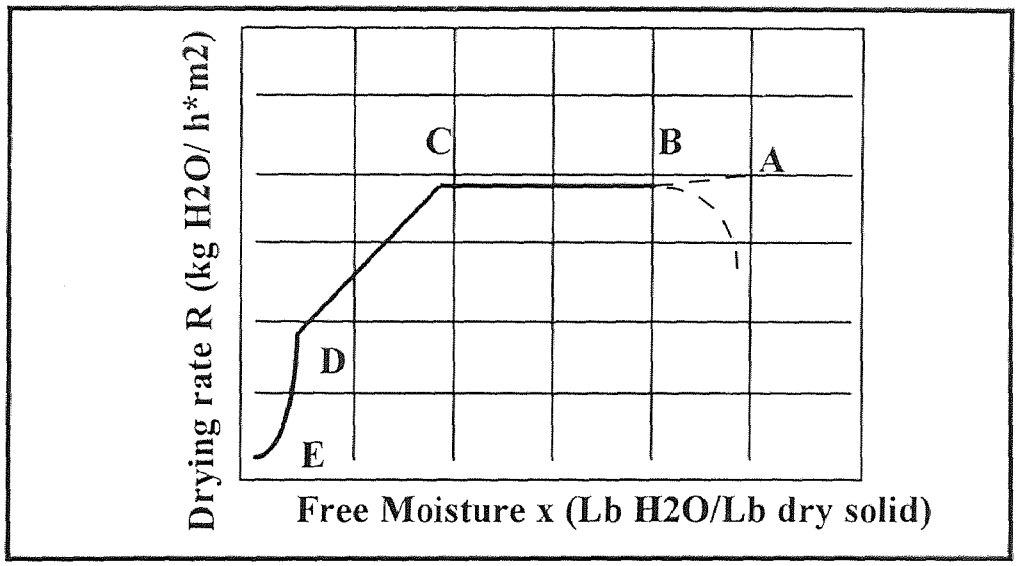

Figure 2.2*Typical Drying Rate Curve for a Granulated Solid Showing the Four Regions of Drying: The Transient Region AB, The Constant Rate Region BC the First Falling Rate Region CD and the Second Falling Rate Region DE.

*Geankoplis, Christie J. 1993 Transport Process and Unit Operations Third Edition, Simon and Schuster, Englewood Cliffs, NJ

were not present. Drying data in this region can be obtained by running batch experiments as described earlier or can be calculated using mass and energy relations.

The easiest of the drying regions that lends itself to theoretical treatment is the constant drying rate region due to the homogenous nature of the liquid film coating the soil (Geankopolis 1993). In order for the moisture sitting on the solid to evaporate, energy must be supplied to it. This energy comes from the gas flow above the saturated surface. The gas flow provides the evaporation energy needed for the liquid to undergo a phase change. At steady state, which is the case in the constant drying rate region, the convective heat transfer into the liquid determines the mass transfer out of the material. The rate of convective heat transfer is defined by the following equation:

$$q = h\,A\,(T - T_S) \tag{2.4}$$

In this Equation 2.4, q is the rate of heat transfer in energy per time, h stands for the heat transfer coefficient in energy per time per surface area per degree, A is the heat transfer area, T is the temperature of the air stream coming in contact with the material and T_s is the temperature of the liquid and the solid at the surface that is being dried. Since the mass transfer is related to the heat transfer, the heat transfer into the liquid can also be written in terms of mass transfer,

$$q = M_A\,N_A\,\lambda_w\,A = R\,\lambda_w\,A \tag{2.5}$$

In Equation 2.5, M_A is the molecular weight of the of the liquid undergoing phase change, N_A is the mass transfer from the liquid to the vapor phase with units of mole per time per surface area and λ_w is the latent heat of evaporation of the liquid undergoing phase change. The mass transfer of liquid into the gas phase is given by:

$$N_A = k_y (y_w - y) \tag{2.6}$$

In Equation 2.6, y_w is the mole fraction of the liquid at the gas-liquid interphase, k_y is the mass transfer coefficient of the vapor in mol per time per area per mol fraction and y is the mole fraction of vapor in the bulk air flow.

By substituting Equation 2.4 and 2.6 into Equation 2.5 and rearranging, an equation to estimate the removal rate of liquid in the constant drying rate region can be constructed as follows:

$$R_c = R = \frac{q}{A\,\lambda_w} = M_A k_y (y_w - y) = \frac{h\,(T - T_S)}{\lambda_w} \tag{2.7}$$

Geankopolis (1993) reported that the heat transfer coefficient is a function of the tangential air flow as follows:

$$h = 0.0204\ G^{0.8} \tag{2.8}$$

Hence, the constant drying rate, R_c, can be predicted for a given air flow rate. In Equation 2.8, the coefficient is in SI units with tangential air flow velocities between 0.9 m/s to 4.6 m/s and G is the air mass flow rate in SI units of mass per hour per surface area.

Rearranging Equation 2.3 and integrating between limits of the constant drying rate gives:

$$(X_o - X) = \frac{R_C A}{W_S} t \tag{2.9}$$

Substituting for R_c using the relationship in Equation 2.7 gives:

$$(X_o - X) = \frac{hA(T - T_S)}{W_S \lambda_W} t = \frac{M_A k_y (y_w - y) A}{W_S} t \tag{2.10}$$

Equation 2.10 predicts that for the classical constant drying region, a plot of (X_0-X) versus time should be linear and pass through the origin. Furthermore, Equation 2.9 and Equation 2.10, show that the slope of the line is determined by the drying rate R_c, and that R_c, is related to the heat transfer coefficient and the mass transfer coefficient. Thus, the slope of the line will indicate any improvements in drying rate.

2.3.2 Theoretical Prediction of Drying Rate Curves in the First Falling Rate Period.

In **Figure 2.1 and 2.2**, the first falling drying rate region is shown by the length of the curve labeled CD in both plots. In the first falling rate period, there is not enough liquid on the surface of the solid to maintain a constant drying rate so the liquid flows to the surface of the solid where it is evaporated. For the region CD in Figure 2.2, the slope of the line is

$$a = \frac{R_C - R_o}{X_C - X_D} \tag{2.11}$$

and thus

$$R = aX + b \tag{2.12}$$

Rearranging Equation 2.3 and substituting Equation 2.12 for R and integrating between limits resulting in

$$X = \left[\frac{aX_C + b}{a}\right] e^{-\frac{aA}{W_s}t} - \frac{b}{a} \tag{2.13}$$

Equation 2.13 suggest a semi-logarithmic correlation in the first falling rate region.

2.3.3 Theoretical Prediction of Drying Rate Curves in the Second Falling Rate Period.

In **Figure 2.1 and 2.2**, the second falling drying rate region is shown by the length of the curve labeled DE in both plots. In the second falling rate region, the moisture is trapped in the solid particles and it travels out of the solid via diffusion. In this phase of drying, diffusion controls the overall drying process and drying occurs very slowly. The fraction of free moisture not only varies with time as in the first falling rate region but it is also a function of the depth. of the bed through which the material has to diffuse. Assuming that diffusion is occurring through a bed of known height and surface area, a unidirectional material balance yields the following partial differential equation:

$$\frac{\partial X}{\partial t} = D_L \frac{\partial^2 X}{\partial x^2} \tag{2.14}$$

The solution to this partial differential equation is an infinite Fourier series. Hence, based on Equation 2.2, Geankopolis (1993) shows that

$$\frac{X - X^*}{X_{t_1} - X^*} = \frac{X}{X_1} = \frac{8}{\pi^2} e^{-D_L t (\pi/2x_1)^2} \tag{2.15}$$

which for long drying times has been truncated at the first term and with the equilibruim moisture content, X^*, essentially equal to zero. Since $X_1 = X_D$, Equation 2.15 can be rewritten as

$$X(x_1, t) = X_D \frac{8}{\pi^2} e^{-D_L t (\pi/2x_1)^2} \tag{2.16}$$

In Equation 2.16, $X(x_1,t)$ is the average free moisture content at a distance x_1 from the surface at time t, x_1 is the depth of the bed through which the moisture has to desorb, X_D

is the initial moisture content of the bed at the start of the second drying rate period and, D_L is the diffusivity which is assumed constant in this equation, but in reality it is a function of temperature, moisture content, soil type, and packing density.

2.3.3.1 Simplified Theory: In some special cases, the entire drying curve may be approximated by two regions, BC and CD as shown in Figure 2.1 and Figure 2.2 with $X^* = 0$. Hence, the graph passes through the origin.

In this case, the entire falling rate period is uniform with a slope,

$$a = \frac{R_C}{X_c} \tag{2.17}$$

or

$$R = aX \tag{2.18}$$

Therefore, rearranging Equation 2.3, subtracting Equation 2.18 and integrating gives:

$$\frac{X}{X_C} = e^{\frac{Aa}{W_s}(t-t_C)} \quad t > t_C \tag{2.19}$$

Equation 2.19 suggests that the entire falling rate region can be correlated using a semi-logarithmic relationship and the slope, a, is measure of improvement in drying rate.

2.4 Overview of Acoustics

A mechanical wave is a disturbance from some equilibrium position in a homogeneous continuous material. The disturbances create a mechanical wave which travels though the material or medium slowly diminishing in strength as the mechanical wave moves away from the point of origin. Mechanical waves can be characterized into two types of waves. The first is a transverse wave which displaces the medium perpendicular to the direction of propagation of travel of the wave (Sears 1986). An example of this kind of

wave motion are the waves crashing on a shoreline. Contrary to this motion is the second type which is a longitudinal wave. This type of wave creates a medium displacement in the same direction of propagation. A good example of this type of wave is sound. In both cases, the medium oscillates back and fourth about its equilibrium position with zero displacement. Mechanical waves only transport energy but no matter along the medium and they can not travel through space.

2.4.1 Speed of Sound in Air

Mechanical waves travel through a continuous homogeneous material at a fixed speed which is known as the wave speed. The wave speed is a characteristic of the medium or material where it is traveling and is the product of the wavelength and the frequency. The characteristic of the medium is represented by a quantity known as the bulk modulus, B, in gases such as air. The bulk modulus of air is defined as an infinitesimal pressure change denoted by the differential of p, dp, over the ratio of an infinitesimal volume change to the original volume of the gas. The relationship is as follows:

$$B = -V_o \frac{dp}{dV} \tag{2.20}$$

Equation 2.20 relates the physical properties, pressure and volume of the medium, in our case air. The minus sign is placed in front of the V_o to make B a positive quantity because when dp is positive, dV is negative, and vise versa.

By a simple momentum balance given elsewhere (Sears 1986), the physical properties of the medium which are denoted by the bulk modulus, B, can be related to the speed of sound. The outcome of this derivation for gases only is as follows:

$$c = \sqrt{\frac{B}{\rho}} \tag{2.21}$$

Equation 2.21 is the speed of a transverse wave in a gas and ρ is the density of the gas. Through experimentation, it was found that sound travels in a gas or air adibatically at frequencies that range from 20 Hertz to 20,000 Hertz. The derivation of the speed of sound for adiabatic propagation of sound in air is given elsewhere (Sears 1986) and the result is as follows:

$$c = \sqrt{\frac{\gamma\ p}{\rho}} \tag{2.22}$$

In Equation 2.22, γ is the ratio of heat capacities of an ideal gas at constant pressure to that at constant volume and for air is equal to 1.4.

2.4.2 Speed of Sound in Liquids and Homogeneous Solids

When sound waves travel through an isotropic solid whose properties do not change with direction, two kinds of waves, longitudinal and transverse waves can propagate through that solid. When a longitudinal wave is propagating through an isotropic solid, the speed of sound is related to the amount of compression that the material can endure. If the amount of compression and stretching is small, the speed of sound in that solid is related to Young's Modulus of Elasticity in the solid by the following equation:

$$c = \sqrt{\frac{Y}{\rho}} \tag{2.23}$$

In Equation 2.23, Y is Youngs Modulus of Elasticity and ρ is the density of the isotropic solid.

A transverse wave is created by applying a shear force on the isotropic solid in a pulse type fashion. This action creates a wave front that propagates perpendicular to the medium through which it is traveling. A good example of this type of wave is a vibrating guitar string. The speed at which this type of wave propagates through an isotropic solid is related to the compression or tension applied to the material and the mass per unit length, area, or volume depending on the geometry of the material. The speed of a transverse wave in a thin solid such as a guitar string is related to the tension, S, of the string and the mass per unit length δ as follows:

$$c = \sqrt{\frac{S}{\delta}} \tag{2.24}$$

Equation 2.24 states that the more tension the string or solid material possesses, the faster sound will travel and the more mass per unit length, the slower sound will travel. In the case of a liquid, no transverse waves can exist because any shear force applied to the surface of the liquid will dissipate immediately due to the low viscosity of liquids compared to solids.

2.4.3 Propagation of Sound in Air

In order to create a sound wave, work must be done on a given volume of air either by momentarily creating a high pressure region in that given volume of air or a low pressure region on that given volume of air. The result of this work is a pressure wave that travels through the air by carrying this energy in the form of a high or low pressure distortion. A one dimensional wave equation is presented in Equation 2.25 and the derivation is found elsewhere (Sears 1986):

$$p(x,t) = B\frac{2\pi}{\lambda} A_p \cos\left(\frac{2\pi}{\lambda} ct - \frac{2\pi}{\lambda} x\right) \quad (2.25)$$

In Equation 2.25 the term A_p stands for the amplitude or maximum particle displacement from equilibrium, x is the particle displacement from equilibrium, λ is the wavelength and t is the time. Furthermore, in Equation 2.25, the maximum pressure in the system occurs when the cosine terms equals one. Therefore, Equation 2.25 gives an indication of how the longitudinal wave propagates in air when the physical properties of a gas are known.

2.4.4 Standing Waves

When the string of a guitar is plucked, the result is a system of standing waves. A standing wave is a mechanical wave having the same frequency with one or more mechanical waves traveling in opposite directions from the other and meeting in the same point in space. The result is a single wave with amplitude equal to the algebraic some of all the waves amplitudes at that point in space where they meet. This newly formed wave is call a standing wave.

A node is formed where the algebraic sum of all the amplitudes of the mechanical waves that form the standing wave is zero and an antinode is formed where the standing wave has maximum amplitude. The distance between a node and an antinode is a quarter wavelength and the difference between adjacent nodes is half a wavelength.

In the case of plucking a guitar string, the string forms a system of standing waves which vibrate with different frequencies known as the harmonic series. A harmonic series of frequencies are frequencies which are multiples of the first fundamental frequency. The first fundamental frequency is the lowest possible frequency of the harmonic series. The harmonic series is related to the speed of sound in the vibrating body and the length

vibrating body. The first term in the series is the first fundamental frequency. The following equation relates these quantities:

$$f = \frac{c}{2L}, \frac{2c}{2L}, \frac{3c}{2L}, \ldots = \frac{nc}{2L} \quad (n = 1,2,3..) \tag{2.26}$$

Any one of these frequencies correspond to a normal mode of the vibrating body and if a force is applied to the vibrating body at any one of these frequencies, large amplitudes of vibration can build up. This phenomenon is known as resonance.

2.4.5 Overview of Wave Energy

Wave energy is measured in intensity which is essentially the average power transported per unit area through a surface which is perpendicular to the direction of travel. The derivation is performed elsewhere (Sears 1986) and the result of this derivation is as follows:

$$I = \frac{1}{2} c \left(\frac{2\pi}{\lambda}\right)^2 B A_p^{\,2} \tag{2.27}$$

Equation 2.27 is the average intensity of a sound wave moving through a gaseous medium. A further observation of Equation 2.27 reveals the important relationship between intensity and amplitude A_p. According to Equation 2.27, the intensity increases by the square of the amplitude.

Sound intensity is normally measured in units of decibels. A decibel is ten times the base ten logarithm of the ratio of the measured intensity to some reference intensity I_o. Normally the reference intensity is the threshold of human hearing which is 10^{-12} Watts per centimeter squared. The formula is as follows:

$$\beta = 10 \log \frac{I}{I_0} \tag{2.28}$$

where β is the dimensionless unit called the decibel.

2.4.6 Wave Attenuation

When a sound wave propagates from one point in a medium to another say x_1 to x_2 the wave "loses energy to the medium" (Meyer 1972 and Crawford 1955). This "energy loss" is due to the conversion of sound energy to other forms of energy or deflection of some of the wave energy by scattering, diffraction, refraction and reflection.

Energy in a wave can also be absorbed by the conversion of some of the wave energy into random molecular motion other than wave motion. In thermal conduction, temperature gradients develop between regions of compression and rarefaction in the wave path and since the compression and rarefaction regions are formed adiabatically, heat flows from these two regions. This heat which comes from the wave energy, flows from the compression region to the rarefaction.

The last type of mechanism that reduces wave energy as the wave propagates in air is thermal relaxation. To understand the mechanism of thermal relaxation, it is essential to recognize that in a gas such as air, the molecules have translational kinetic energy and internal kinetic energy. The internal kinetic energy of a molecule is composed of kinetic energy of rotation and kinetic energy of vibration. Thermal relaxation is the conversion of wave energy into internal kinetic energy, either translational or rotational kinetic energy.

Normally, the attenuation coefficient represents the combination of all these mechanisms and is usually expressed as the quotient of a constant and the frequency for a given range of frequencies. Generally, the attenuation coefficient is higher for gases and is

smaller in liquids and solids. Attenuation α_p is expressed mathematically by adding a exponential decay term to Equation 2.25.

$$p(x,t) = e^{-\alpha_p x} B \frac{2\pi}{\lambda} A_p \cos\left(\frac{2\pi}{\lambda} ct - \frac{2\pi}{\lambda} x\right) \tag{2.29}$$

Equation 2.29 represents the propagation of a mechanical wave through a continuous medium in the x direction with an attenuation term driving the function to zero as x goes to infinity.

2.4.7 Overview of Sound Behavior at Interphases Between Two Mediums

When a sound wave reaches a boundary between two mediums, the sound wave can transmit itself completely into the next medium, it can reflect off of that next medium and back into the original medium and, it can refract into the next medium or it can diffract from the next medium (Cracknell, 1980).

2.4.7.1 Reflection: Sound waves will reflect back into the media of origin, when the sound wave encounters a discontinuity or an interphase between the medium where it is propagating and the other medium with which it has an encounter. The sound wave will reflect at the angle of incidence

$$\theta_i = \theta_r \tag{2.30}$$

In Equation 2.30, θ_i represents the angle of incidence and θ_r represents the angle of reflection.

2.4.7.2 Refraction: Refraction occurs when a sound wave penetrates a second medium. .The angle of transmissions θ_t of the sound wave is related to the angle of incidence of the sound wave by Snell's Law,

$$\sin \theta_i / c_1 = \sin \theta_r / c_2 \tag{2.31}$$

Snell's law also shows that for angles greater than the critical angle, the sound wave is reflected completely back to the original media and no transmission occurs. The critical angle θ_c is defined as:

$$\sin \theta_c = c_1/c_2 \tag{2.32}$$

2.4.7.3 Diffraction: Diffraction occurs when a sound wave hits a body with dimensions similar to those of the sound wave's wavelength. This causes the sound wave to spread around the edges of the body by changing its direction of propagation.

2.4.7.4 Scattering: Scattering is a phenomenon observed when a sound wave strikes a body with dimensions small compared to the sound wave's wavelength. This phenomenon affects the amplitude of the wave and hence the energy of the wave. Scattering is the main cause of attenuation of a sound wave when traveling through soil or other heterogeneous materials and it increases as the third power of the grain size and the fourth power of the frequency as long as the grain size remains smaller than the wavelength of the sound wave.. The amplitude of the scattered sound wave at great distance from the grain is directly proportional to the volume of the particle and inversely proportional to the square of the wavelength.

2.4.7.5 Acoustic Coupling: When the properties two media are alike and if the angle of incidence between these two media is less than the critical angle, most of the wave energy is transmitted efficiently among either media. On the other hand if the properties of the two media in question differ greatly, the sound wave and its corresponding energy is reflected completely into the medium of origin.

The properties that acoustically differ in two media are the wavelength, the density and the speed of sound. Acoustic impedance, w, is the term that combines these properties. This relation is as follows:

$$w = c^2 \rho \frac{2\pi}{\lambda} \tag{2.33}$$

If the acoustic impedance of two media say medium A and medium B are known, then a reflection, an incident and a transmission coefficient for the sound wave's energy can be estimated. The relationship is as follows:

$$a_r^2 = \left(\frac{w_A - w_B}{w_A + w_B} \right)^2 a_i^2 \tag{2.34}$$

$$a_t^2 = \left(\frac{2w_A}{w_A + w_B} \right)^2 a_i^2 \tag{2.35}$$

In Equations 2.34 and 2.35, a_r , a_i and a_t are the reflection coefficient, the incident coefficient and the transmission coefficient respectively. These coefficients represent the fraction of the sound wave's energy that is reflected at the interphase of the two media, the fraction of the sound wave's energy that arrives at the interphase of the two media and the incident coefficient and the fraction of the sound wave's energy that is transmitted into the next medium.

Two extreme cases can be seen examined in Equations 2.34 and 2.35. The first case is when the acoustic impedance of Medium B is much greater than Medium A ($w_B >> w_A$). By substituting back into Equations 2.34 and 2.35, it is evident that the square of the reflection coefficient is approximately equal to the square of the coefficient of

incidence. The square of the transmission coefficient is very small and approximately zero. This proves that when two media have different acoustical impedances all the wave energy is reflected back into the medium of origin. On the other hand, if the acoustic impedance of Medium A is equal to the acoustic impedance of Medium B, the reflection coefficient is zero and the transmission coefficient is equal to the square of the incidence coefficient thus proving that when two materials are acoustically matched, all of the energy is transmitted into the next medium.

2.4.8 Resonance Phenomenon

Resonance is a phenomenon that occurs when a periodic force matching the natural frequency of a vibrating body is applied (Kleppe 1989). As mentioned earlier, a vibrating body of definite size and shape contains what is known as normal modes of motion. This means that each particle on the body vibrates sinusoidally with the same frequency. When a periodic force is applied intermittently at this frequency, the vibration energy in the body builds up. The result is the build up of large amplitudes of vibrations that can cause the vibrating body to break apart.

In Section 2.4.7.5 it was mentioned that if two materials are acoustically mismatched, the wave is reflected back into the medium where the sound originated. This does not apply if the frequency of that sound wave is at the resonance frequency of a vibrating body. If the frequency of the wave in question is at the resonance frequency of a vibrating body into which it is trying to penetrate, the result is penetration into the vibrating body.

A good example of this phenomenon are two identical tuning forks set some distance apart. One is set in motion while the other remains at rest. The vibrations can then be eventually heard on that tuning fork that was not originally in motion.

The vibrations leaving the tuning fork that was set in motion, have to enter air which is acoustically mismatched with the metal with which the tuning fork is made and then reenter the other tuning fork that is not in motion. However since the emitted frequency is at the second tuning fork's resonance frequency, the sound wave's energy enters the tuning fork with ease.

2.5 Acoustic Properties of Soil

The science that deals with mechanical waves in soil and in rocks is known as seismology. Due to the inhomogeous nature of the soils and rock, mechanical waves tend to attenuate very quickly and have different speeds as the waves enter a leave the rocks and soils of different densities and acoustic impedance. In solid rock mechanical waves can exist as longitudinal waves as well as transverse waves also known as P-waves and S-waves respectively (White 1965). These waves are strongly dependent on the consistency of the shear modulus as well as the bulk modulus as the wave propagates through the rock. Changes of the shear and bulk modulus are dependent on the composition of the rock.

Acoustic properties such as speed of sound, amplitude of sound wave and attenuation of sound in soil are dependent on the mineralogy of the soil, the porosity of the soil, the fluid content of the soil and the state of consolidation of the soil (Blangy 1993). A study conducted by Blangy, Strandenes, Moos and Nur (1993) concluded that ultrasonic velocities in sandstone reflect the changes in bulk and shear moduli due to the lithological changes as the sound wave travels along the length of the sandstone.

Further studies have revealed that there is an extra loss of amplitude in the sound wave as it travels through unconsolidated soils such as sand (White 1965). This is due to geometric spreading and reflection at boundaries and discontinuity. Studies also revealed that in tightly packed clays, sound waves travel faster and with little change in velocity and with some attenuation. It was concluded that tightly packed clays can be treated as homogeneous materials (Han 1986). **Table 2.1** represents attenuation coefficients of sound wave for different types of rocks.

2.6 Mechanical Waves in Cylindrical Bore Holes

Sound waves are normally created in bore holes for many purposes. One of these applications is to search for oil in the ground. Sound waves are created in a borehole by first drilling a cylindrical borehole and filling it up with water (White 1965). Then another borehole is drilled some distance away and also filled with water. A receiver is placed on one of the bore holes and a transducer in the other. The waves received by the bore hole where the receiver is located, reveal many characteristics of the soils and rock between bore holes. This information also reveals whether there is oil or other fluids between the bore holes.

2.7 Overview of Sonic Drying

The use of airborne ultrasound to enhance mass transfer of liquids in solids is not a new idea. It was discovered in 1936 and has been in use ever since as an enhancement technology in drying of solids (Burger 1961). Sonic drying which refers to the expulsion of water from solid materials was first suggested by F. J. Burger and K. Sollener (1936) when they attempted to dry quartz sand using an intense air-coupled sound field. Since then, there have been numerous studies concerning the drying of solids. All of the

Table 2.1 Measured of Attenuation Coefficient for Several Rock Types*

ROCK TYPE	FREQUENCY CPS	ATTENUATION COEFFICIENT	METHOD
Granite:	$1 * 10^6$	$\alpha_p = 0.044$/cm at 10^6 cps	Multiple reflection of sine-wave train
Kamyk	$(0.2\text{-}2) * 10^6$	$\alpha_p = 3.9 \times 10^{-8} f$ sec/cm	Short pulse, direct path only
Limestone: Solenhofen	$(3\text{-}15) * 10^6$	$\alpha_p = 5.2 \times 10^{-8} f$ sec/cm	Multiple reflection of sine-wave train
Sandstone: Amherst	$1 * 10^6$	$\alpha_p = 0.035$/cm at 10^6 cps	Multiple reflection of sine-wave train
Chalk: Chiselhurst	600	$\alpha_p \sim 6 \times 10^{-6}$ /cm at 600 cps	Bulk medium, sine-wave train
Shale:	$(3\text{-}12) * 10^3$	$\alpha_p = 45 \times 10^{-8} f$ sec/cm	Long. Resonance
Sylvan	$(6\text{-}20) * 10^3$	$\alpha_p = 4 \times 10^{-6} f$ sec/cm	Bulk medium, Fourier analysis of pulses

*White, J.E. 1965 Seismic Waves: Radiation, Transmission and Attenuation, International Series in the Earth Science, McGraw-Hill Book Company, New York, NY

researchers claimed that airborne ultrasound increases the drying rate of solids exposed to a sound field but the extent of the enhancement varies considerably with the material (Muralidhara 1984 and Swamy 1983). Furthermore, the generator type, size and frequency varied from experiment to experiment but they all showed enhancement. A review of all these articles concluded that sonic drying is best at sound frequencies between 7 kHz and 20 kHz and sound intensities greater than 145 dB (Boucher 1958).

Presently, sonic drying is being used to dry heat sensitive compounds, degrease metal parts, to agglomerate particulate matter in dusty environments such as mines and to defoam fermentation brothes in the beer brewing industry (Boucher 1961,Chendke 1975 and Borisov 1966).

2.7.1 Mechanism of Sonic Drying

There are several mechanisms taking place when a granulated material is being dried (Greguss 1963 and Judhav 1989). The first mechanism that is encountered is the diffusion of the liquid from the surface of the material into the air. The liquid must first evaporate then diffuse through the gas film and then into the bulk air flow. Once sufficient liquid has left the material, a concentration gradient of liquid develops between the interior of the material and the surface of the material. This concentration gradient drives the liquid to the surface of the material. The primary mechanism that controls the removal of liquids from a wet solid is the temperature gradient between the air and the wet surface. When the temperature of a tangential air stream is higher than the surface of a granulated material and its liquid content, heat transfer between the air, the granulated solids and the liquid within the granulated solids will cause the liquid to evaporate into the tangential air stream. In the case of sonic drying, temperature gradients are not measured and yet sound

is able to remove liquids from solids at higher rates. This mechanism is known as sonic diffusion because it is observed when a sound field is applied to a wet material.

Thus far, there has been little theoretical work on relationships between parameters such as acoustical power, radius of influence and radius of penetration in granulated solids containing liquids. Furthermore, the small amount of theoretical work concerning these relationships has not been proven experimentally. The first of these theoretical relationships attempts to relate, the acoustical power, the radius of penetration in a granular material of a known thickness and of infinite length and width, and the moisture conductivity. The model assumes that the droplet of moisture loses kinetic energy uniformly as it works its way to the top of the material within the penetration radius. Greguss (1963) predicted the distance traveled by the moisture droplet from a distance, x_p, inside the material within the penetration radius of the sound field to the top of the surface by the following formula:

$$s = \frac{x_p}{\cos \varphi} \tag{2.36}$$

In Equation 2.36, φ is the angle at which the particle is moving with respect to the surface of the granular solid material and s is the distance traveled by the droplet. Greguss (1963) then related the intensity of sound I to Equation 2.36 in the following manner:

$$I(1 - s / r) = I(1 - x_p / r \cos \varphi)... \tag{2.37}$$

In equation 2.37 r is the distance penetrated by the sonic energy into the granulated solid.

Greguss also derived a relationship between sound intensity and penetration range for vapor trapped in a granular solids subjected to a sound field. He called k_∞ the fraction

of vapor arriving at the surface of the granular material. The relationship is an infinite series of the ratio of penetration range r of the sound field to the thickness of the slab, H. The equation is as follows:

$$k_{\infty} = \frac{2}{3}\frac{r}{H}\left[1-\left(1-\frac{H}{r}\right)\right]^{\frac{3}{2}} - \frac{H}{4r}\ln\frac{r}{H} + \frac{H}{2r}\ln\left(1+\sqrt{1-\frac{H}{r}}\right) - \frac{1}{6}\left(1-\sqrt{1-\frac{H}{r}}\right) + \frac{r}{6H}\left(1-\sqrt{1-\frac{H}{r}}\right)^{2}\cdots \quad (2.38)$$

Greguss (1963) also explained that in an element of surface area dA, the differential of the total kinetic energy of the moisture within that surface has to be directly proportional to the number of droplets n, within that surface area A, the intensity of the sound field I, the penetration range r, and the surface area element dA. The formula is as follows:

$$dK \propto n\, I\, r\, dA \quad (2.39)$$

In Equation 2.39, dK is the total kinetic energy of the moisture particles within the surface area element dA. Greguss (1963) further explained that by dividing the kinetic energy by half the mean moisture droplet velocity squared υ^2, the total amount of moisture brought into motion by the sound field I, in the element dA, can be obtained. The mean particle velocity is related to the overall mass transfer coefficient k_m by the following relationship:

$$\upsilon = \frac{k_m}{H}\cdots \quad (2.40)$$

The overall mass transfer coefficient can be broken down into the liquid mass transfer coefficient k_w, and the vapor mass transfer coefficient k_v, so that the sum of the reciprocal of each is equal to the reciprocal of the overall mass transfer k_m.

Greguss (1963) cites the work of Likov which shows that the mass transfer coefficient for liquids diffusing through pores in a bed of granulated solids is proportional to the surface tension of the liquid σ and inversely proportional to the viscosity of the liquid μ as shown in the following equation:

$$k_w = \frac{\sigma}{4\mu} k \tag{2.41}$$

In Equation 2.41, k is a coefficient which represents the distribution of the pores in the bed, μ is the liquid viscosity and k_w is the liquid phase mass transfer coefficient.

2.8 Overview of Sonic Generators

There are many types of sound generators in the market today. They may be divided into five categories in accordance with how they produce the sound and the materials with which they are made (Manthey 1992). These five categories of generators are:

1. Electrostatic Generators
2. Electrodynamic Generators
3. Magnetostrictive Generator
4. Piezoelectric Generators
5. Pneumatic Generators

Electrostatic Generators are based on the principle that the spacing between the plates of a condenser can be changed by electrostatic forces between them. The plates are made out of a flexible metallic material which attract and repel one another in the presence of an alternating voltage. This motion creates sound vibrations in the air that is near the plates. These sonic generators are used for low power applications such as distance measurements and censoring.

Electrodynamic generators are the most common sound emitters in the market. They work on the principle that when an electrical current is passed through a coil, it produces a magnetic field which moves a small magnetic plate back and forth. This magnetic plate is attached to a material which acoustically matches that of air to enhance the sound being generated.

Magnetostrictive generators are based on the principle that when a voltage is applied to a metallic material such as nickel or steel, the material will expand and when that voltage is removed, the material will return to its original shape. An alternating voltage at the resonance frequency of that material will result in an efficient oscillation of the metal which will produce a sound field in all directions. This group of generators is durable and they are mostly used for degreasing mechanical parts that are submerged in a cleaning fluid.

Piezoelectric generators are the most common industrial generators in the market today. They work on the principle that when a voltage is applied to a crystal that has piezoelectric properties, the crystal will develop a charge and will be attracted to an oppositly charge plate or crystal. When the charge is reversed, the opposite will be true. When this procedure is repeated, numerous times, the result is a vibration of the crystal. If the crystal vibrates at its resonance frequency, the result is the generation of a powerful sound field.

The last class of sound generators are the pneumatic generators. These generators produce sound waves using air. There are numerous types of pneumatic generators and they are divided into two subclasses: Static Generators and Dynamic Generators.

2.8.1 Static Generators

Static generators are based on the principle that when a jet is accelerated to a velocity close to that of the speed of sound by a converging nozzle, a crossover of gas results due to the oblique shock waves formed at the tip of the nozzle. This action causes a pressure variation in the gas stream (Gallego-Juarez 1988 and Graham 1970). By placing a resonant cavity in a point within this unstable region, the gas inside the resonant cavity will be exited into resonance and further reinforcing the sound waves created in the unstable region. The frequency of sound at which the generator operates and the intensity of the sound field emitted by the generator is a function of the mass flow of air. These authors report that this type of generator was conceived by Hartmann in the 1930's.

During the 1960's, Soloff developed an improved version of the Hartmann Whistle which later became known as the Stem Jet Whistle (Soloff 1964). Similar to the Hartmann Whistle, the Stem Jet Whistle creates sound by a high velocity jet of air and a resonance cavity of known depth and diameter, but unlike the Hartmann Whistle, the cavity in the Stem Jet Whistle is located along the center axis and parallel to the emission of sound and held together by a stem. Hence this is where the Stem Jet Whistle acquired the name Stem Jet.. The cavity in the Hartmann Whistle is located perpendicular to the sound field emission.

The next type of static generator is The Vortex Whistle. The Vortex Whistle works on the principle that when a jet of air is forced through a circular conduit of decreasing diameter, the result is the generation of a sound field which is proportional to the inlet gas pressure and the number of turns the gas makes inside the circular conduit

before exiting through the smaller diameter pipe. The intensity at which the sound is generated is proportional to the mass flow of air that is fed into the whistle.

2.8.1.1 Principles of the Hartmann Type Whistles: A Hartmann Whistle is based on the principle that when a jet of air (gas) is accelerated to a velocity close to that of the speed of sound by a converging nozzle, a crossover of gas results due to the oblique shock waves formed at the tip of the nozzle which causes a pressure variation in the gas stream. According to Merle's (Boucher 1957 and Swamy 1980) formula, the frequency of sound can be calculated from the geometry of the converging nozzle and the resonator cavity:

$$f = \frac{c}{D_o}\frac{\left(K_1 + K_2\right)}{\sqrt{r_r - r_c}} \tag{2.42}$$

In Equation 2.42, c is the velocity of sound, D_o is the nozzle orifice, r_r is the ratio of the reservoir pressure to atmospheric pressure, r_C is the critical ratio at which the speed of sound is reached at the nozzle orifice and K_1 and K_2 are characteristics of the whistle. The constant r_C is defined by the following thermodynamic relation:

$$r_C = \frac{P_A}{P_R}\left(\frac{2}{\gamma + 1}\right)^{\frac{\gamma}{\gamma+1}} = 0.527 \tag{2.43}$$

In this relationship, P_A is the atmospheric pressure, P_R is the reservoir pressure and γ is the ratio of the heat capacity of air at constant pressure to the heat capacity of air at constant volume. The sound intensity generated by a Hartmann type whistle at the source and the sound intensity generated by a Stem Jet Whistle at the source can be estimated by the following two formulas respectively:

$$I_o = 3O^2\sqrt{P_R - 0.9} \tag{2.44}$$

$$I_o = K'\left(P_R - 0.3\right) \tag{2.45}$$

For both devices, the corresponding wavelength at the sound source is:

$$\lambda_0 = .0193O \text{ (ft)} \tag{2.46}$$

In Equation 2.46, O, stands for the resonator cavity opening and I_o is the sound intensity at the source measured in decibels. In equation 2.39 K' is a proportionality constant. In Equation 2.46, λ_o is the wavelength of sound at the source of the two whistles. The two whistles can operate best when the frequency of sound generated by the whistle is equal to the frequency of resonance of the cavity. This phenomenon is due to vibrations in the cavity which enhance the intensity of the sound being emitted. Typical efficiencies of a Hartmann type whistle range from 6% for a Hartmann Whistle to 20% for a Stem Jet Whistle. The efficiency of a whistle is calculated by dividing the acoustical power generated by the whistle over the total power consumed by the whistle.

2.8.1.2 Principles of the Vortex Whistle: The Vortex Whistle is a device which consists of a circular opening through which compressed gas enters tangentially and is forced to rotate through a cylinder of converging diameter. The gas then escapes through a small circular opening where the gas tangential velocity is greatest. This fast rotating gas produces powerful oscillations (Boucher 1961). Although very little work has been done to determine sound intensities and wavelength produced by this type of whistle, a rough estimate of the frequency generated by this type of whistle can be obtained using a formula developed by Vonnegut and reported by Boucher(1961):

$$f = \alpha\left[\frac{c}{\pi D}\right]\left[\left(P_1 - P_2\right)/P_2\right]^{\frac{1}{2}} \qquad (2.47)$$

In Equation (2.47) α is constant, P_1 is the pressure of the gas entering the device and P_2 is the pressure of the gas leaving the device, and D is the outlet diameter of the vortex which changes. There has been no work done on efficiency of this type of whistle although powerful emissions have been observed.

2.8.2 Dynamic Generators

The basic principle governing dynamic generators is that when a jet of air is periodically interrupted by a rotating device, the result is the generation of sound waves with frequencies which are proportional to the number of interruptions the jet of air is subjected to in a period of one second (Allen 1947 and Wood 1937)). The intensity of sound generated by this type of generator depends on the amount of gas that is "blocked off" when the jet of air is interrupted (Allen 1959). In a siren, which is a dynamic generator based on this principle, the amount of air that is "blocked off", meaning the air that can not penetrate when the holes in the siren are closed, is determined by the clearance between the rotating part and the moving part. The percentage of air that is "blocked off" from the total air flow is known as the acoustical flow. The acoustical flow is a function of the power and hence the intensity of the sound and these are related by the following equation:

$$W_p = \left(\frac{\left(\omega - \omega_o\right)^2}{2\sin\theta\rho_2 S_2}\right) \qquad (2.48)$$

In equation (2.48), W_p is the acoustical power generated by the siren, ω and ω_o are the total mass flow of air and the average mass flow of air respectively. The variable θ is a function of time and represents the rotor angle multiplied by the number of ports. Variables ρ_2 and S_2 are the density of air and the cross sectional area of all the holes.

Like whistles, sirens are use for industrial gas cleaning, coagulation of particles in aerosols and drying of heat sensitive materials.

2.9 Coupled Sonic Drying-Pneumatic Fracturing Overview

Focusing sonic energy into a fracture can theoretically have many beneficial effects that can lead to an enhancement in the removal rate of liquids that are trapped inside tightly packed geologic formations. This effect can vary from enhanced volatilization rate to cavitation of the liquid on the surface of the fracture under the intense sonic energy. Based on studies performed on drying of solids in the presence of a sonic field, the following effects are probable when a intense sound field of about 145 Db is applied in a fracture:

1. Decreasing the gas film at the gas-liquid interface. The sonic energy decreases the gas-liquid interface film by increasing the turbulence around the boundary layer of the liquid and the gas. The decrease in the film causes a greater concentration gradient for the liquids to move from the liquid phase into the vapor phase. Furthermore, the decrease in the stagnant gas film length between the gas and the liquid due to the turbulance created by the pressure waves, increases the heat transfer coefficient and henceforth heat is transferred more efficiently into the liquid to be evaporated.

2. Decreasing the net total pressure in the fracture. An intense acoustical field of about 150 decibels, causes the gas in a fracture to compress and dilate. At these sound levels,

the dilation regions are approximately 18% below atmospheric pressure and since it is known that dilation regions dominate over compression regions, the net pressure in the fracture will be lowered and hence liquid will be pulled into the fracture. Furthermore, since the net pressure is lowered in the fracture, some of liquid in the fracture will tend to vaporize and be carried away by the airflow in the fracture.

3. Increasing moisture conductivity in solids. Liquid conductivity of moisture trapped in capillaries around a fracture area will also be enhanced and will be compelled to flow into the fracture. It has been demonstrated that liquids trapped in capillaries are not always continuous. The moisture is separated by vapor or air bubbles. An intense sonic field can cause the bubbles trapped in these capillaries to warm up and this causes a migration of the contents in the capillaries toward the fracture zone since it is at a lower pressure due to the intense acoustical field. The name given to this phenomenon is sonic moisture conductivity.

4. Causing cavitation of the liquid near the sound source and henceforth faster evaporation of the liquid. Liquids in close proximity to the sonic device will be subject to cavitation due to the intense sound field. Also, if the fracture is in a rock, the acoustical energy will be attenuated slower and this will lead to a higher radius of influence for cavitation effects. The gases formed during cavitation will be carried away by the same air used to create the intense sound field. This effect will contribute in a positive way to the removal rate because it will further enhance the removal rate of contaminants from the fracture.

CHAPTER 3

3. EXPERIMENTAL APPROACH

The objective of the present work is to establish whether or not airborne ultrasonic methods can be coupled with pneumatic fracturing to enhance the removal of volatile organic contaminants from soil *in situ*. These tests were conducted in bench scale experiments using two air coupled transducers, a siren and a stem jet whistle in soil testing cells.

The approach was to pack sand in a tank containing an artificial fracture made of a sandwiched geotextile embedded within the sand layer inside the tank. Prior to packing the tanks, two 3/4 inch PVC pipes were inserted in the tank. These pipes were used to extract the vapors originating from the volatilization of the contaminants. The same tank was also used with an air coupled ultrasonic transducer aligned with the fracture in the tank. The weight of the tanks during the experiment was recorded by a scale composed of three sandwiched load cells between two 1/2 inch thick aluminum plates. The concentration of volatiles in the effluent gas stream over the course of the experiment was recorded by a gas chromatograph with a flame ionization detector. Furthermore, the temperature was monitored at 4 different points along the fracture to measure any temperature change caused by the sonic energy. The temperature in the fracture was measured with 4 type J thermocouples placed at the sound source, half way between the sound source and the extraction pipes in the fracture, outside the extraction pipe and inside the extraction pipe. The resulting data were analyzed using standard methods for analyzing the drying of materials describe in chapter 2. Based upon the measured data

and using standard drying theory, conclusions will be made to determine whether ultrasound is effectively enhancing the removal rate of contaminants from soil.

3.1 Setup of Experimental Apparatus

Before setting up the experimental apparatus, one must identify the variables that will be measured while keeping the rest of the parameters constant. According to drying theory, the variables that must be monitored are concentration of liquid in the effluent air stream over time, and mass removal over time. The remaining variables; packing density, composition of solid matrix and air flow rates should be kept constant.

3.1.1 Setup of Tanks

Two tanks made out of Plexiglass™ were constructed at NJIT. Twelve pieces of acrylic Plexiglas 3/4 inch thick were purchased from Grewe Plastics in Newark, New Jersey. Eight of the pieces were 11 and 3/4 inches wide by 23 and 3/4 inches tall and 3/4 inch thick. These pieces formed the walls of both tanks. Two of the pieces were 18 inches square by 3/4 inch thick formed the base of both tanks. The top of the tanks were made by bonding a 11 inch square by 3/4 inch thick Plexiglass™ plate onto the center of a 12 and 1/2 inch square by 1/2 inch thick Plexiglas piece (**See Figure 3.1**). These pieces of Plexiglass™ were bonded together using Rez-N-Bond acrylic bonding compound. The top of the tanks were bonded onto the tanks during each of the runs by using Silicone II Window and Door Sealant. Silicone II was used to enable the top of the tank to be removed at the end of a run. The edges of the tank were reinforced by angle iron to prevent the tank from bursting open during an accidental over pressurization.

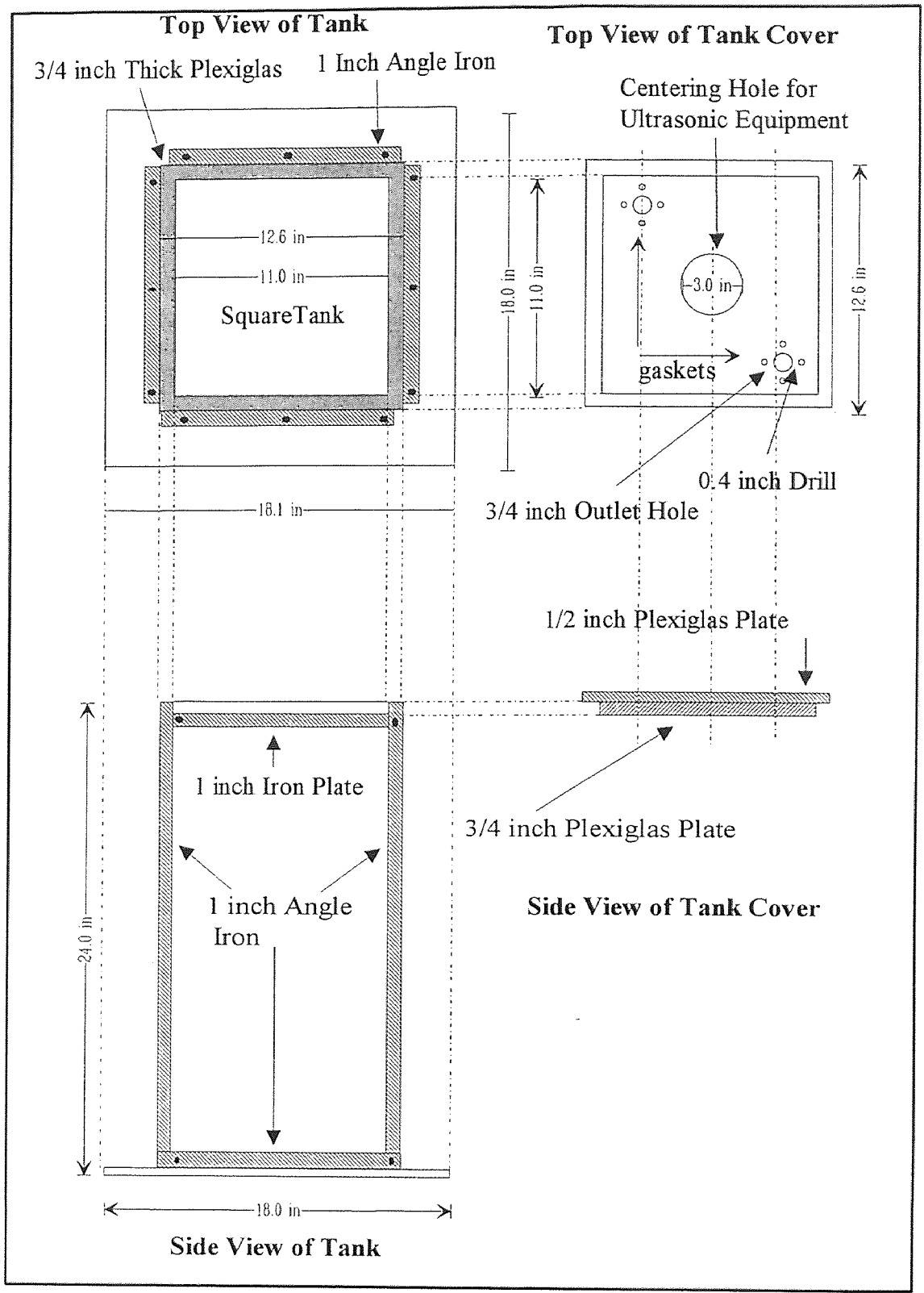

Figure 3.1 Experimental Tank Design

After the tanks were assembled, they had a 11 and 3/4 inch opening on top and stood 23 and 3/4 inches tall with a base of 18 inch square. The tanks were made of clear material to make observations and to position the ultrasonic equipment properly.

A 3/8 inch diameter pressure hose was inserted at one corner of the tank or at the center of the tank, depending and the transducer that was being tested. The hose penetrated through the Plexiglas and fed the ultrasonic equipment located in the fracture. In opposite corners of the tank, two perforated 3/4 inch Chloronated Polyvinyl Chloride (CPVC) pipes were inserted to collect the gas coming out of the fracture. These pipes were attached to flanges which were attached to the top of the tank. From the top of the cell, the flanges connected the top of the tank to the rest of the piping including the sampling filter for the gas chromatograph.

3.1.2 Setup of Electronic Scale System

The electronic scales were built by sandwiching three electronic load cells between two aluminum plates for each of the scales (**See Figure 3.2**). The electronic signal was sent to a computer terminal and turned into a reading in pounds. The plates were 20 inches square by 1/2 inch thick and purchased from Roncocas Metal Corporation in Roncocas, New Jersey. The GSE Precision Load Cells model number 5353 (**See Figure 3.3**) were placed in a triangular arrangement between the two aluminum plates. A Radio Shack DC regulated power supply of 13.8 volts was used to excite the load cells. A built in Wheatstone bridge inside each of the load cells provided a resistance to the voltage which varied with weight. Each of the voltages generated by each of the load cells was transferred separately to a Data Translations terminal block, model number 707 (DT707).

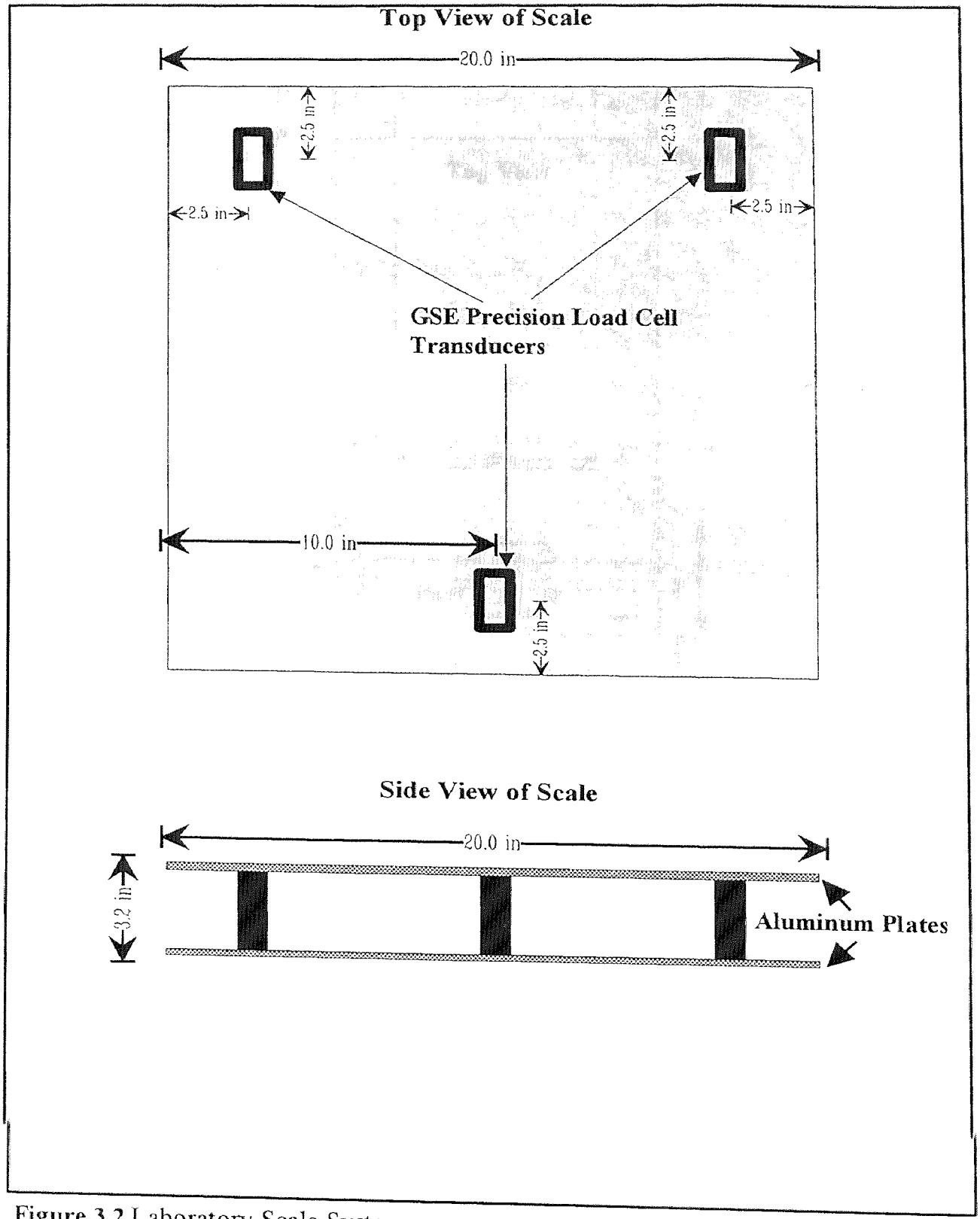

Figure 3.2 Laboratory Scale System

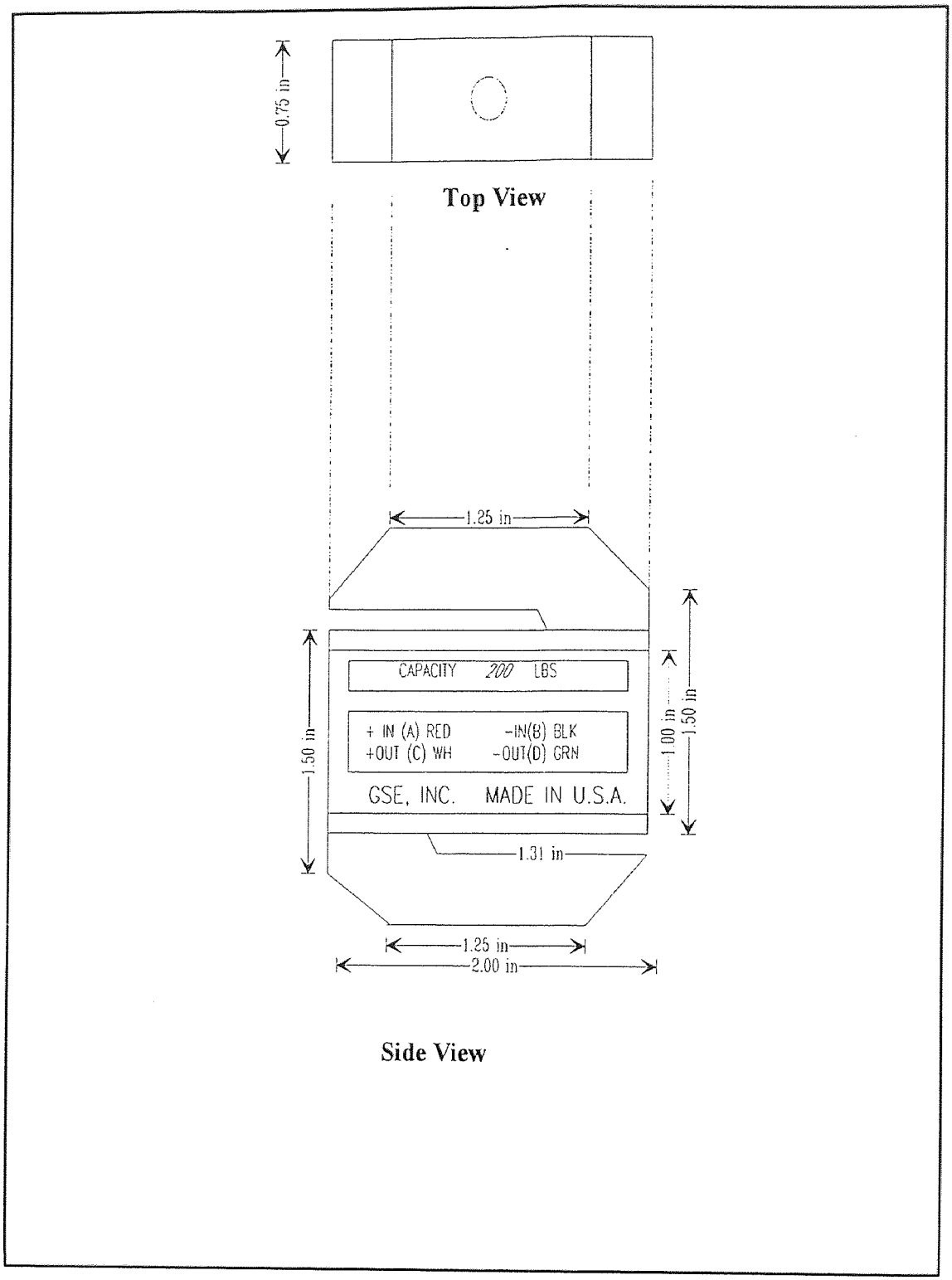

Figure 3.3 GSE Precision Load Cell

The DT707 sent the signals to a Data Translation Computer Card (DT2805) which converted the analog signals to a digital signals. The digital signals were read by a computer software, Labtech Note Book which added the signal and applied the proper calibration constants. The calibration constants changed the signal into a reading in pounds which was displayed in the computer monitor and recorded to the computer hard disk. The calibration line is shown in **Figure 3.4**.

3.1.3 Gas Analysis

Monitoring the concentration of volatile compounds emerging from the fracture was accomplished by attaching a Matheson Gas Product Particle Filter model number 6120 with 0.2 micron efficiency to the extraction line coming out of the tank. The sample gas stream was fed into a 3 milliliter sampling loop inside a gas chromatograph. The sampling loop is part of a six way valve system which when activated, feeds the contents of the loop with carrier gas nitrogen at 24 liters per hour into the gas chromatograph's column. The gas chromatograph's column is made of Carbopack with a length of 10 feet and a column diameter of 1/8 inch. The oven temperature which houses the column was always set at 100 ^{o}F. This temperature successfully separated the water vapors from the gas to be analyzed. The sample along with the carrier gas was fed to a flame ionization detector. The detector burned the hydrocarbons and generated a signal which was sent to the terminal block (DT707). The computer monitored the signal and when the signal went above the threshold value assigned by the user through the Labtech Note book software, the computer recorded the signal and captured the peaks. The data collection was conducted at a rate of 2 samples per second or 2 hertz. Then the peaks were integrated

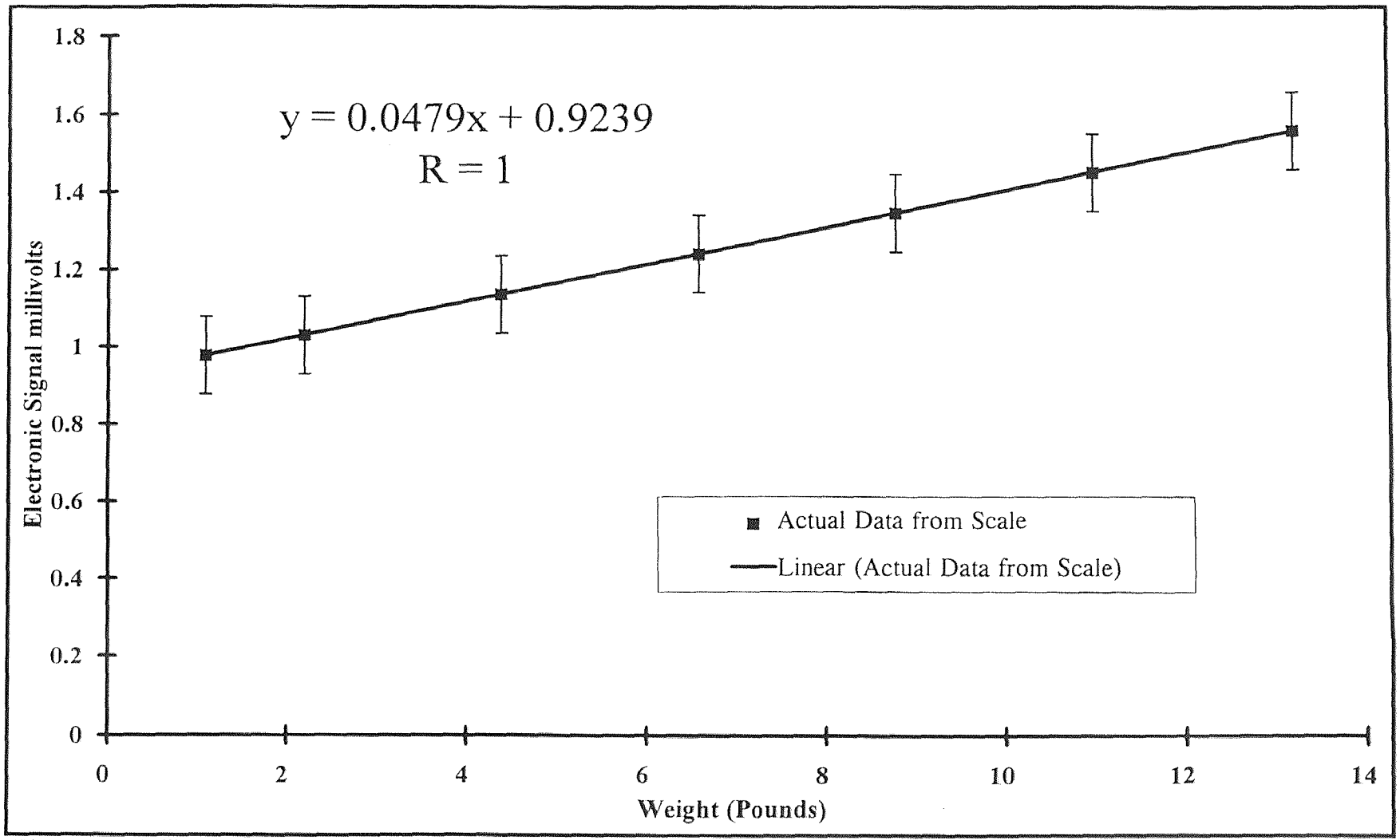

Figure 3.4 Calibration Line For Scale System

by using the trapezoidal rule. Since the total area underneath the signal generated by the ion detector is proportional to the total number of moles in the sample, the concentration of VOCs in the effluent gas was known and monitored over the duration of the run. The gas chromatograph was calibrated by preparing a solution of the contaminant ethanol in water which extended from a range of .03 moles per liter to 0.0003 moles per liter. Injections of 0.2 microliters where made and the area was obtained for each of the concentrations. The log of the number of moles contained in each of the injection was plotted on the y axis versus the log of the total area for the corresponding solution. A straight line equation was obtained which relates the number of moles of ethanol to the corresponding area **(See Figure 3.5)**.

3.1.4 Siren Design

Two sound generators were built to enhance the removal rate of liquids trapped in the experimental tank. The first sound generator, a siren, was constructed at NJIT. This sound generator was built based on the concept of Allen and Rudnick (1947) who state that when a jet of air is periodically interrupted by a rotating device, the result is a sound wave whose frequency is given by the product of the angular velocity of the rotating device and the number of periodic interruptions. The siren was built by coupling an Atlas Copco Air Motor model number LZB 46 AR to a perforated hollow cylindrical steel tube open at one end. The cylinder contains 56 radial perforations with diameter of 2.1 millimeter equally spaced in a row of 6. The perforated cylindrical steel tube is coupled to a Barden Precision Bearing Series Number 205. The bearing prevents the cylinder from vibrating while in motion. This entire assortment is 12 inches tall and is encased in a

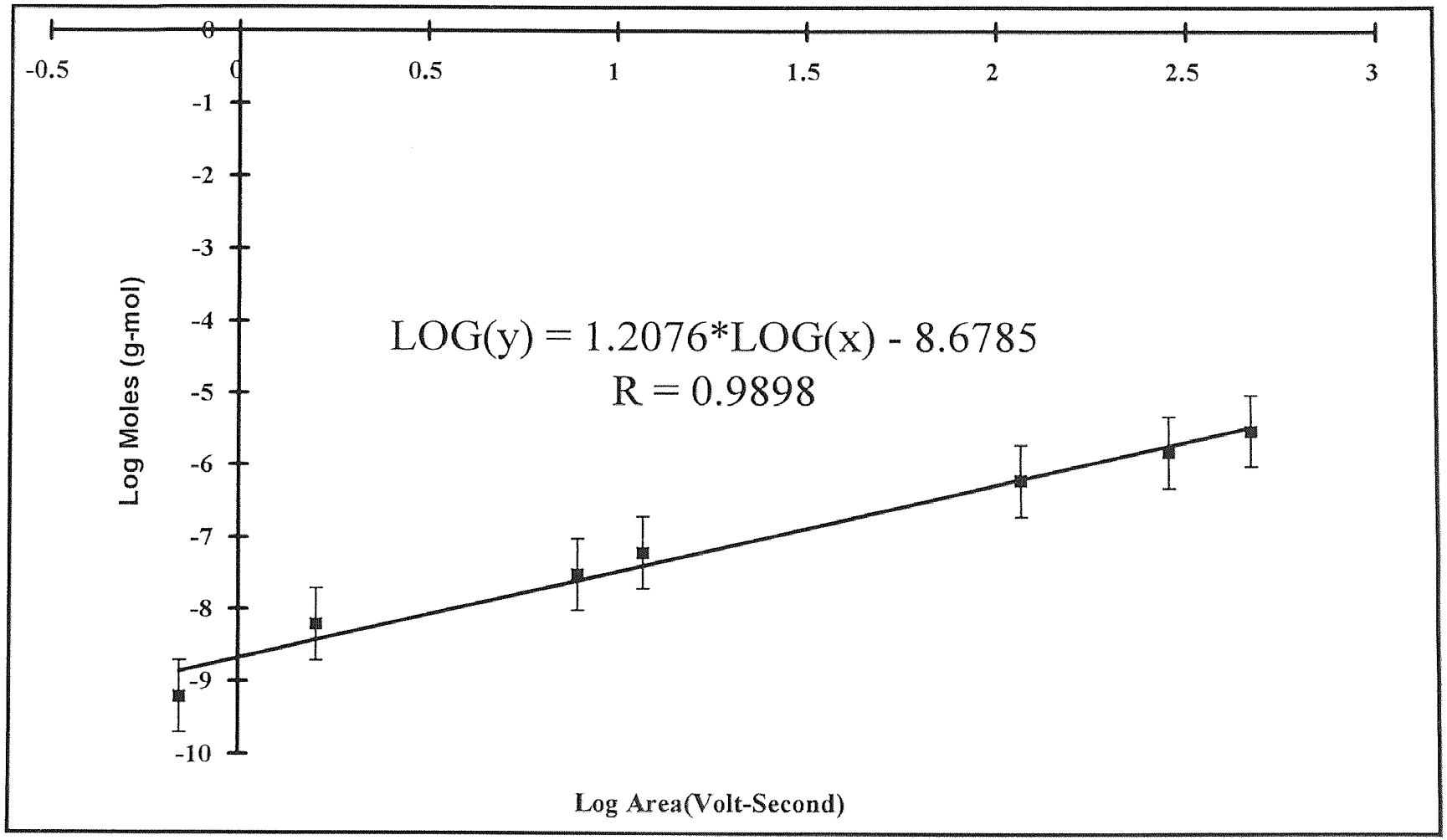

Figure 3.5 Gas Chromatograph Calibration Calibration Line For Ethanol by Using the Trapazoidal Rule

3 inch diameter cylinder with the same perforations as the rotating cylinder which are aligned with one another. Air is fed from the top of cylinder through a 1/4 inch swagelock opening (**See Figure 3.6**). After the siren was assembled, it was calibrated with a Digistrobe, Digital Stroboscope model number 1965 by establishing a known air pressure feed to the motor and measuring the revolutions per minute of the motor. The calibration curve for the siren is shown in **Figure 3.7**.

The siren is operated by aligning the holes with the fracture in the middle of the tank and feeding air of known air pressure and known flow to the siren and the motor. Typical sound levels and corresponding air flow rates and pressures are displayed in **Table 3.1**.

Table 3.1 Siren Performance Characteristics

Siren Characteristics		Operational Parameters				
Outer Diameter (Inches)	**Number of Holes**	**Motor Speed (RPS)**	**Freq. (Hz)**	**Inlet Air Pressure (PSIG)**	**Inlet Air Flow (CFM)**	**Sound Level (db)**
3.0	56	64	3,584	5	1.5	98
3.0	56	120	6,720	10	2.0	102
3.0	56	233	13,048	15	2.5	110
3.0	56	317	17,752	30	3.0	112
3.0	56	233	13,048	50	4.0	122
3.0	56	233	13,048	60	4.5	122
3.0	56	233	13,048	70	5.0	125

3.1.5 Whistle Design

The second sound generator built for the purpose of enhancing the volatilization rate of volatile organic compounds from soil is a Stem Jet Whistle. This whistle was designed and built by Applied Ultrasonics Inc. and purchased by NJIT. It consists of a

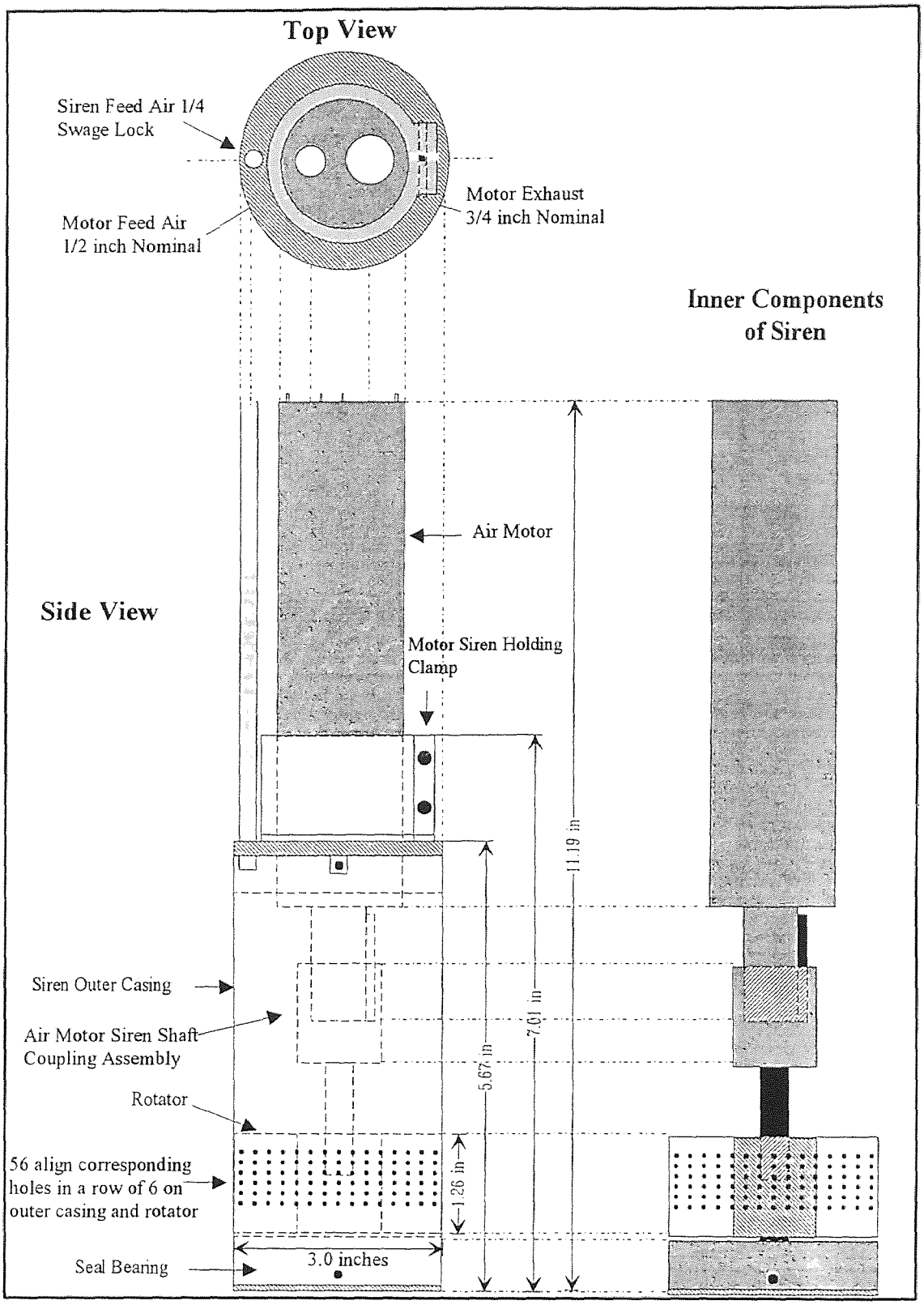

Figure 3.6 NJIT Siren Design

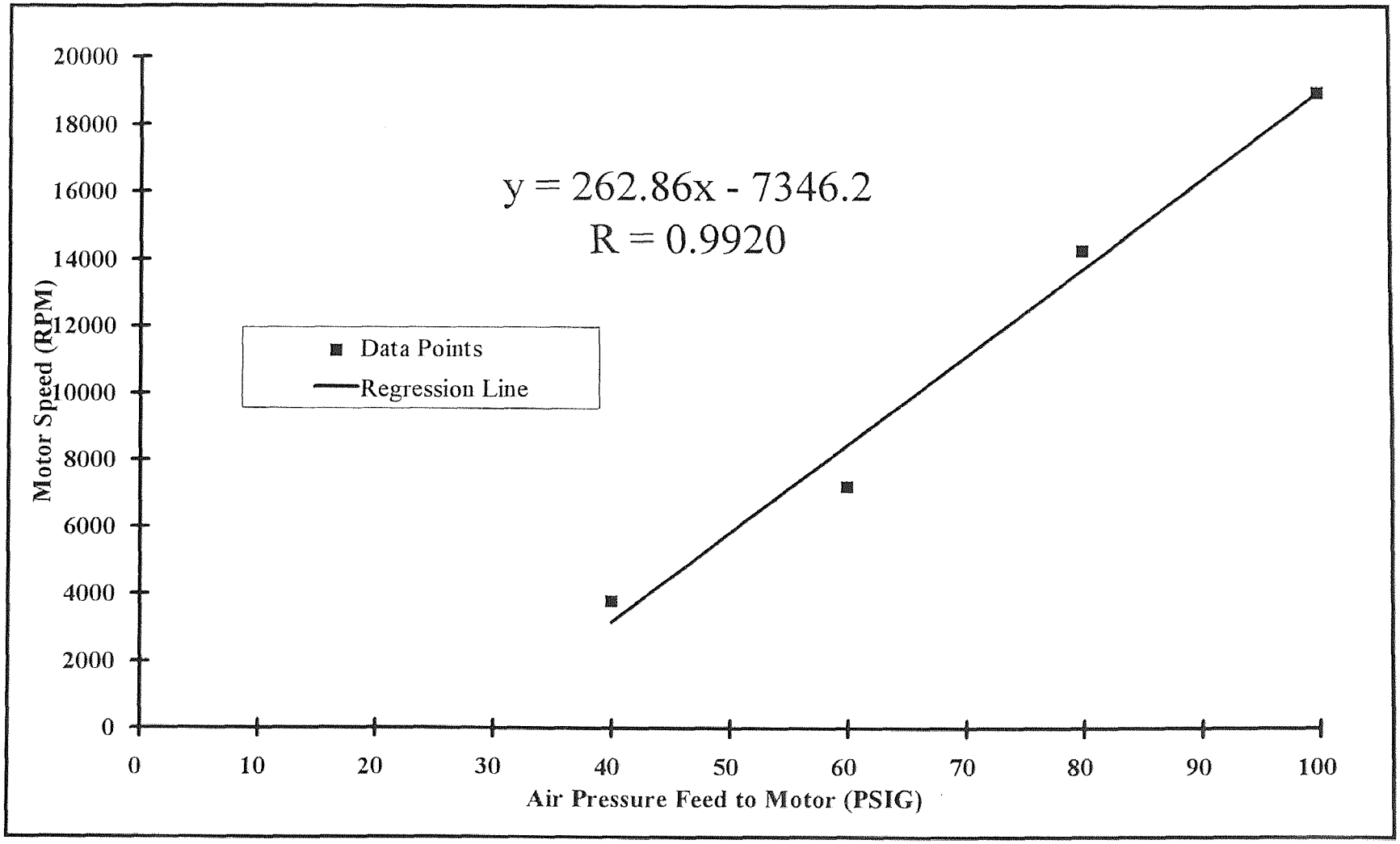

Figure 3.7 Siren Air Motor Calibration Line

converging nozzle which accelerates the gas and impinges this high velocity gas onto a cavity. The result is periodic expulsions of air at supersonic speeds. The amount of gas expelled and the frequency at which the gas is expelled determines the sound power and the frequency respectively. The whistle is approximately three inches in length and is equipped with a converging nozzle (**See Figure 3.8**).

3.2 Experimental Procedure

The experiment was initiated by measuring 1.1 pounds of the contaminant which consisted of a solution of 90 percent by volume ethanol, 5 percent by volume methanol and 5 percent by volume isopropyl alcohol. The small amount of methanol and the isopropyl alcohol in the solution were assumed to be ethanol as well since the peaks overlap each othr when the gas was sample in the gas chromatograph. The measured contaminant was mixed with 10 pounds of water and agitated to ensure proper mixing.

A 400 mesh size sand was purchased from a local construction company. A total of 100 pounds of this 400 mesh sand was measured out and deposited in a pan. This 100 pounds of dry sand was mixed with the ethanol, methanol, isopropanol and water solution. One of the constructed tanks was selected and placed on the electronic scale. This tank was first packed to a height of three inches with the mixed sand. At the three inch level, the sandwiched layer of geotextile material approximately 1/2 inch thick was placed and followed by the extraction pipe and the ultrasonic equipment. The ultrasonic equipment was placed either at a corner of the tank if it was the whistle or in the center of the tank if it was the siren. The thermocouples were then placed at the sound source in the fracture, half way between the extraction pipe and the sound source in the fracture,

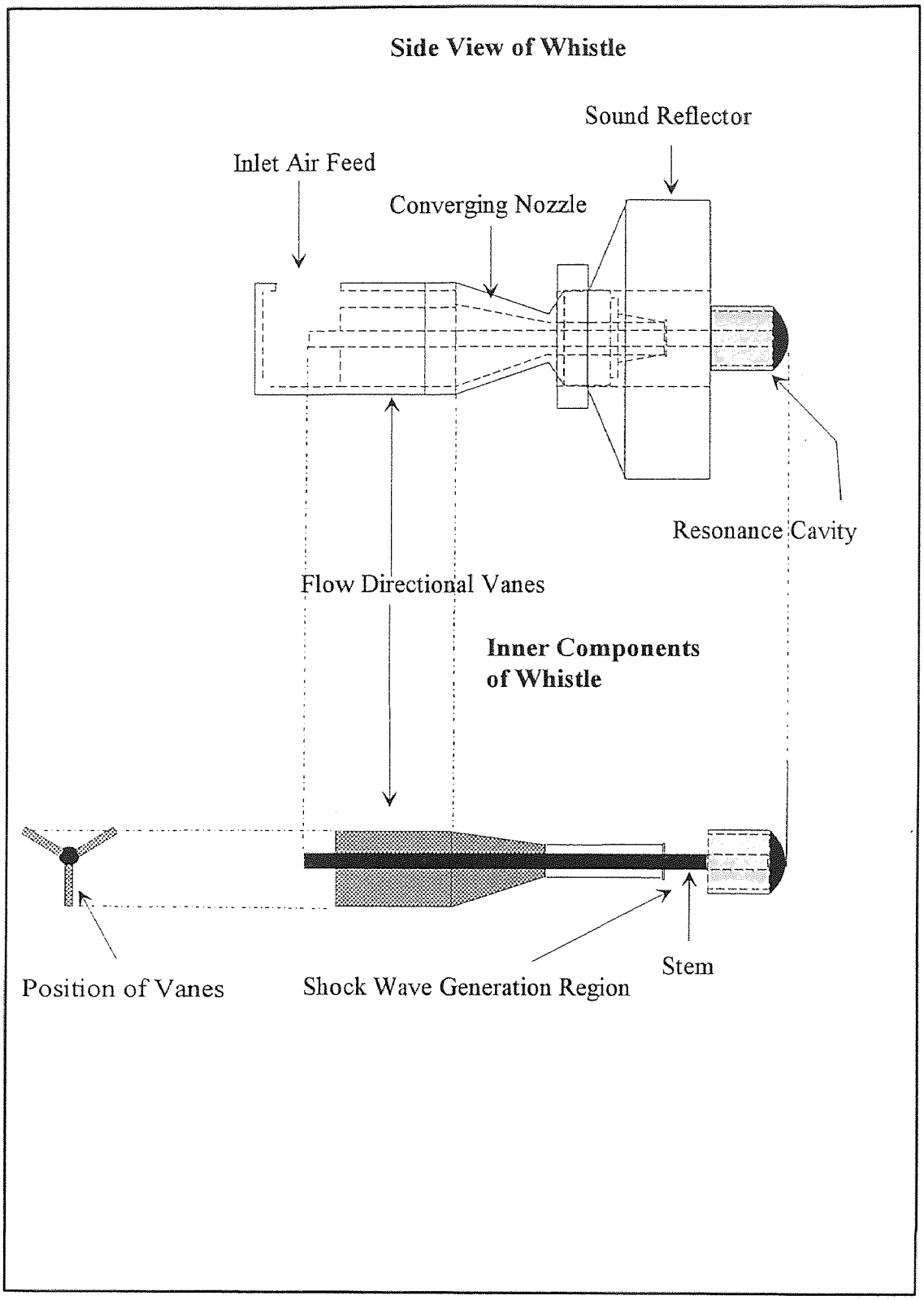

Figure 3.8 Applied Ultrasonic Whistle Design

next to the extraction pipe and inside one of the extraction pipe. Then, the equipment was the covered up with sand.

Following the whistle or siren runs a control run was conducted for comparison with the siren or whistle run. The control run was prepared by aligning with the artificial fracture a 3 inch diameter CPVC pipe with a perforation pattern the same as the siren in the middle of the tank. The thermocouples were then placed at the sound source in the fracture, half way between one of the extraction pipes and the sound source in the fracture, next to that same extraction pipe and inside that same extraction pipe. Then the assembly was covered up with sand just as with the siren run. The whistle control run was prepared by inserting a 3/8 inch elbow in place of the whistle at one corner of the tank aligned with the artificial fracture. The thermocouples were then placed at the sound source in the fracture, half way between the extraction pipe and the sound source in the fracture, next to the extraction pipe and inside the extraction pipe.

The tank was packed in three inch heights which extended to 16 inches from the base of the tank. The approximate packing density was 100 lb. of sand and contaminant per cubic foot of tank. Once the tank was packed and sealed with silicone sealant it was left undisturbed for 72 hours to allow any excess liquid in the sand to migrate to the bottom of tank near the fracture region. Then after 72 hours, the experiment was initiated by setting an inlet airflow of 7.0 standard feet cubic per minute at a pressure of 35 psig to the ultrasonic equipment. The outlet flow rate of contaminant was 12.5 standard feet cube per minute at 90 inches of water. In the first few hours of the experiment some of the liquid was observed blowing out of the tank in two phase flow. This was followed by a period of vapor extraction which lasted for the remainder of the experiment. The

experiments lasted for approximately 40 to 60 hours depending on how quickly the contaminants where removed.

3.2.1 Experimental Procedure Using the Siren

The NJIT Siren's 56 holes in a row of 6 were covered with a 500 mesh stainless steel net to prevent sand particles from penetrating the space between the stator and rotor in the siren. Then, the siren was placed in the center of the test cell with its holes aligned with the 1/2 inch geotextile fracture approximately 3 inches from the bottom of the tank. The air pressure to the siren motor was set at 90 PSIG and the motor speed was approximately 18,000 revolutions per minute. The air fed to the siren was set at 7 standard cubic feet minute at pressures which varried from 35 psig to 50 psig and the outlet air flow rate was measured at 12.5 standard cubic feet minute and 85 inches of water (**See Figure 3.9**). The rotameter calibrations were provided by the manufacturer. Extraction pipes at opposite corners of the tank removed the air and vapors and liquids that were removed from the soil by the pressure gradient. The fluids entered the extraction pipes through 1/8 inch perforations approximately 1/2 inch apart and repeated for 4 inches in the near by fracture zone. The concentration of contaminants was monitored as described in section 3.2 and the weight was monitored by the electronic scale system as described in section 3.2

3.2.2 Experimental Procedure Using the Whistle

The whistle was placed in the test cell approximately 3 inches from the bottom, aligned with the fracture and facing the opposite corner of the tank. At the opposite corner of the tank, near the fracture zone, an extraction pipe with 1/8 inch perforations approximately

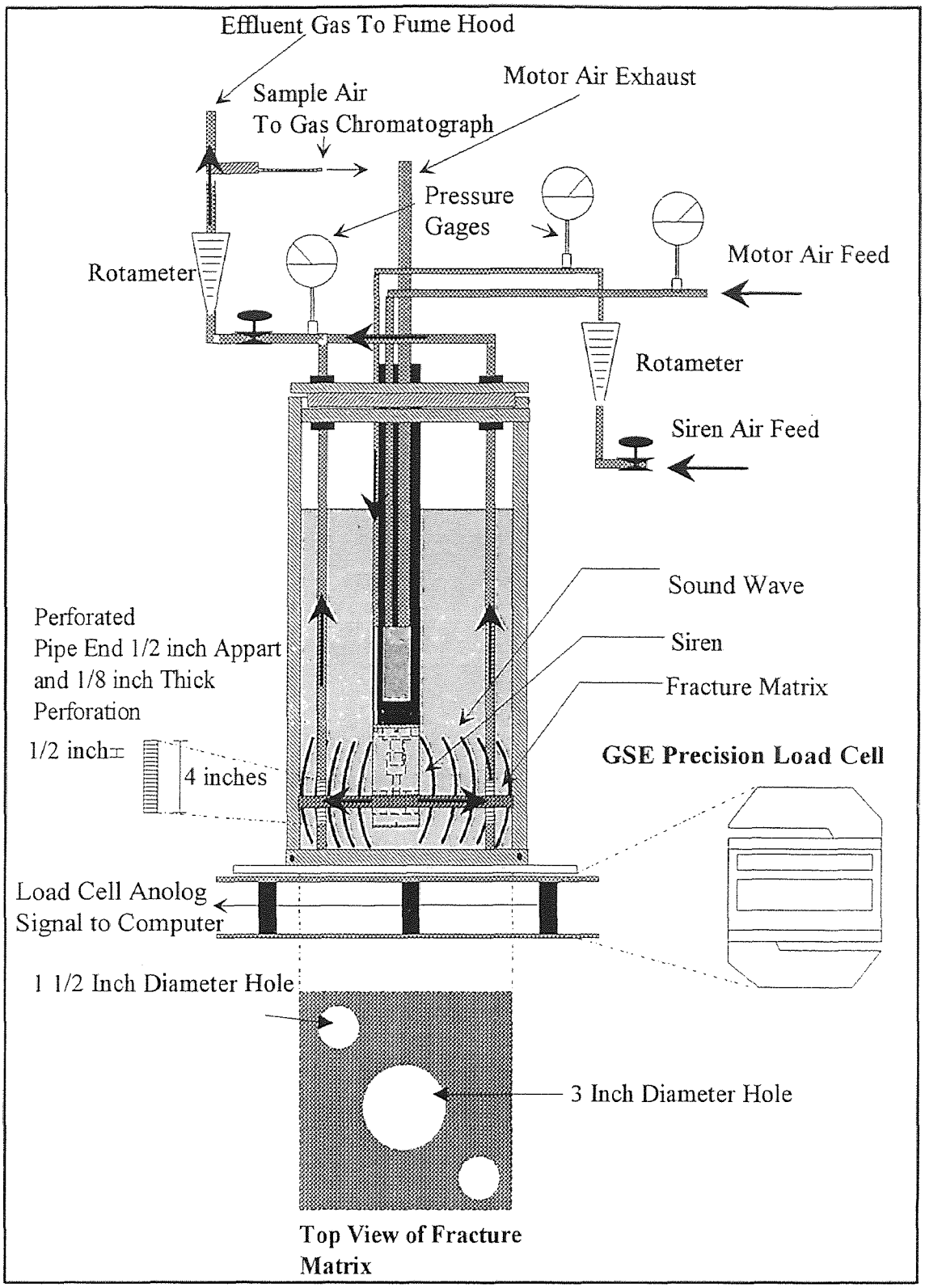

Figure 3.9 Experimental Apparatus for Siren Test

1/2 inch apart and repeated for 4 inches was used to collect the contaminantsbeing carried by the air stream. The whistle was turned on by setting the inlet air flow to approximately at 7 standard cubic feet minute and 35 PSIG. The air entered the whistle and a sound wave of approximately 11 Khz and 160 Decibels was generated (**See Figure 3.10**). The outlet air flow rate was measured at 12.5 standard cubic feet minute and 85 inches of water. The contaminants concentration was monitored as described in Section 3.2 and the weight was monitored by the electronic scale system as described in Section 3.2.

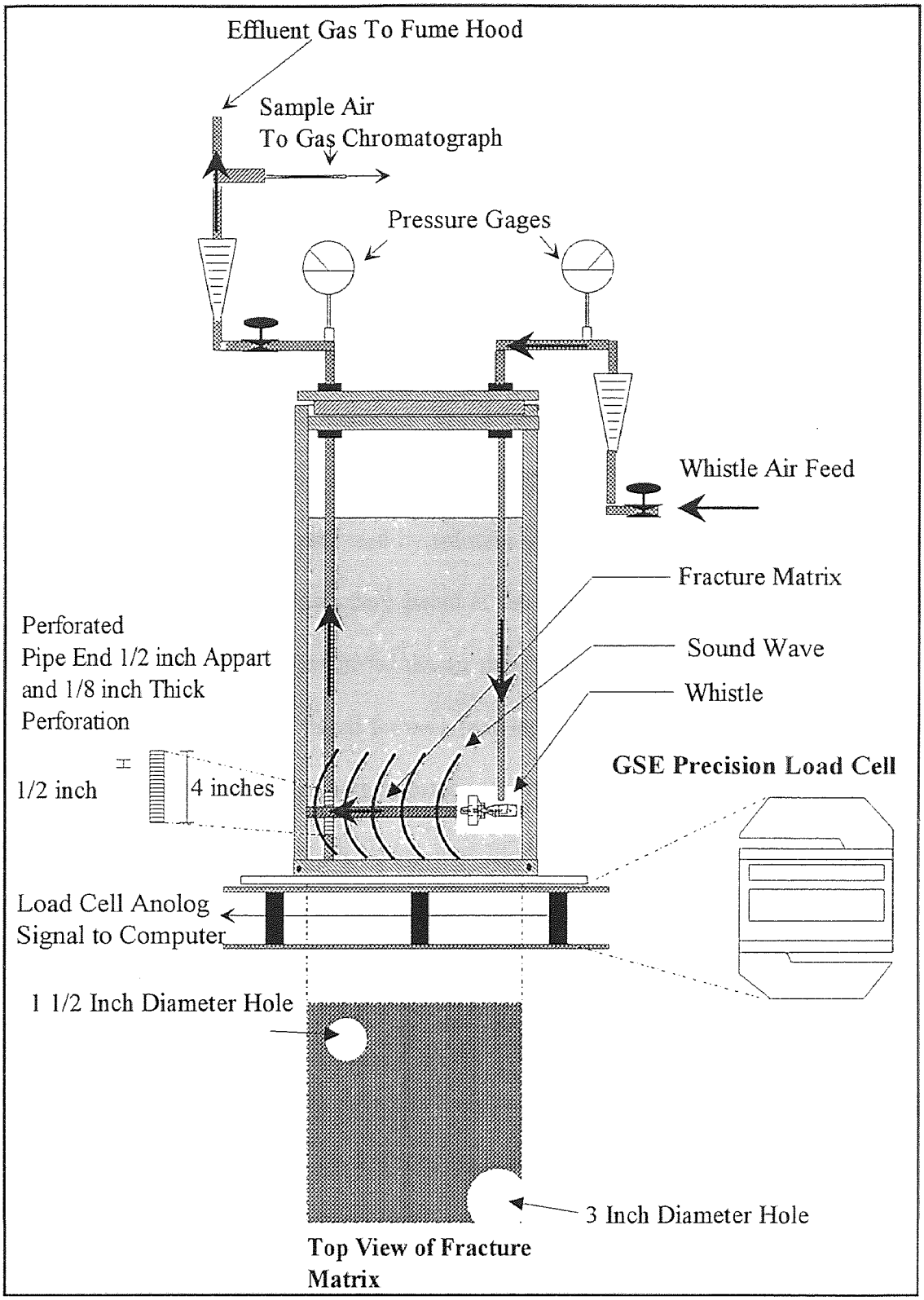

Figure 3.10 Experimental Apparatus for Whistle Test

CHAPTER 4

4. EXPERIMENTAL RESULTS AND DISCUSSION

Experimental test runs were conducted for both the siren and whistle devices. Each set of experiments involved a run with the sonic device as well as a corresponding baseline run. In total, three experimental sets were run for the siren type device and three sets were run for the whistle type device. For each test run, moisture loss from the test cell versus time in hours was recorded. In addition, the concentration of ethanol in parts per million volume (ppmv) in the effluent stream was monitored.

4.1 Data Analysis Method

The experimental data were analyzed by splitting the curves into two regions. The first region was the transient region where liquid in the artificial fracture in the test cell was observed to be physically entrained by the air flow through the fracture region in the test cell. This "blow out" period varied for each individual run but fell in the range of three to ten hours after the experiment was initiated. For this two phase flow region, the data were correlated with a power fit which best fit the data and plotted on a logarithmic coordinates so that the data appeared linear. The slopes for each of the control tests and the test of the corresponding sonic devices were obtained and compared with a Student's t test (Mendenhall and Beaver 1994) in this transient region.

The second region is the falling rate region where all of the contaminants coming out of the test cell (water and ethanol) were removed in the vapor phase (no liquid visible). The data in the falling rate region were fitted using an exponential curve fit which best represented the data and plotted on semi logarithmic coordinates so that it appeared

linear. The slopes for each of the control tests and the test of the corresponding sonic devices were obtained and compared with a student t test in this falling region.

4.2 Results of Tests with the Siren

The test results for test for Set 1 of the siren tests are presented in seven figures. **Figure 4.1** represents the complete data collected by the laboratory scale system for siren test 1 and the corresponding control test or baseline test for free moisture in the test cell versus time. The data in **Figure 4.1** were then averaged in five minute intervals and the average was plotted in **Figure 4.2**. **Figure 4.2** is plotted on semi logarithmic coordinates and represents the five minute average of free moisture in the test cell versus the five minute average time in **Figure 4.1**. **Figure 4.2** was then divided into two graphs, **Figure 4.3** and **Figure 4.4**. **Figure 4.3** is the transient behavior of free moisture in the tank versus time with its corresponding control test. The data in **Figure 4.3** were plotted on logarithmic coordinates and correlated with a logarithmic curve fit. The corresponding correlation coefficients are shown. The transient region in **Figure 4.3** is shown and correlated well with a logarithmic fit between the time range of 0.05 hours to 10.0 hours for both the control test 1 and the siren test 1 in the transient region.

Figure 4.4 represents the falling rate region of siren test 1 and the control test 1 where the free moisture versus time is correlated with an exponential fit on semi logarithmic coordinates. The correlation equations and the correlation coefficients are shown in **Figure 4.4**. **Figure 4.5** represents the concentration of ethanol obtained for

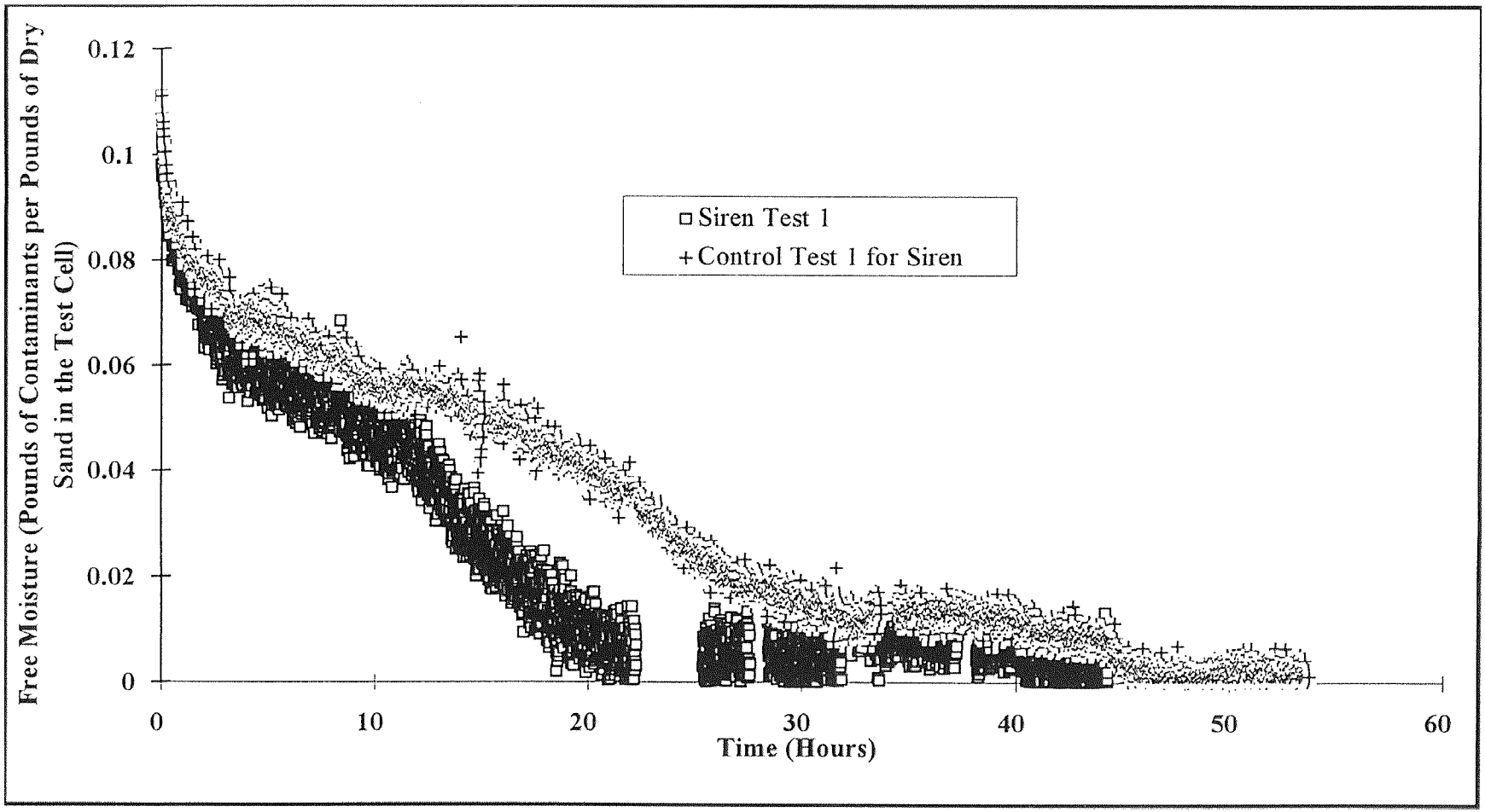

Figure 4.1 Measured Data of Free Moisture Versus Time for Siren Set 1

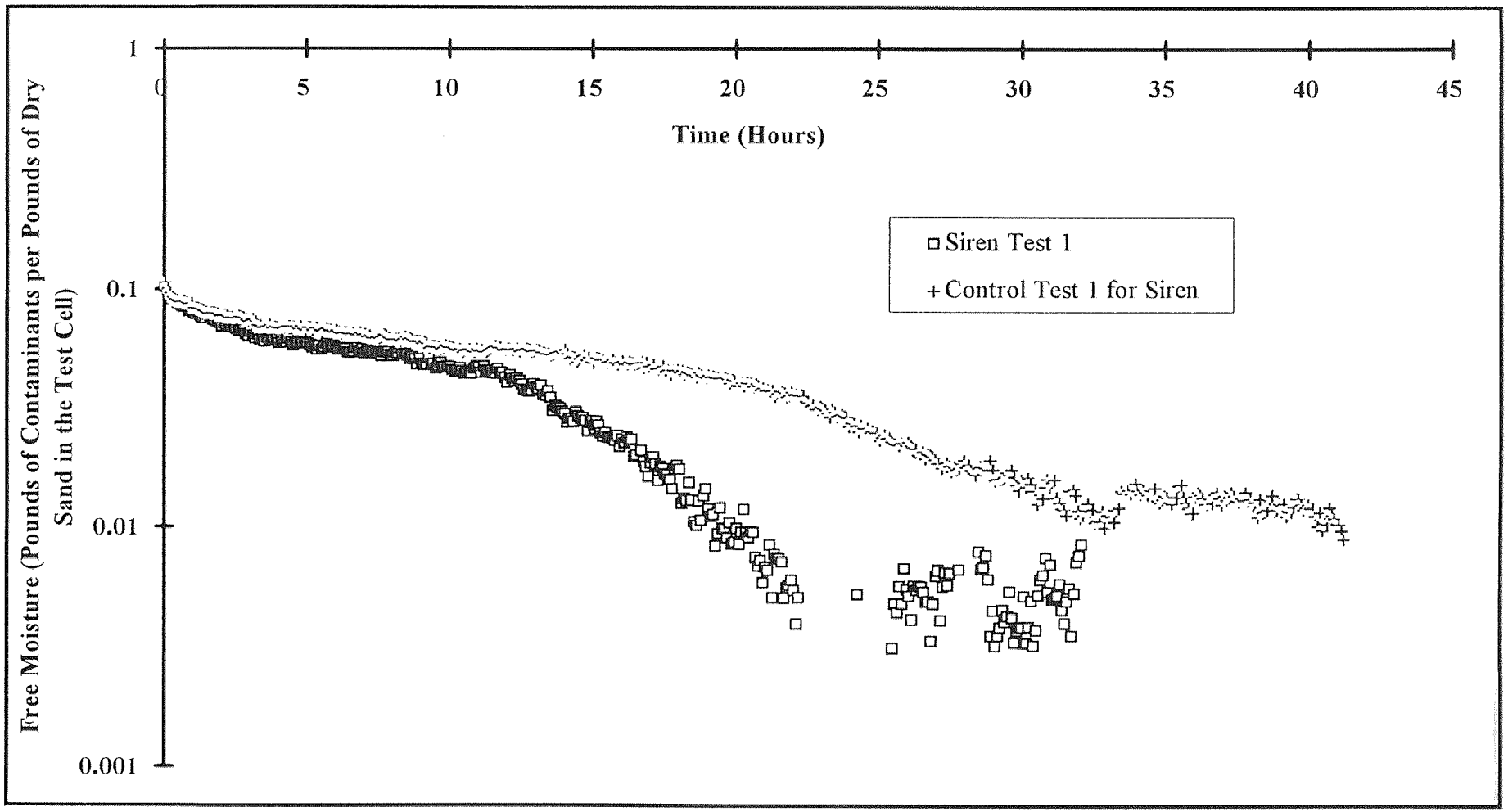

Figure 4.2 Average Semi Logarithmic Plot of Free Moisture Versus Time for Siren Set 1

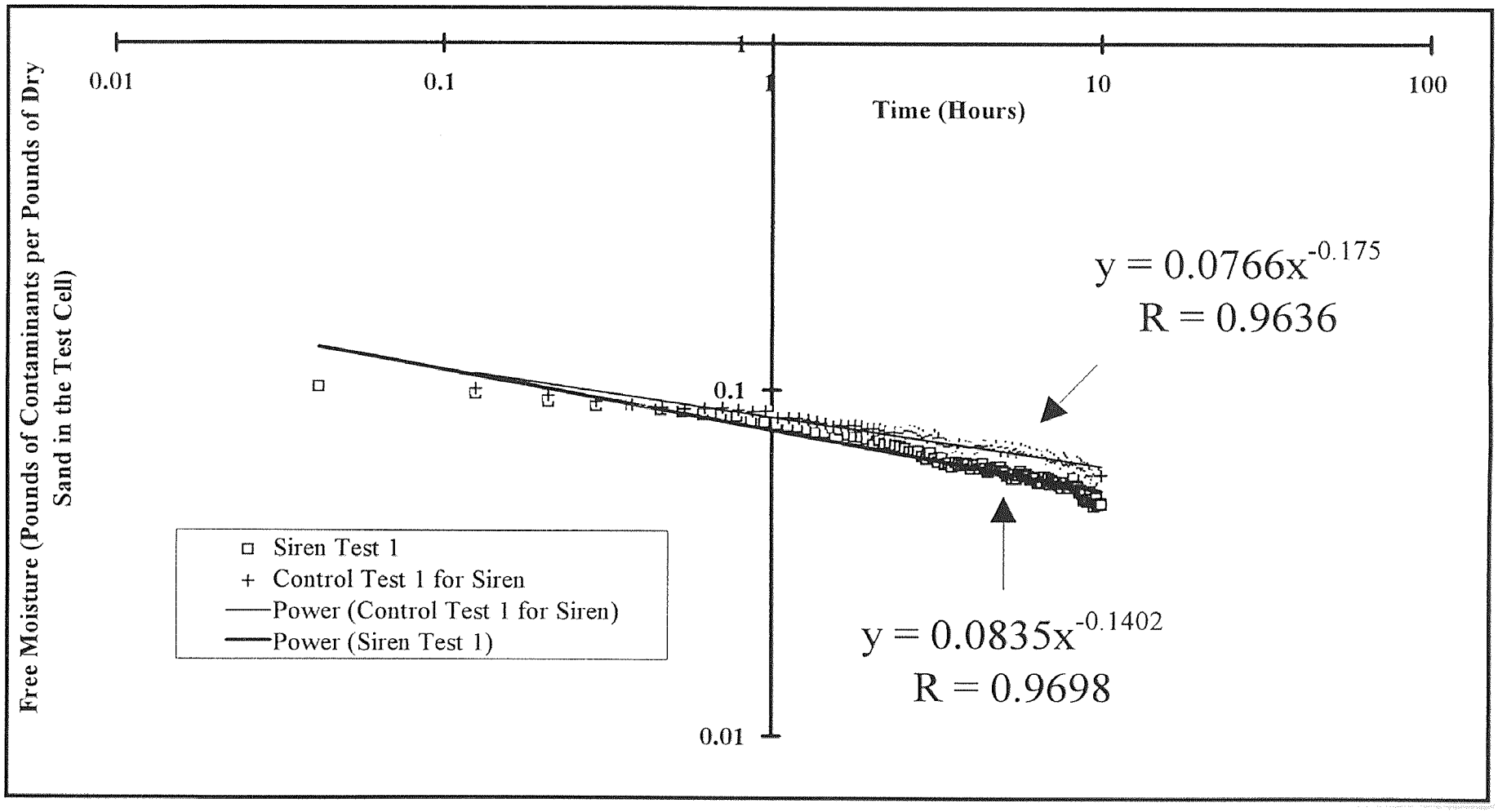

Figure 4.3 Average Logarithmic Curve Fit of Free Moisture Versus Time for Siren Set 1 in the Transient Region

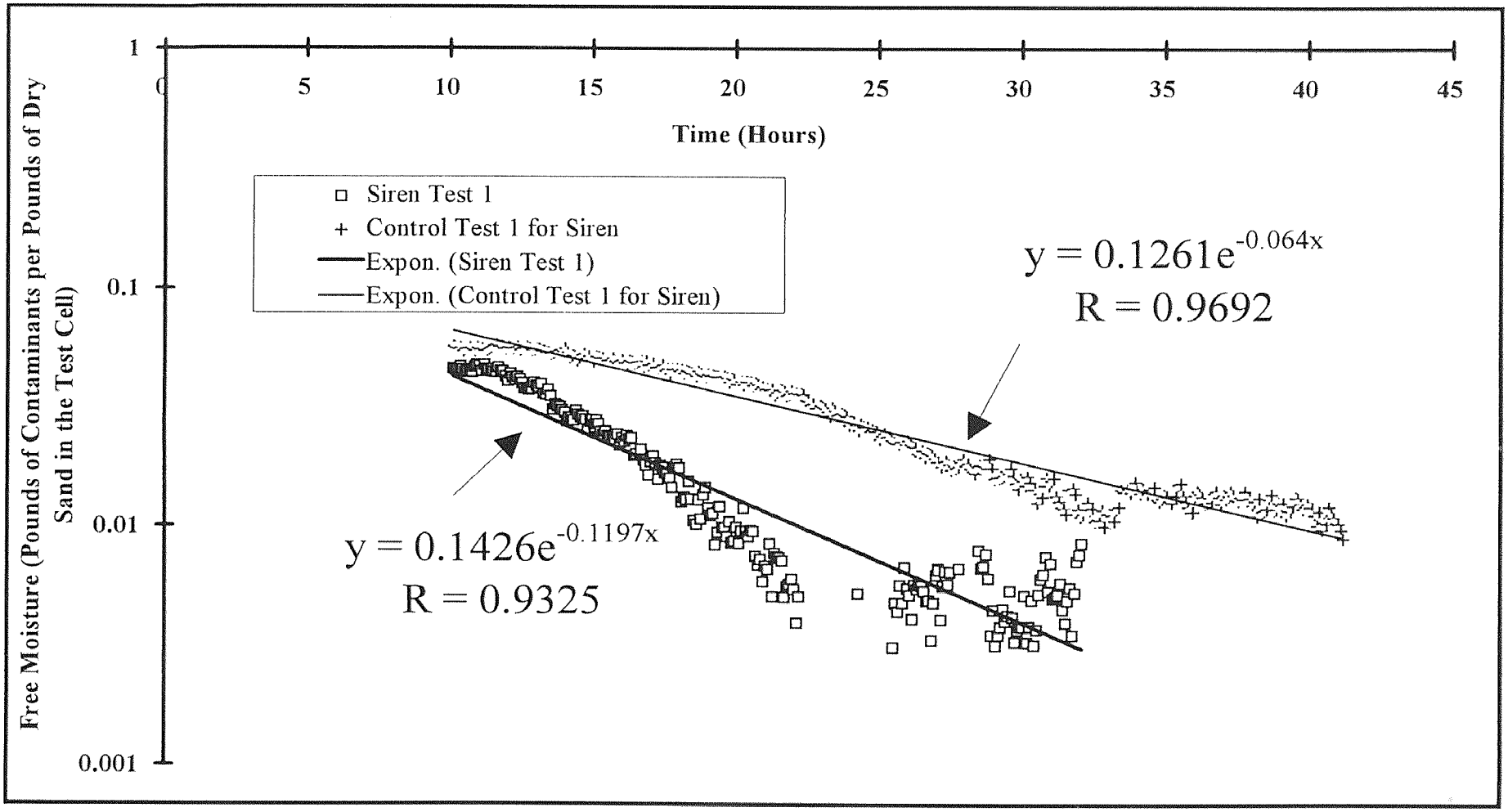

Figure 4.4 Average Semi Logarithmic Curve Fit of Free Moisture Versus Time for Siren Set 1 in the Falling Rate Region

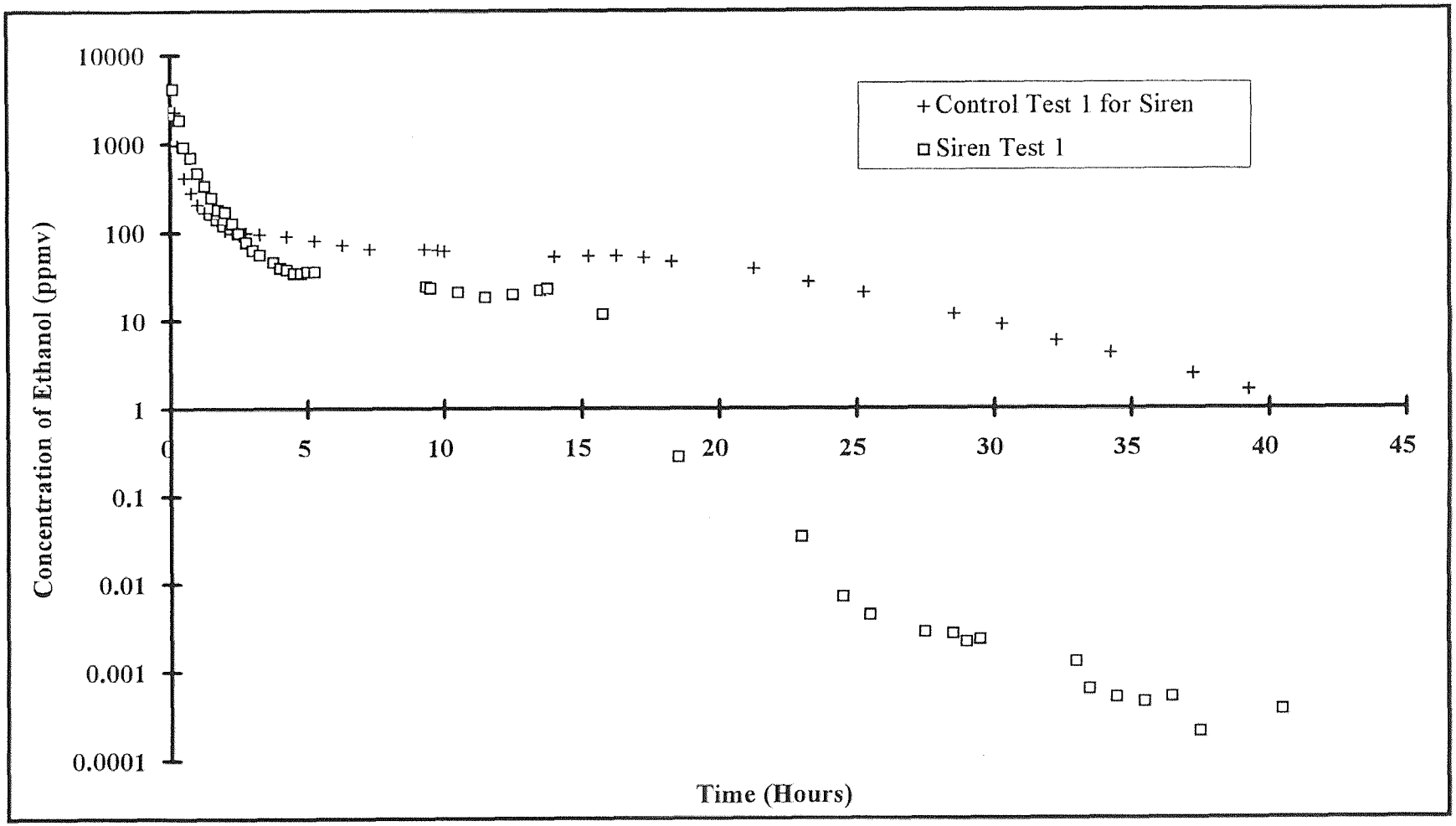

Figure 4.5 Semi Logarithmic Plot of Concentration Versus Time for Siren Set 1

siren test 1 and control test 1 versus time. The data are once again broken into two regions, the transient region and the falling rate region (**Figure 4.6** and **Figure 4.7** respectively) and these two regions are correlated on logarithmic coordinates and a semi logarithmic coordinates respectively. The correlated equations and the correlation coefficients are shown in **Figures 4.6** and **4.7**.

Analysis of the siren set 2 data was performed similarly to the set 1 siren data. **Figure 4.8** represents the complete data collected by the laboratory scale system for the siren test 2 and the corresponding control test or baseline test for free moisture in the test cell versus time. The data in **Figure 4.8** were averaged in five minute intervals and the average was plotted in **Figure 4.9**. **Figure 4.9** is plotted in semi logarithmic coordinates and it represents the five minute average of free moisture in the test cell versus the five minute average time in **Figure 4.8**. **Figure 4.9** was divided into two graphs, **Figure 4.10** and **Figure 4.11**. **Figure 4.10** is the transient behavior of free moisture in the tank versus time with its corresponding control test. The data in **Figure 4.10** were plotted in logarithmic coordinates and correlated with a logarithmic curve fit. The transient region in **Figure 4.10** is shown and correlated well by a logarithmic curve fit between the time range of .05 hours to 10 hours for both the control test 2 and the siren test 2 in the transient region. **Figure 4.11** represents the falling rate region of siren test 2 and the control test 2 where the free moisture versus time is correlated with an exponential fit on semi logarithmic coordinates for both tests (siren test 2 and control test 2). The correlation equations as well as the correlation coefficients are shown in **Figure 4.11**. **Figures 4.12** represents the concentration of ethanol obtained for siren test 2 and

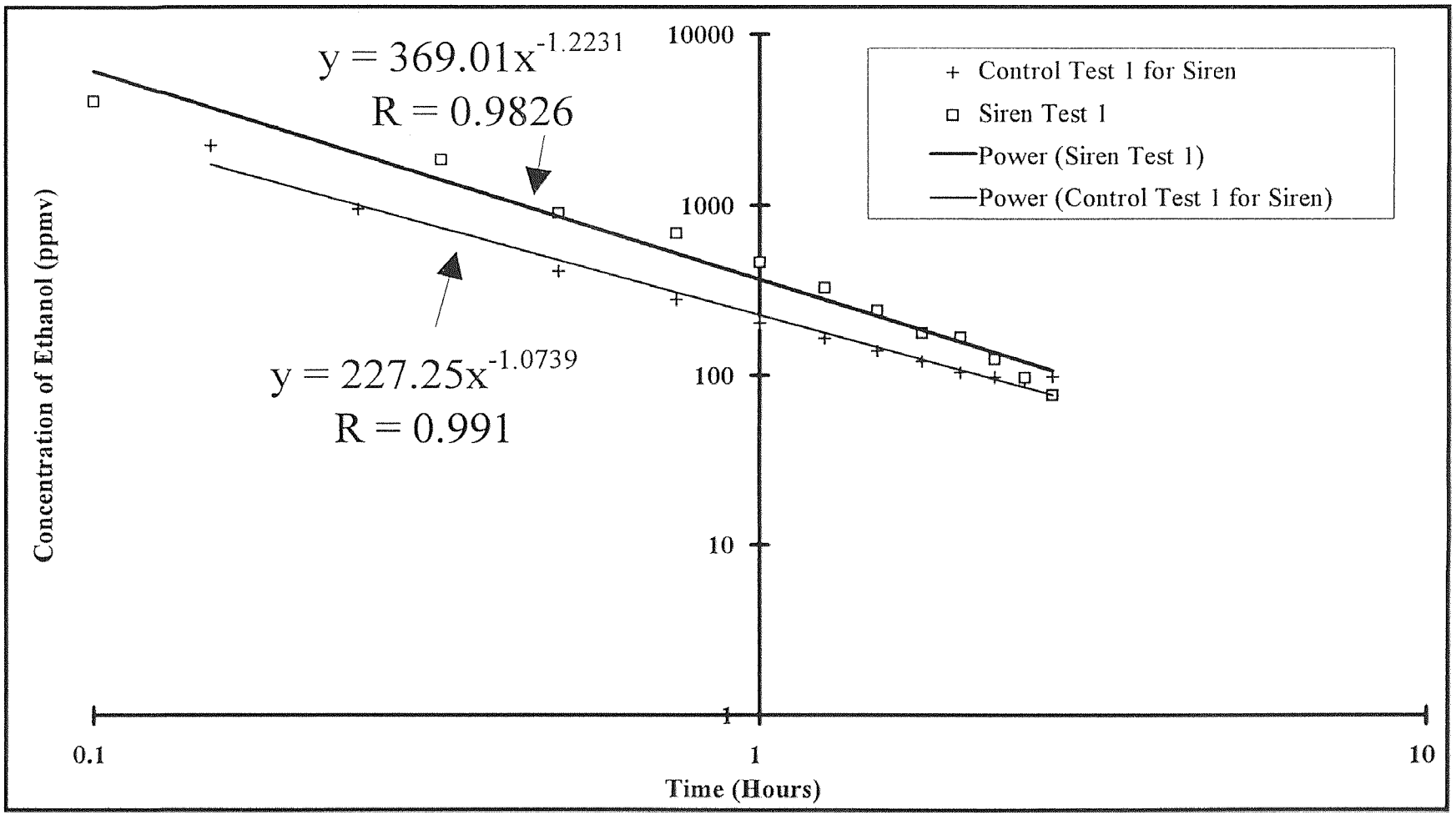

Figure 4.6 Logarithmic Curve Fit of Concentration Versus Time for Siren Set 1 in the Transient Region

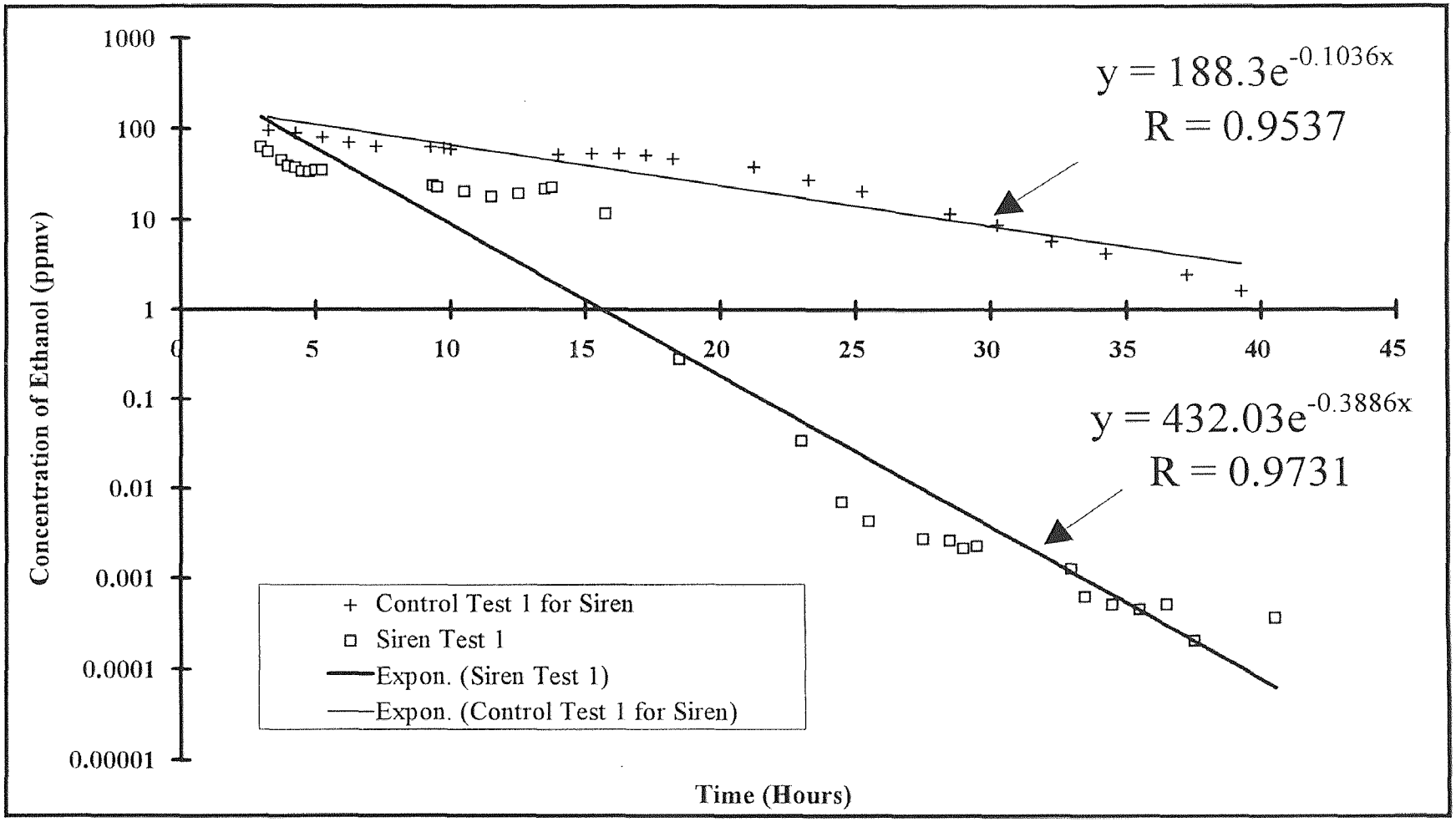

Figure 4.7 Semi Logarithmic Curve Fit of Concentration Versus Time for Siren Set 1 in the Falling Rate Region

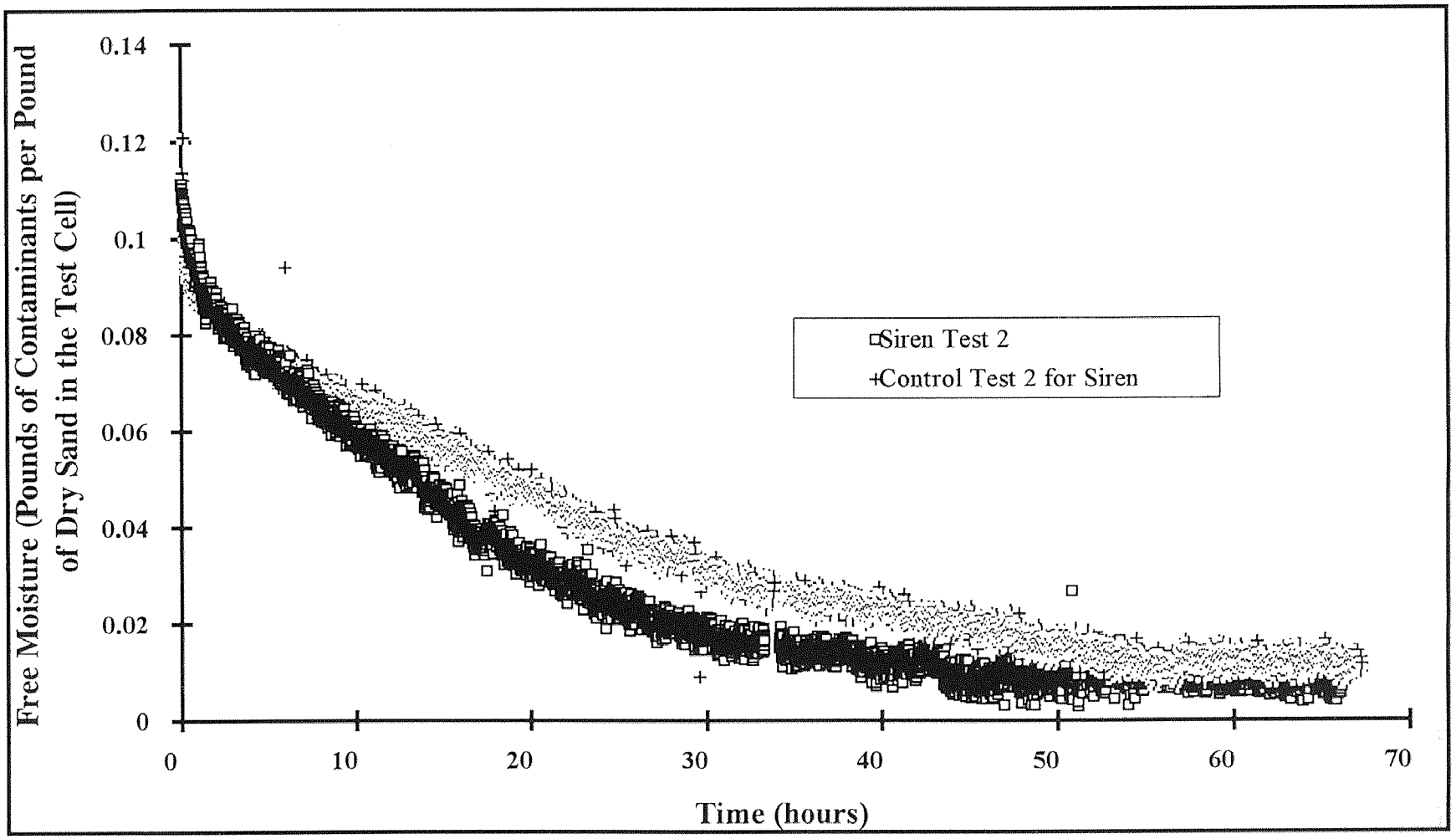

Figure 4.8 Measured Data of Free Moisture Versus Time for Siren Set 2

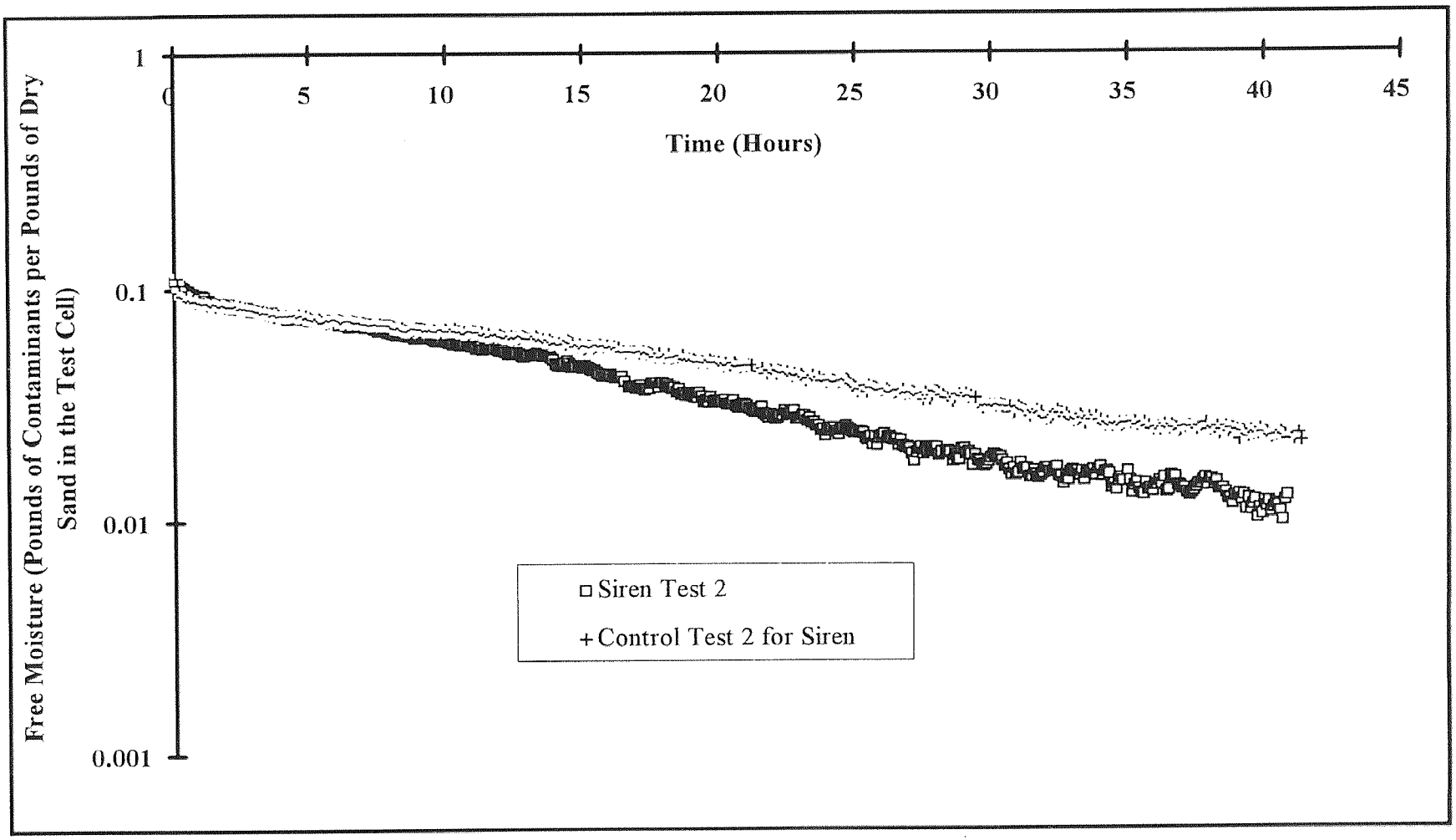

Figure 4.9 Average Semi Logarithmic Plot of Free Moisture Versus Time for Siren Set 2

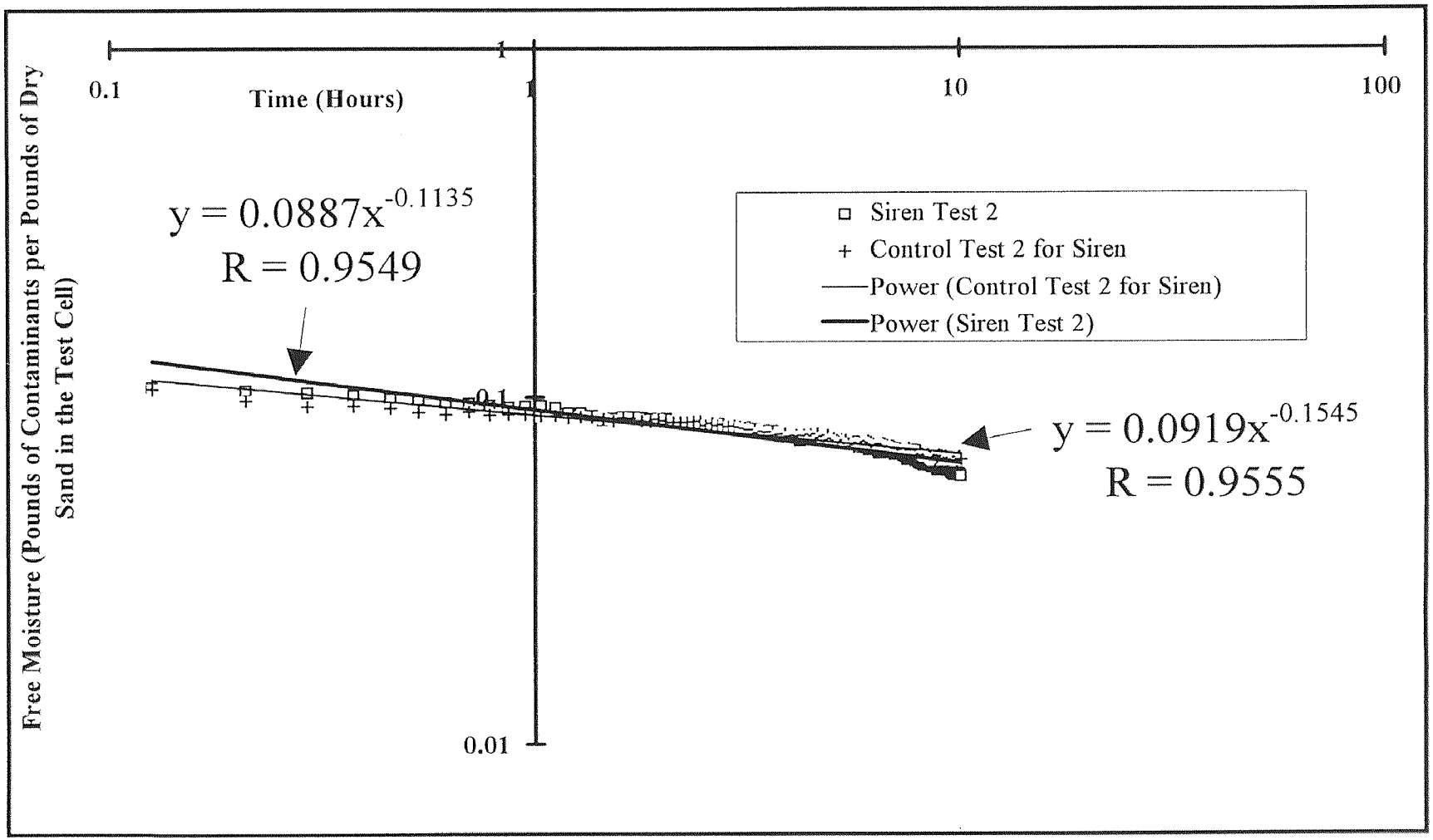

Figure 4.10 Average Logarithmic Curve Fit of Free Moisture Versus Time for Siren Set 2 in the Transient Region

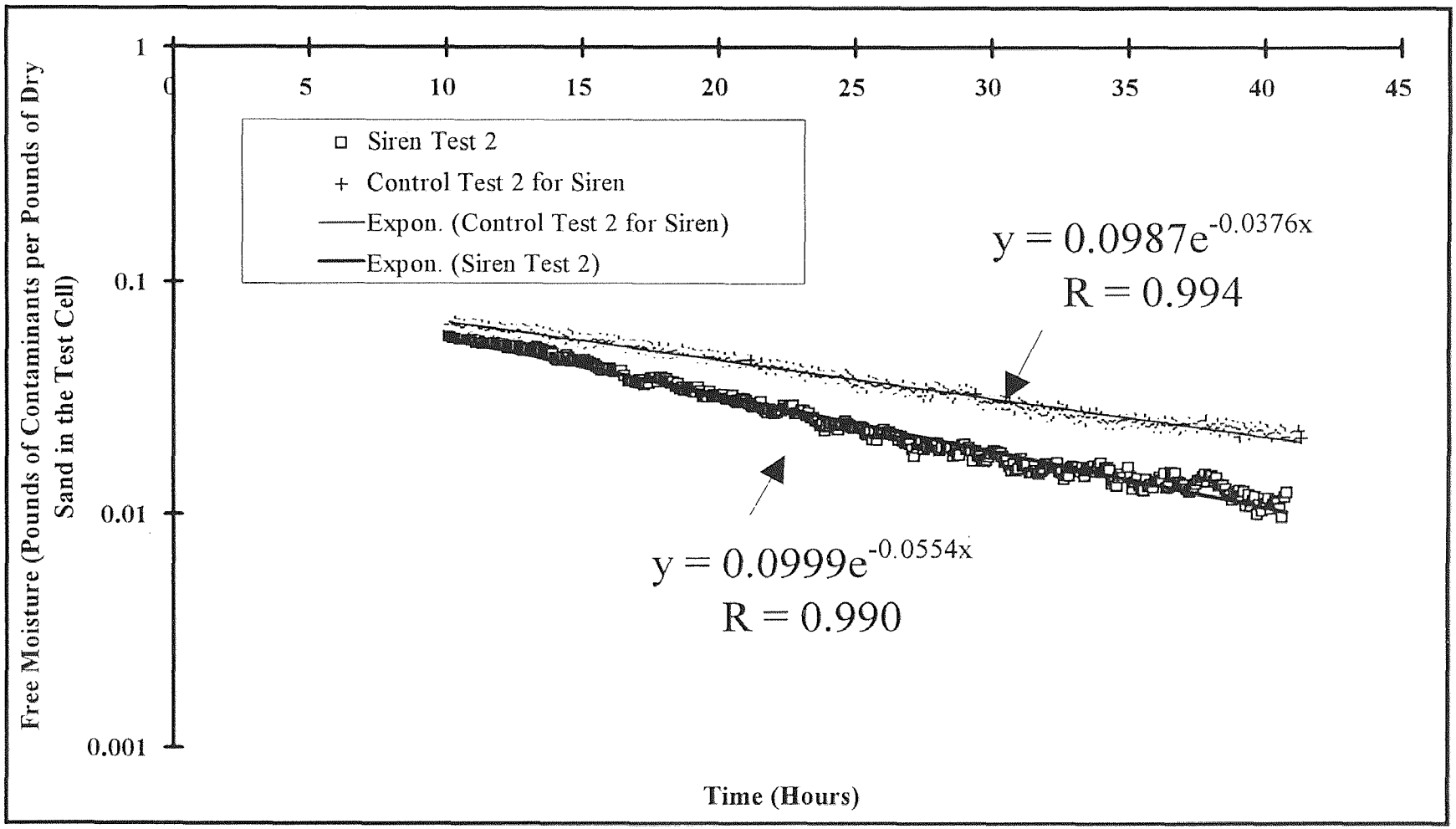

Figure 4.11 Average Semi Logarithmic Curve Fit of Free Moisture Versus Time for Siren Set 2 in the Falling Rate Region

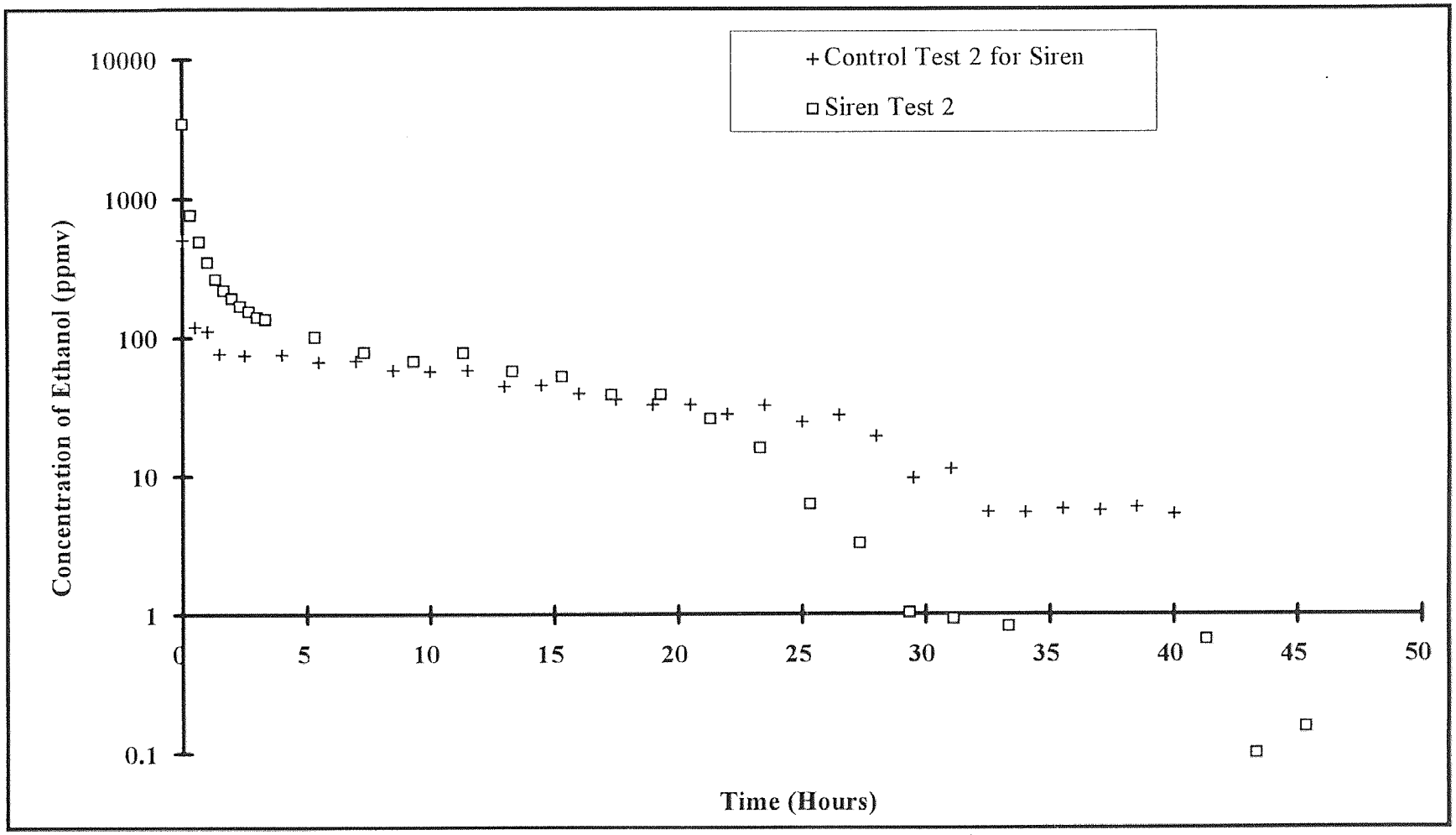

Figure 4.12 Semi Logarithmic Plot of Concentration Versus Time for Siren Set 2

control test 2 versus time. The data are once again divided into two regions, the transient region and the falling rate region (**Figure 4.13** and **Figure 4.14** respectively) and these two regions are correlated on logarithmic coordinates and a semi logarithmic coordinates respectively. The correlation equations as well as the correlation coefficients are **Figures 4.13** and **4.14**.

Set 3 of the siren test was also divided into seven graphs. **Figure 4.15** represents the complete data collected on the laboratory scale system for the siren test 3 and the corresponding control test or baseline test for free moisture in the test cell versus time. The data in **Figure 4.15** were averaged in five minute intervals and the average was plotted in **Figure 4.16**. **Figure 4.16** is plotted on semi logarithmic coordinates and represents the five minute average of free moisture in the test cell versus the five minute average time in **Figure 4.15**. **Figure 4.16** was divided into two graphs, **Figure 4.17** and **Figure 4.18**. **Figure 4.17** is the transient behavior of free moisture in the tank versus time with its corresponding control test. The data in **Figure 4.17** were plotted on logarithmic coordinates and correlated with a logarithmic curve fit. The transient region in **Figure 4.17** is shown and correlated well by a logarithmic curve fit between the time range of .05 hours to 10 hours for both the control test 3 and the siren test 3 in the transient region. **Figure 4.18** represents the falling rate region of siren test 3 and the Control Test 3 where the free moisture versus time is correlated with an exponential curve in semi logarithmic coordinates for both tests (siren test 3 and control test 3). The correlation and the correlation coefficients are shown in **Figure 4.18**. **Figures 4.19** represents the concentration of ethanol obtained for siren test 3 and control test 3 versus

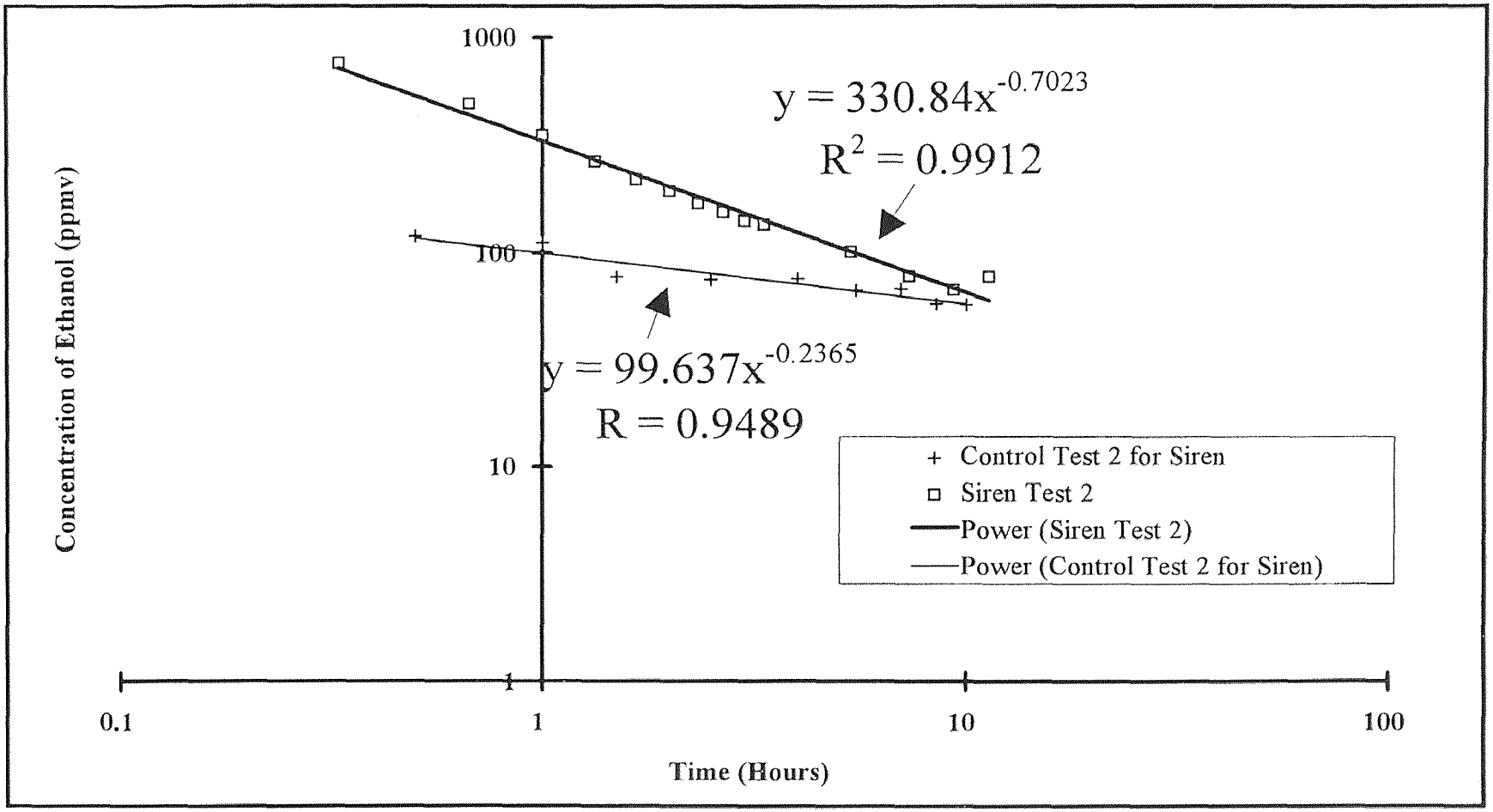

Figure 4.13 Logarithmic Curve Fit of Concentration Versus Time for Siren Set 2 in the Transient Region

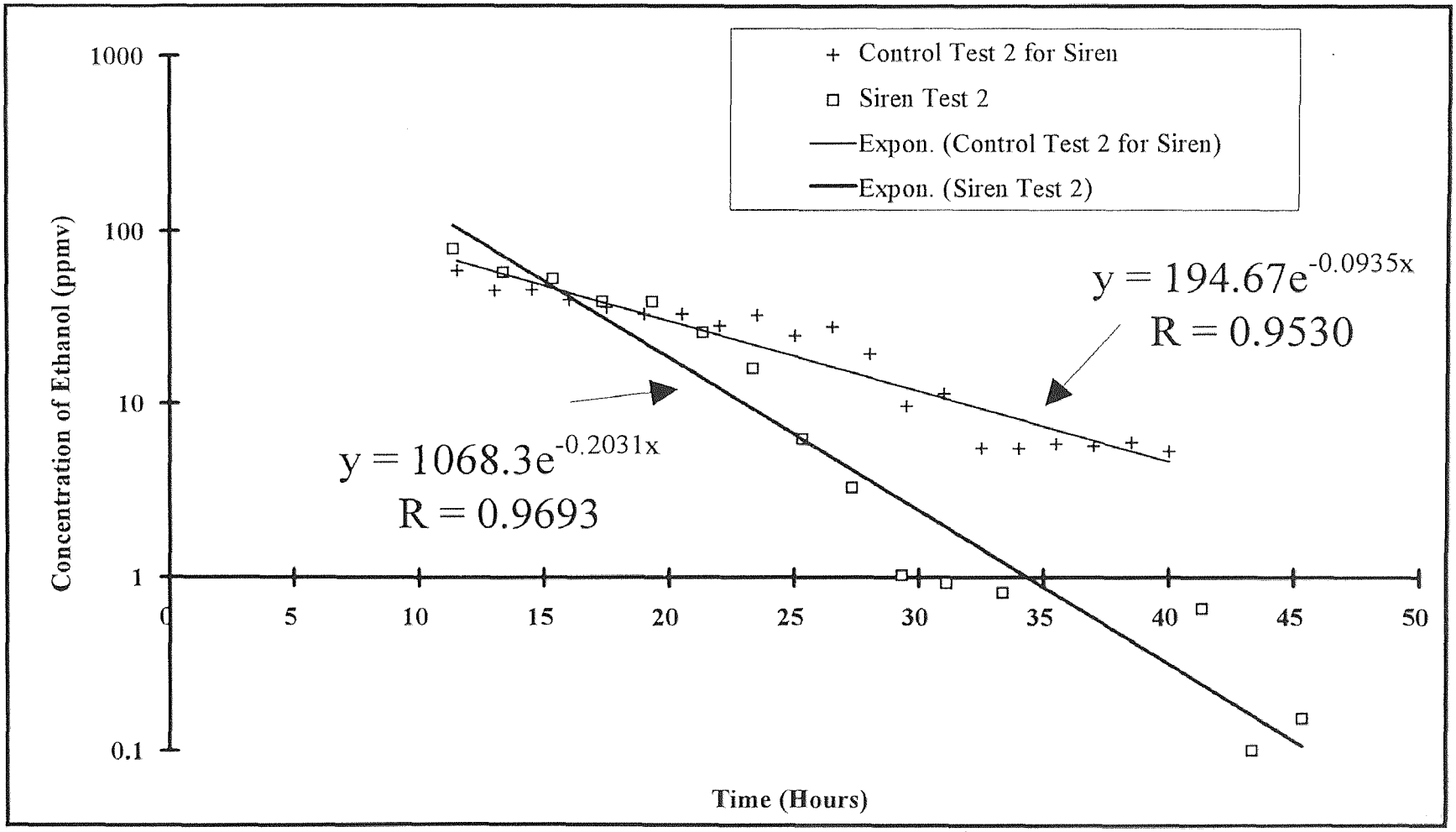

Figure 4.14 Semi Logarithmic Curve Fit of Concentration Versus Time for Siren Set 2 in the Falling Rate Region

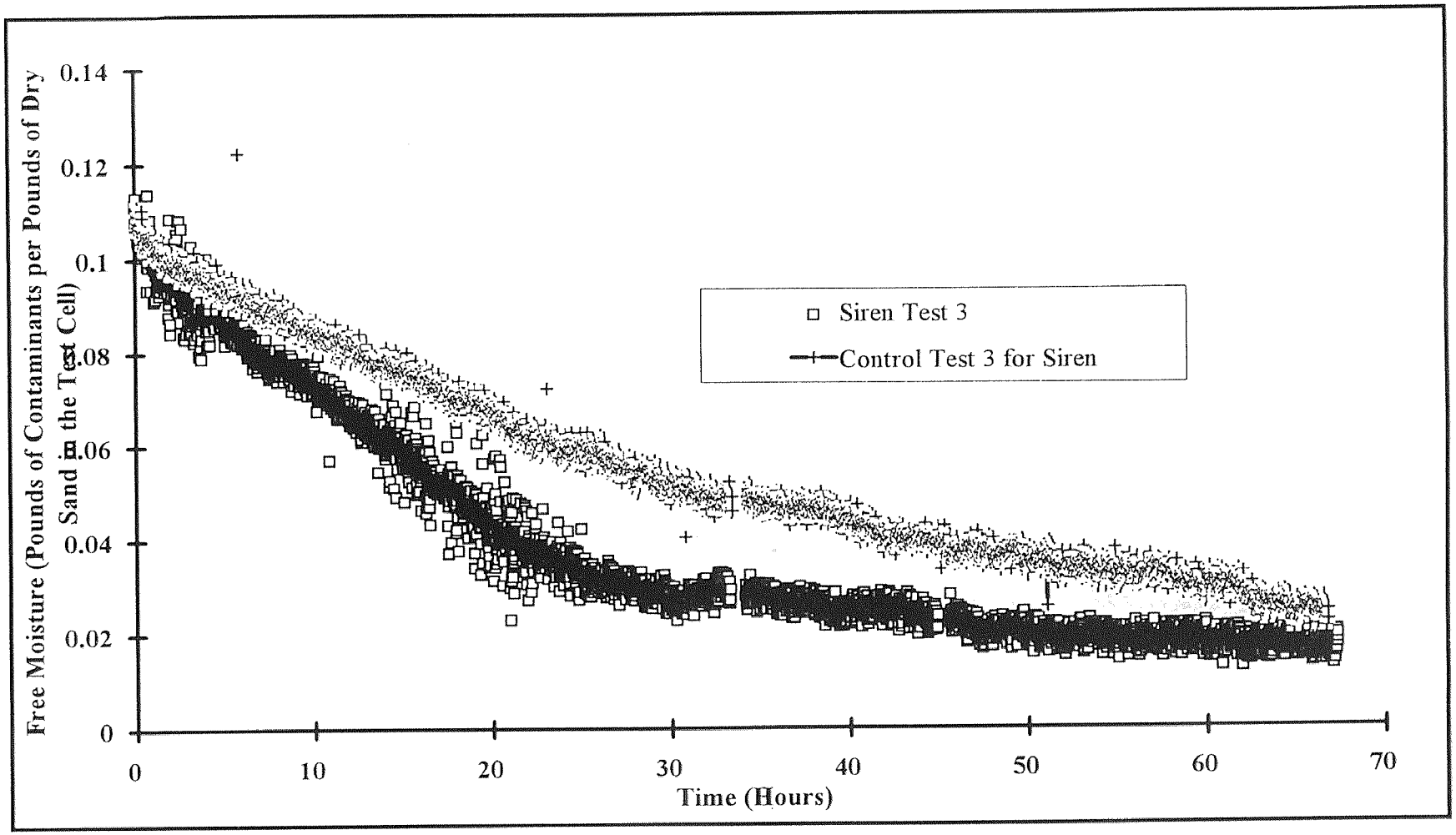

Figure 4.15 Measured Data of Free Moisture Versus Time for Siren Set 3

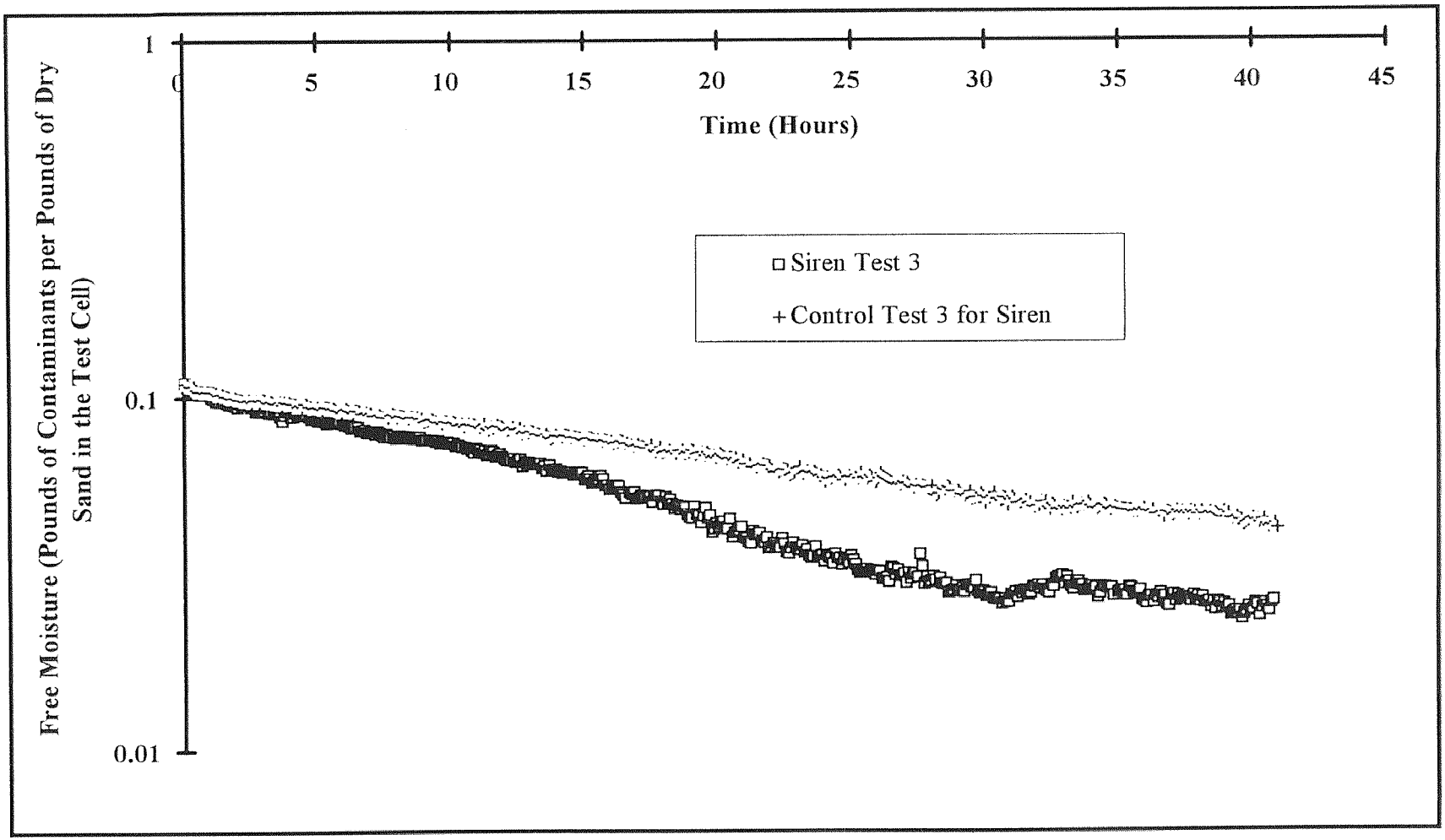

Figure 4.16 Average Semi Logarithmic Plot of Free Moisture Versus Time for Siren Set 3

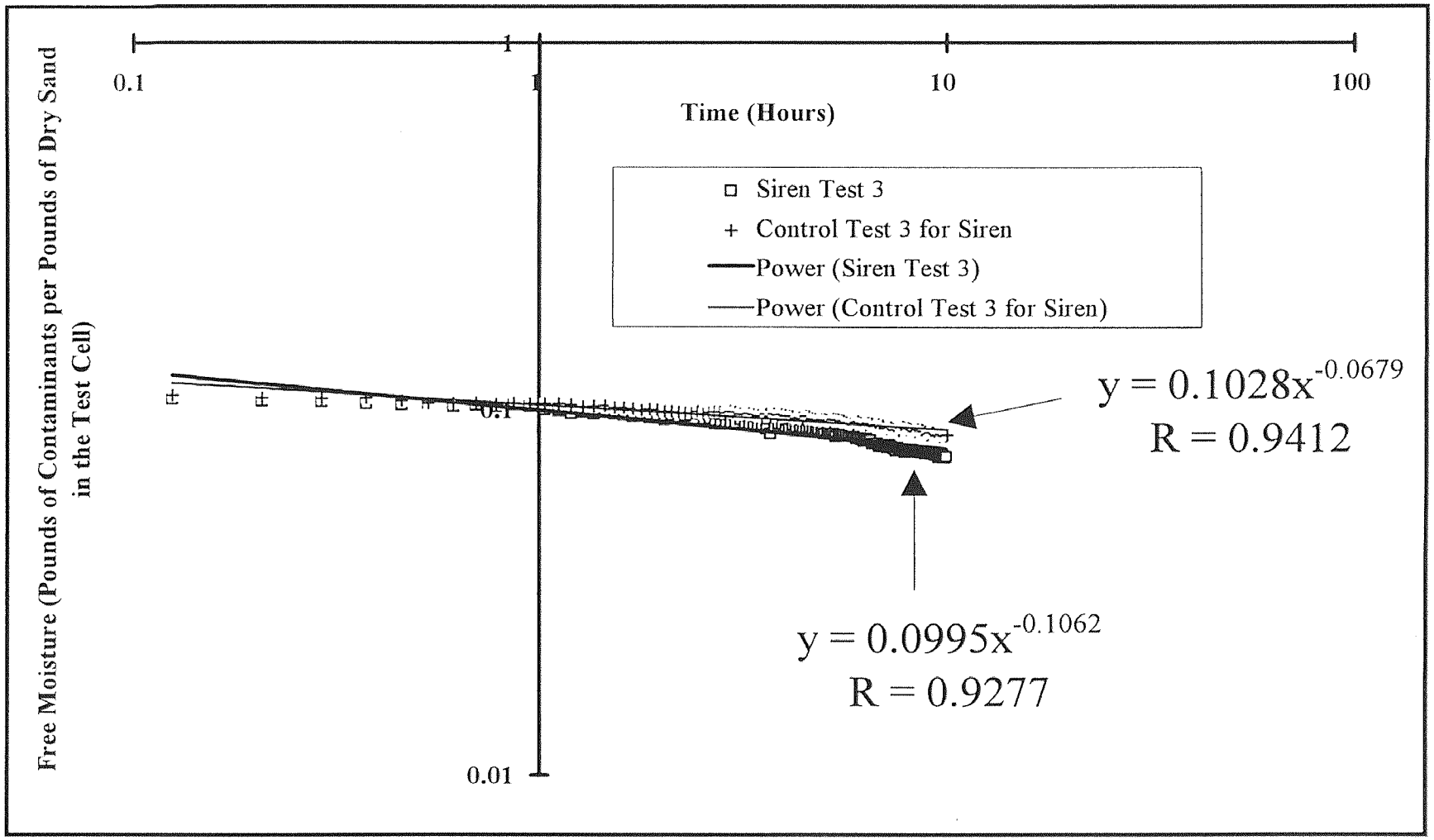

Figure 4.17 Average Logarithmic Curve Fit of Free Moisture Versus Time for Siren Set 3 in the Transient Region

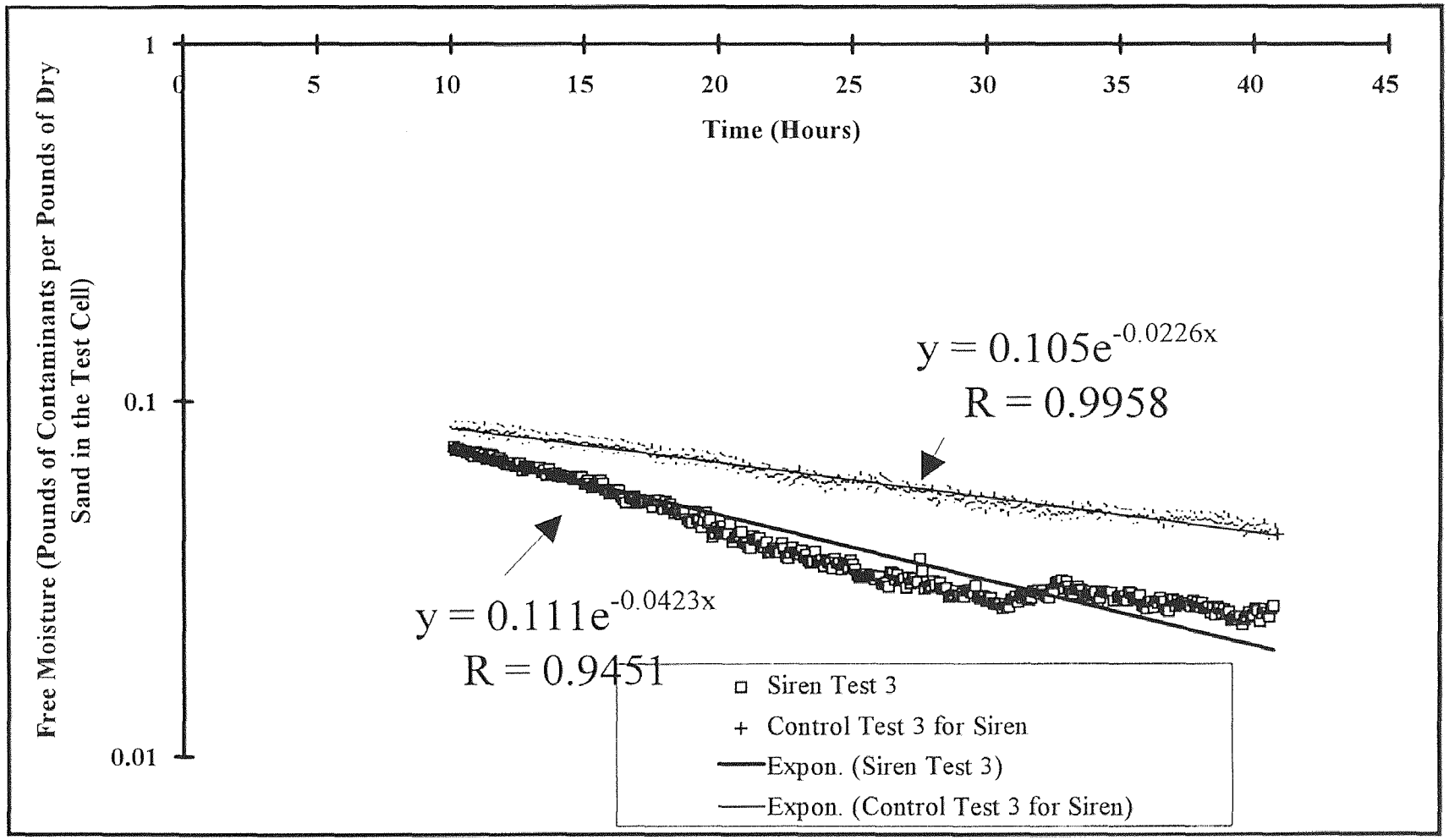

Figure 4.18 Average Semi Logarithmic Curve Fit of Free Moisture Versus Time for Siren Set 3 in the Falling Rate Region

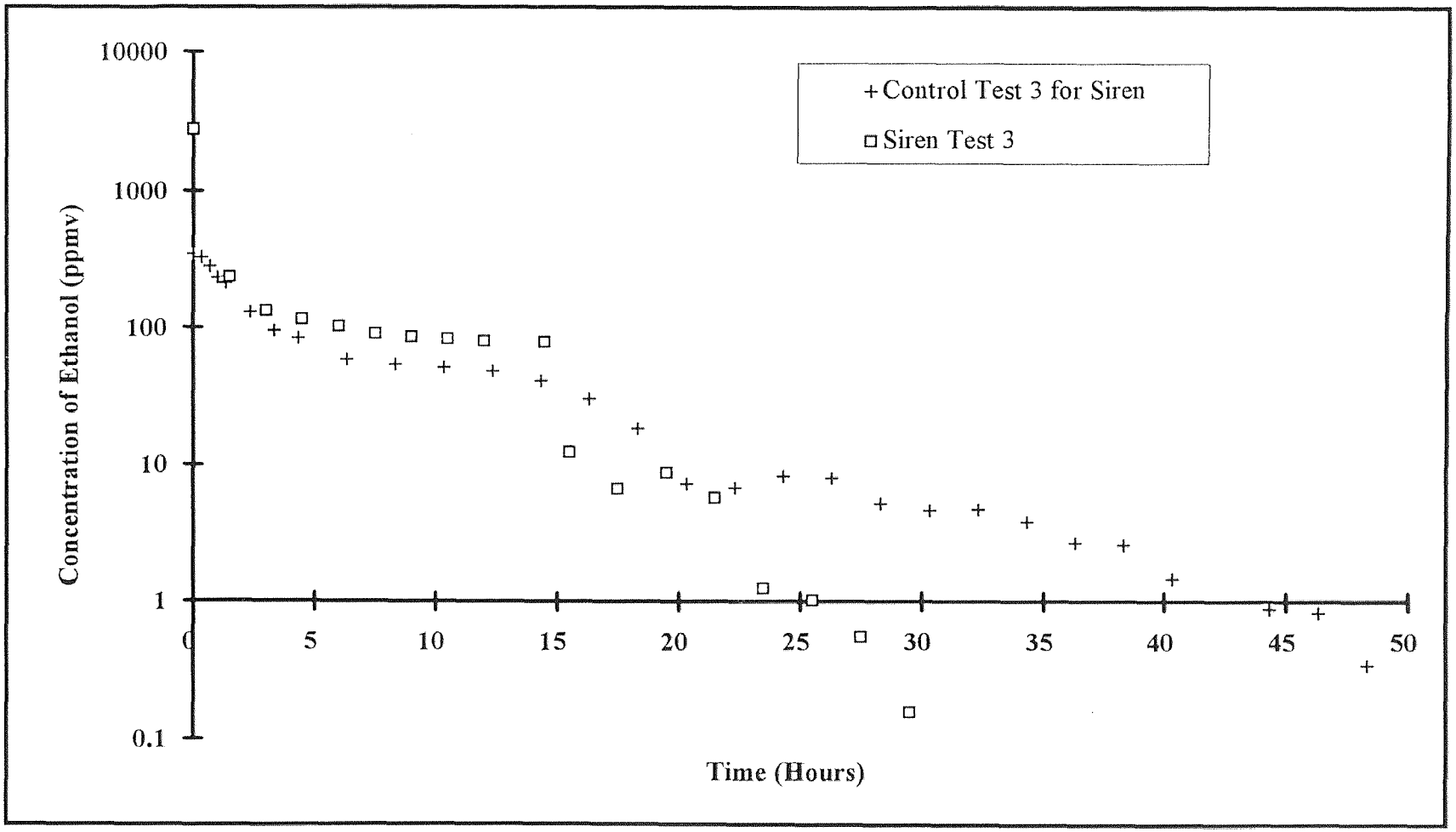

Figure 4.19 Semi Logarithmic Plot of Concentration Versus Time for Siren Set 3

time. The data are once again divided into two regions, the transient region and the falling rate region (**Figure 4.20** and **Figure 4.21** respectively) and these two regions are correlated on logarithmic coordinates and semi logarithmic coordinates respectively. The correlation equations as well as the correlation coefficients are shown in **Figures 4.21** and **4.21**.

A comparison of the complete data in **Figures 4.1**, **4.8**, and **4.15** show in every test that the curves for the siren lie below the curves for the control. This demostrates that for each set of data the ultrasonic device enhanced the removal rate. Furthermore, the average time required to reach a low asymptotic value of 0.01 pounds or 91 percent removal was reduced using the ultrasonic siren from 50 hours to 32 hours. This represents an average reduction in time of 37% with a range of 21-53 percent. These data are summarized in **Table 4.1**. Shorter remediation times can definitely reduce overall clean-up cost. These times can also be estimated from an inspection of **Figures 4.4**, **4.11** and **4.18**. Furthermore, the data in **Figures 4.1**, **4.8** and **4.15** show some beneficial effect of ultrasound during the transient period although the effects during the falling rate period are greater.

Table 4-1 Estimated Time to Reach an Asymptotic Value of 0.01 Free Moisture per Pounds of Solids for the Siren from Figures 4.1, 4.8 and 4.16

Siren Set Number	Time for Control Run	Time for Actual Run	Percent Reduction
	Hours	Hours	Percentage
1	43	20	53
2	56	44	21
3	----------	----------	----------
Average	50	32	37
Range	43-56	20-44	21-53

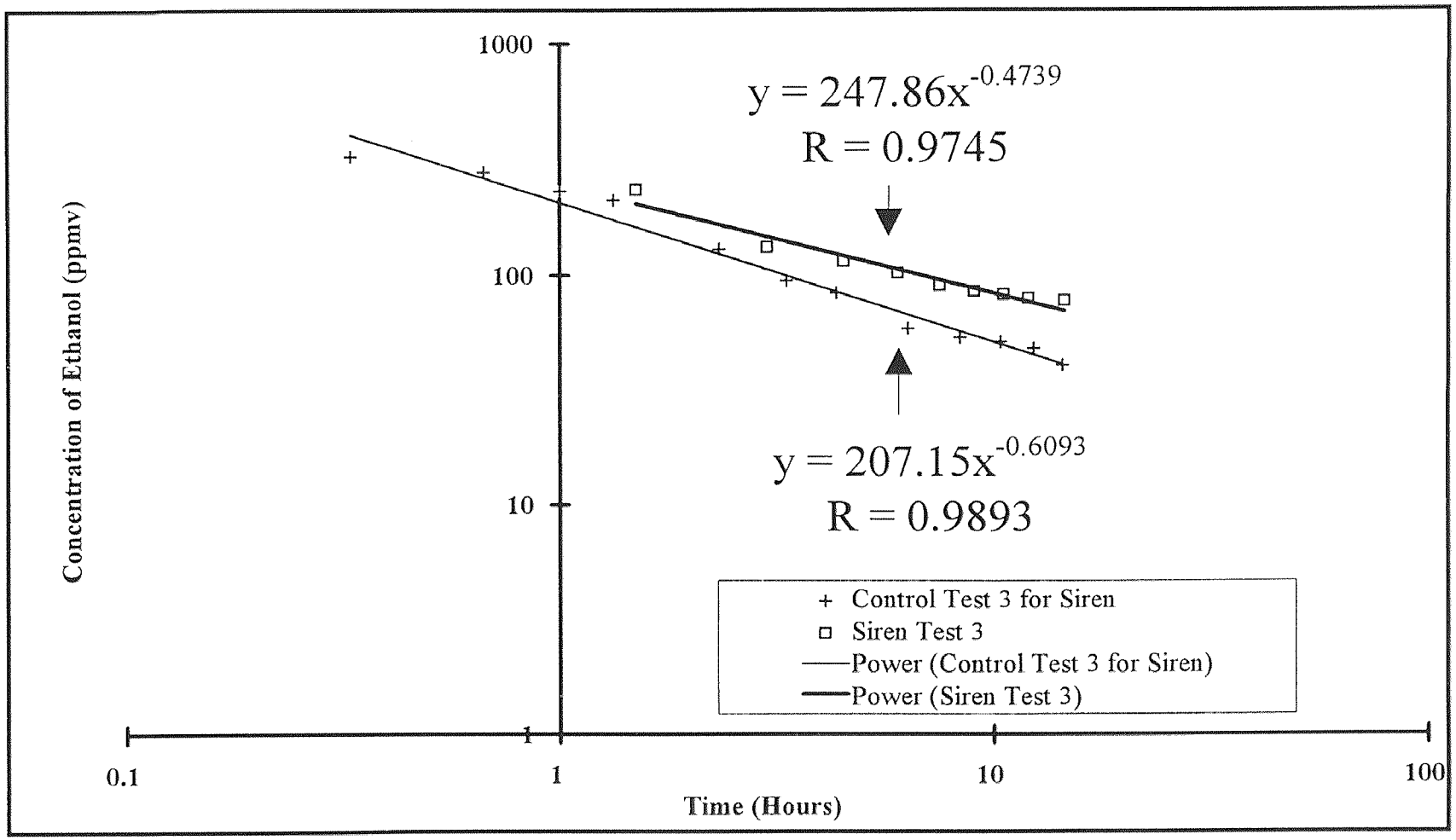

Figure 4.20 Logarithmic Curve Fit of Concentration Versus Time for Siren Set 3 in the Transient Region

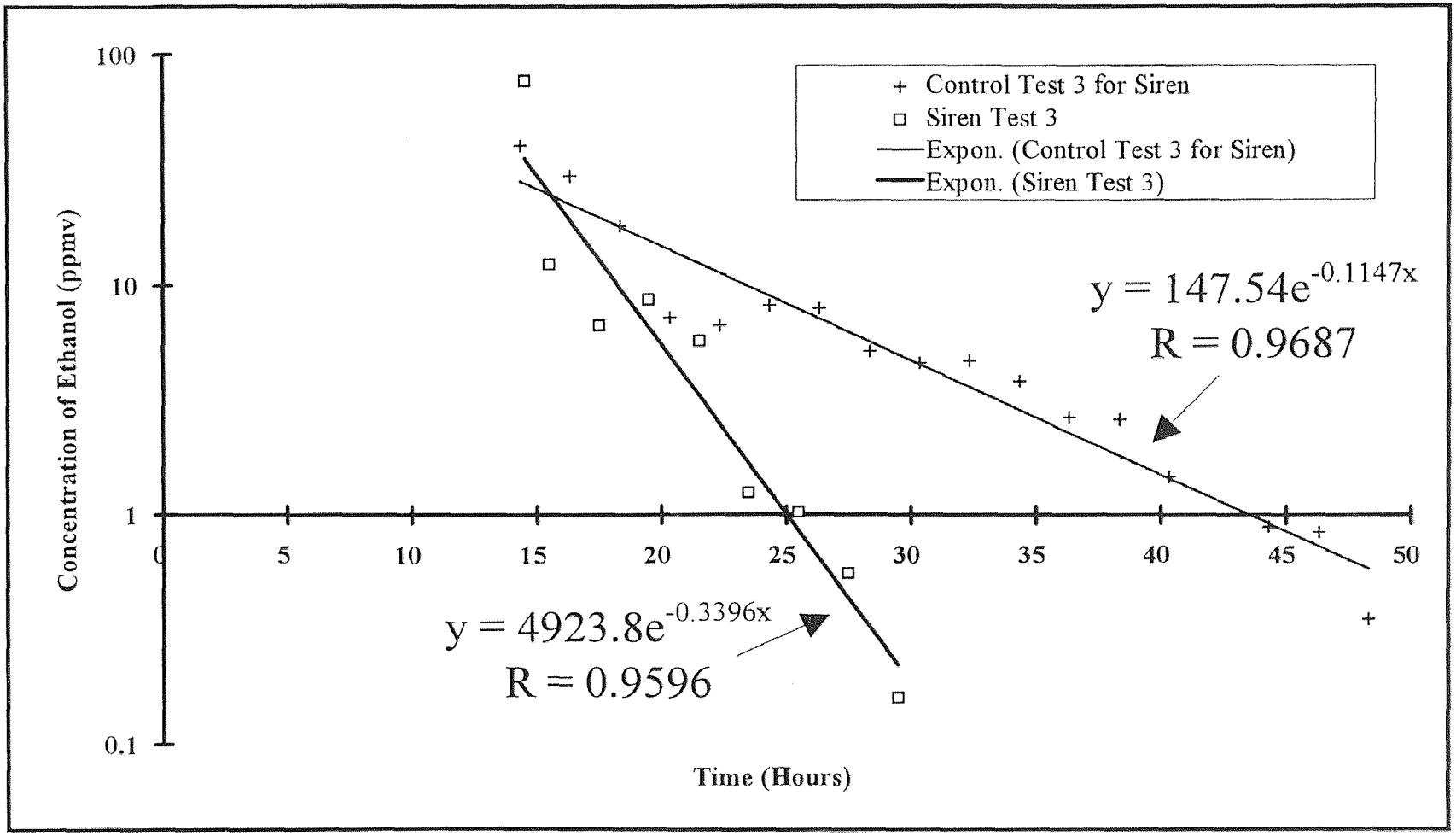

Figure 4.21 Semi Logarithmic Curve Fit of Concentration Versus Time for Siren Set 2 in the Falling Rate Region

An examination of the complete data for concentration versus time in **Figures 4.5, 4.12** and **4.19** show that the removal of ethanol with the ultrasonic siren is greater than the control case. The times needed to reach a low concentration of 1 ppmv ethanol are sumarized in **Table 4.2**. The data reveal an average reduction in time of 41% in the removal rate of ethanol from the soil. These data corroborate the free moisture data and more rapid removal of ethanol using ultrasound with the siren and hence potentially reducing site remediation times and cost. A similar comparison of the estimated time reduction to reach level of 1 ppmv can be obtained from **Figure 4.7, 4.15** and **4.21**.

Table 4-2 Estimated Time to Reach an Concentration of 1ppmv of Ethanol in the Vapor for the Siren from Figures 4.5, 4.13 and 4.20

Siren Set Number	Time for Control Run	Time for Actual Run	Percent Reduction
	Hours	Hours	Percentage
1	>40	18	>55
2	>40	30	>25
3	45	25	>44
Average	>42	24	>41
Range	----------	18-25	----------

Table 4.3 is a summary of the slopes obtained for **Figures 4.1** through **4.21**. The first portion of the table represents the slopes of the transient region for Siren Set 1 through 3 for the free moisture versus time curve. These slopes are averaged at the bottom of the set and the mean is compared statistically using a student t test with the corresponding control mean for the baseline. The Student's t test revealed that for the free moisture versus time correlation in the transient region of the siren sets 1 through 3 there is no significant difference between the control tests and the siren tests at a 90%

Table 4-3 Slopes of Free Moisture Removal With Time in the Transient Region and in the Falling Rate Region for the Siren

Transient Region				Falling Rate Region			
Siren Set Number	**Slope for Control Run**	**Slope for Actual Run**	**Percent Enhancement**	**Siren Set Number**	**Slope for Control Run**	**Slope for Actual Run**	**Percent Enhancement**
	Dimensionless	**Dimensionless**	**Percentage**		**1/Hour**	**1/Hour**	**Percentage**
1	-0.140	-0.175	24.82	1	-0.064	-0.120	87.03
2	-0.114	-0.155	36.12	2	-0.038	-0.055	47.34
3	-0.068	-0.106	56.41	3	-0.025	-0.042	72.65
Mean	-0.107	-0.145	39.12	**Mean**	-0.042	-0.072	69.01
Transient Region				**Falling Rate Region**			
Student t Calulated	**Student t Published 2 tailed**	**Significance Level with 4 Degrees of Freedom**	**Significant Difference (Yes or No)**	**Student t Calulated**	**Student t Published 2 tailed**	**Significance Level with 4 Degrees of Freedom**	**Significant Difference (Yes or No)**
1.296	1.533	90.000	No	0.145	1.533	90.000	No

confidence level. These results are also shown in **Table 4.3** where the calculated "t" is less than the published "t". This result is most likely caused by the small sample size of three and more measurements may change this conclusion.

The slopes for siren set 1 through 3 in **Table 4.3** were averaged and compared in the falling rate region using a Student's t test. The comparison revealed that there is no significant difference between the slopes of the siren sets 1 through 3 and their corresponding baseline. This result indicates that for a sample size of three, a comparison of means slopes shows no difference in free moisture removal versus time in either the transient region or the falling rate region. A comparison of the means with more than three samples is necessary for more conclusive statistical results.

The slopes of the concentration versus time for siren set 1 through 3 in the transient region are presented in **Table 4.4** A Student's t test was also performed on the mean slope of these three tests with their corresponding mean for the control tests. The Student's t test revealed that there is no significant difference between the mean slope of the concentration decay versus time for the siren in the transient region and its corresponding mean for control tests at a 90% confidence level. In other words, in the initial transient region of the siren test, the concentration decay versus time with the sonic energy of 125 Decibels emitted by the siren is not significant to establish a statistical difference when comparing it with its corresponding control tests. This result is probably due to the small sample size of three and a greater sample size may change this conclusion.

The slope of the concentration versus time for siren set 1 through 3 in the falling rate region is presented in **Table 4.4**. A Student's t test was performed on the slopes of

Table 4-4 Slopes of Ethanol Concentration Decay With Time in the Transient Region and in the Falling Rate Region for the Siren

Transient Region				Falling Rate Region			
Siren Set Number	Slope for Control Run	Slope for Actual Run	Percent Enhancement	Siren Set Number	Slope for Control Run	Slope for Actual Run	Percent Enhancement
	Dimensionless	Dimensionless			1/Hour	1/Hour	
1	-1.074	-1.223	13.89	1	-0.105	-0.390	272.14
2	-0.237	-0.702	196.96	2	-0.094	-0.203	117.22
3	-0.609	-0.474	-22.22	3	-0.119	-0.340	186.58
Mean	-0.640	-0.800	62.88	Mean	-0.106	-0.311	191.98

Transient Region				Falling Rate Region			
Student t Calulated	Student t Published 2 tailed	Significance Level with 4 Degrees of Freedom	Significant Difference (Yes or No)	Student t Calulated	Student t Published 2 tailed	Significance Level with 4 Degrees of Freedom	Significant Difference (Yes or No)
0.487	1.533	90.000	No	3.649	3.495	99.500	Yes

these three siren tests and their corresponding mean for the control test. The Student's t test revealed that there is 99.5% certainty that there is significant difference between the mean slope of the siren concentration decay versus time in the falling rate region and its corresponding mean for the control test.

Table 4.3 also shows the percent increase in slope using the ultrasonic siren which is a measure of the improvement in the rate of removal. In the transient regions, a comparison of the slopes for the free moisture removal shown in **Figures 4.3, 4.10** and **4.17** show an average percent enhancement of 39.1% with a range of 24.8% to 56.4% for the three runs. Similarly, from **Figures 4.4, 4.11, and 4.18** for the falling region the percent enhancement averaged 69.0% with a range of 47.3% to 87.0% for the three tests.

Analysis of the data in **Table 4.4** show a similar behavior based upon the concentration of ethanol in the vapor. For the transient region shown in the **Figures 4.6, 4.13** and **4.20** the data show an average improvement of 62.9% with a very wide range of -22.2% to 197.0% for the three tests. For the falling rate period the percent enhancement based upon ethanol concentration in the effluent averaged 192.0% with a range of 117.2% to 272.1% for the three tests.

Based upon this analysis the conclusions are that the ultrasonic siren improves the removal rate and reduces remediation times. With more data points, an improvement in the significance level is likely.

4.3 Results of Tests with the Whistle

The results of set 1 of the whistle test are presented in seven figures. **Figure 4.22** represents the complete data collected by the laboratory scale system for the whistle test 1 and the corresponding control test or baseline test for free moisture in the test cell

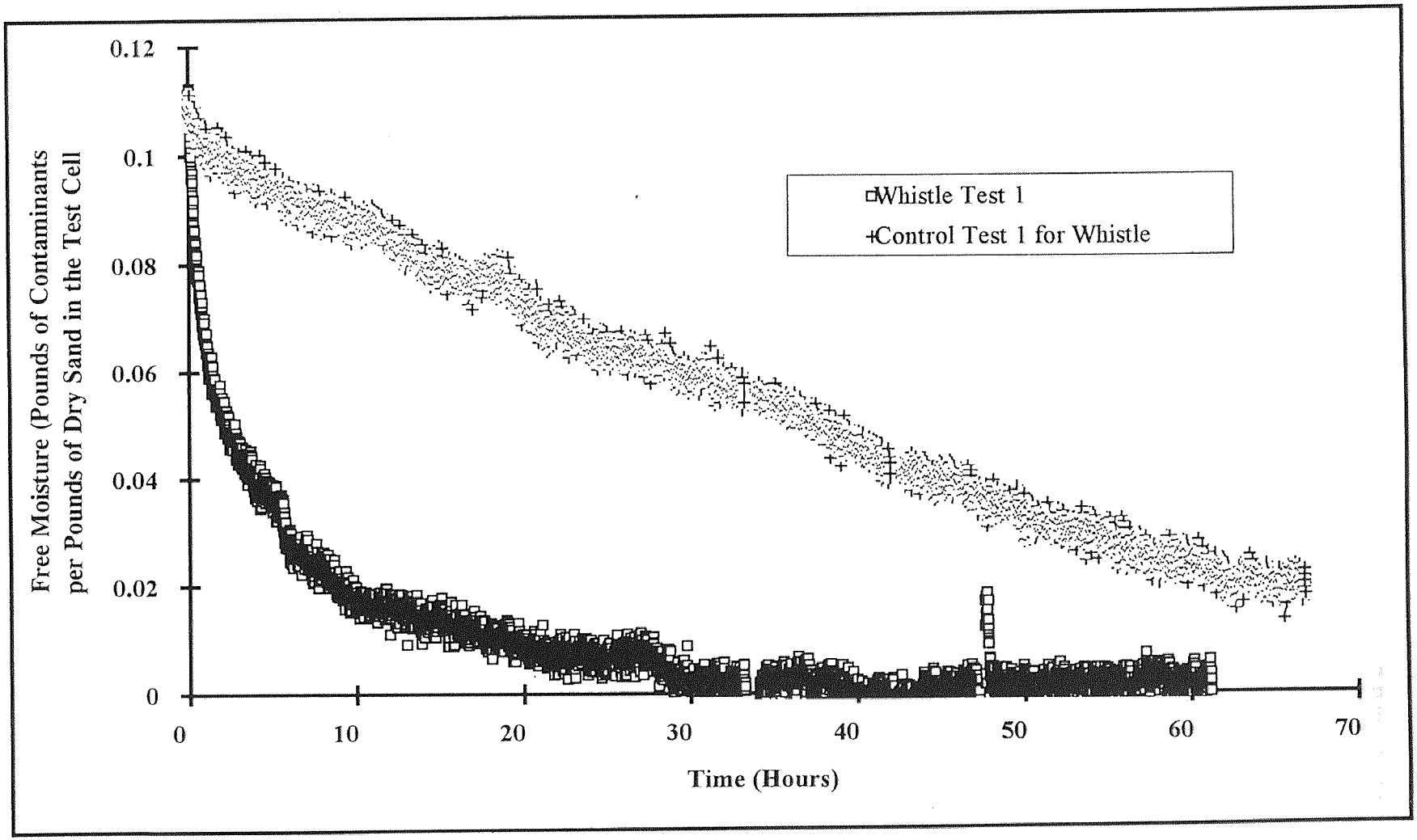

Figure 4.22 Measured Data of Free Moisture Versus Time for Whistle Set 1

versus time. The data in **Figure 4.22** were then averaged in five minute intervals and the average was revealed that there is a 99.5% certainty that there is significant difference between the plotted in **Figure 4.23**. **Figure 4.23** is plotted on semi logarithmic coordinates and represents the five minute average of free moisture in the test cell versus the five minute average time in **Figure 4.22**. **Figure 4.23** was divided into two figures, **Figure 4.24** and **Figure 4.25**. **Figure 4.24** is the transient behavior of free moisture in the tank versus time with its corresponding control test. The data in **Figure 4.24** were plotted on logarithmic coordinates and correlated with a logarithmic curve fit and the corresponding correlation coefficients were calculated. The transient region in **Figure 4.24** is shown and correlated well by a logarithmic curve fit between the time range of .01 hours to 7 hours for both the control test 1 and the whistle test 1 in the transient region.

Figure 4.25 represents the falling rate region of whistle test 1 and the control test 1 where the free moisture versus time is correlated with an exponential curve fit on a semi logarithmic coordinates for both tests (whistle test 1 and control test 1). The correlation equations and the correlation coefficients are shown in **Figure 4.25**. **Figure 4.26** represents the complete data for the concentration of ethanol obtained for whistle test 1 and control test 1 versus time. The data are divided into two regions, the transient region and the falling rate region (**Figure 4.27** and **Figure 4.28** respectively) and these two regions are correlated on logarithmic coordinate and on semi logarithmic coordinates respectively. There was no transient region observed in the concentration decay versus time with the whistle in the whistle test 1. However a transient region was observed for the control test 1 and is plotted in **Figure 4-27** with its correlation equation and correlation coefficient. The falling rate period for both the whistle test 1 and the

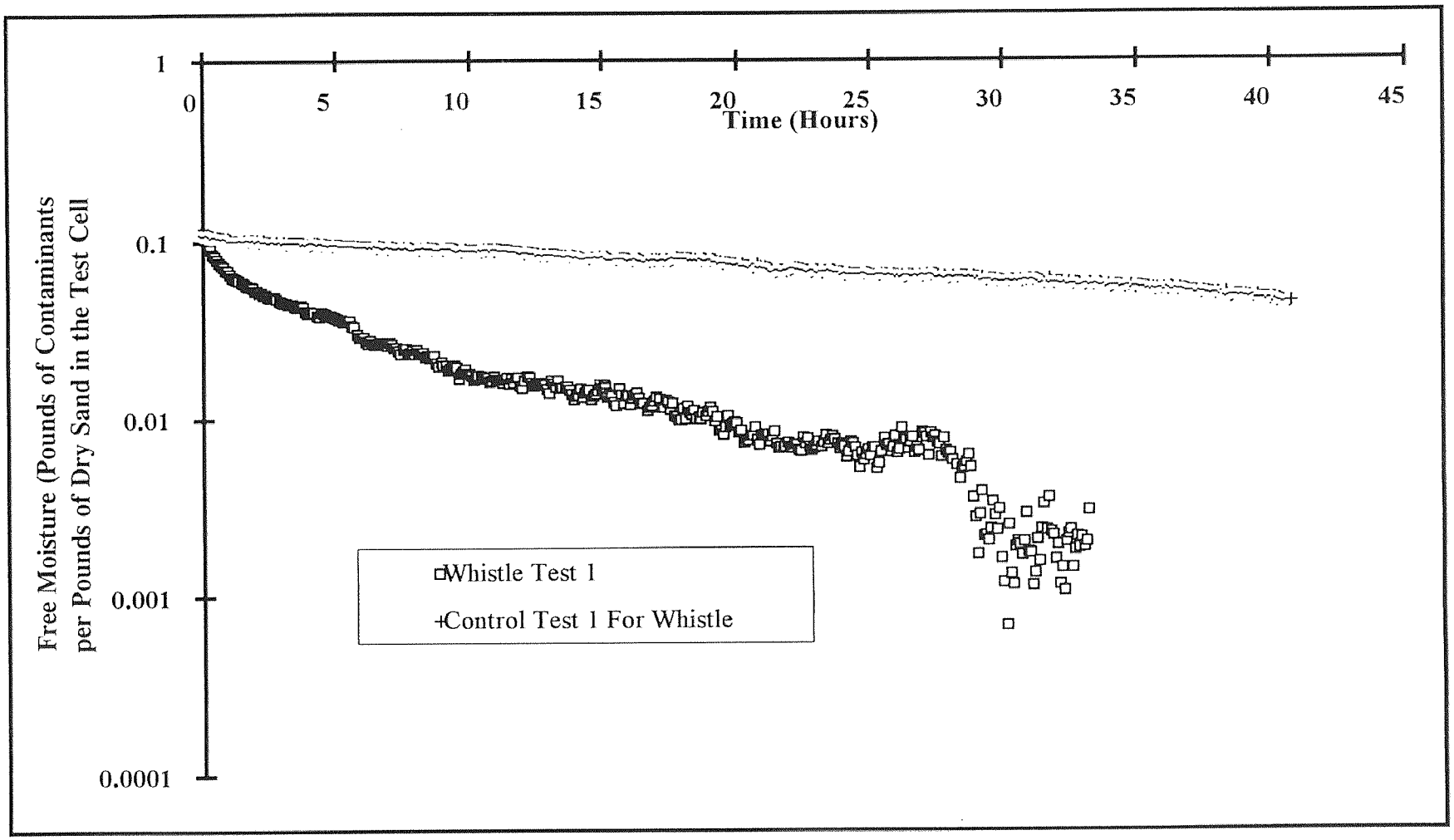

Figure 4.23 Average Semi Logarithmic Plot of Free Moisture Versus Time for Whistle Set 1

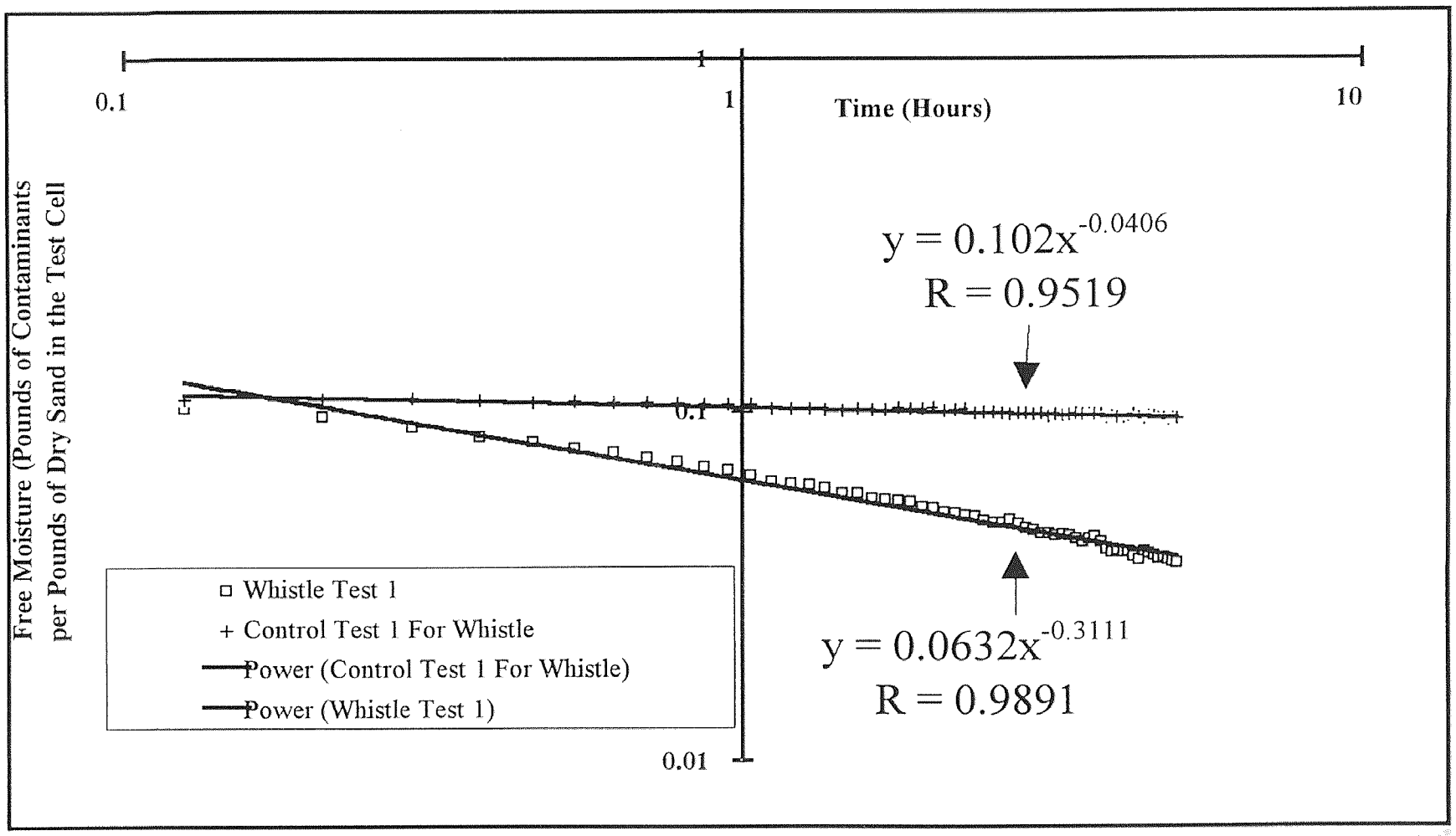

Figure 4.24 Average Logarithmic Curve Fit of Free Moisture Versus Time for Whistle Set 1 in the Transient Region

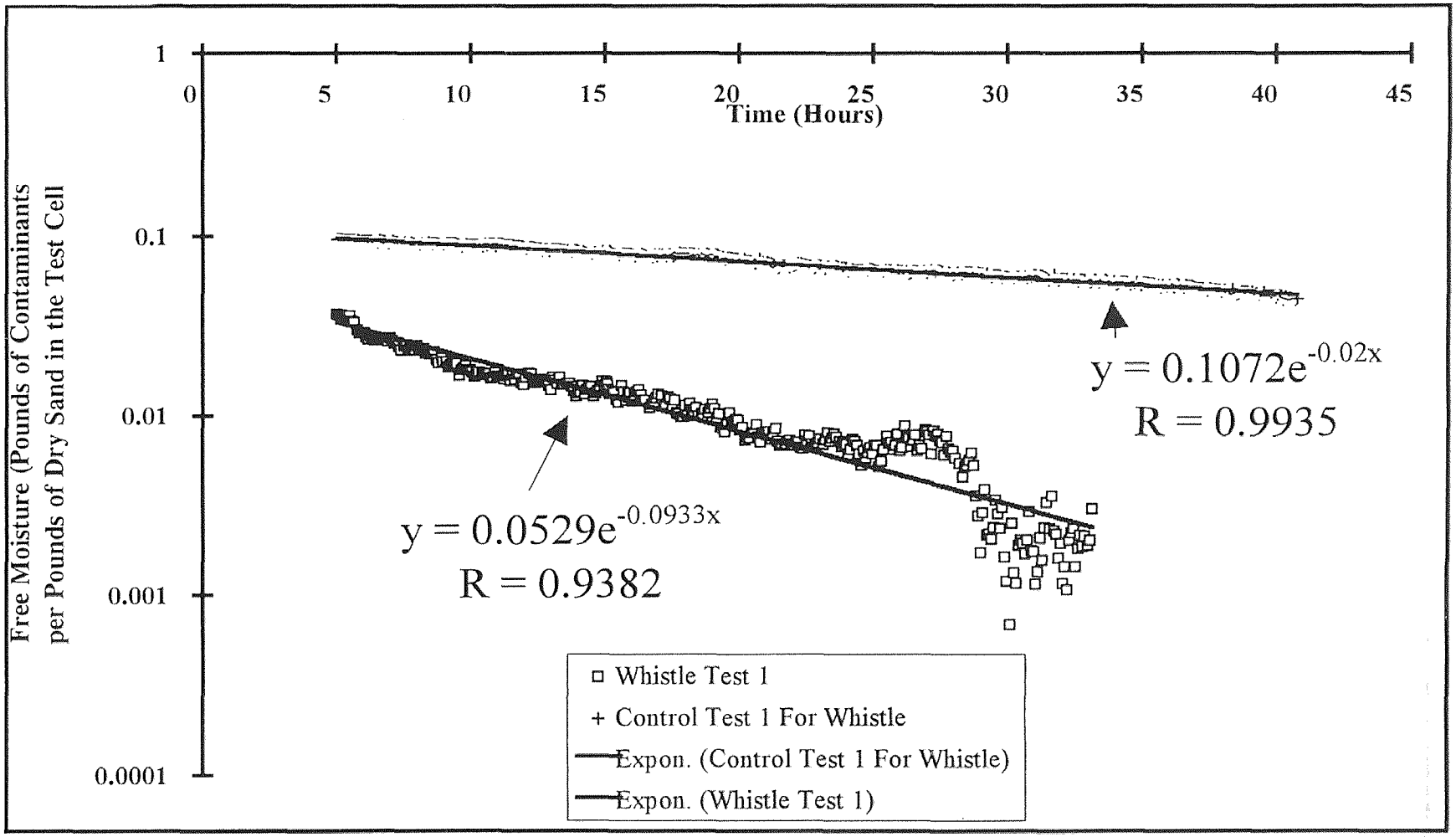

Figure 4.25 Average Semi Logarithmic Curve Fit of Free Moisture Versus Time for Whistle Set 1 in the Falling Rate Region

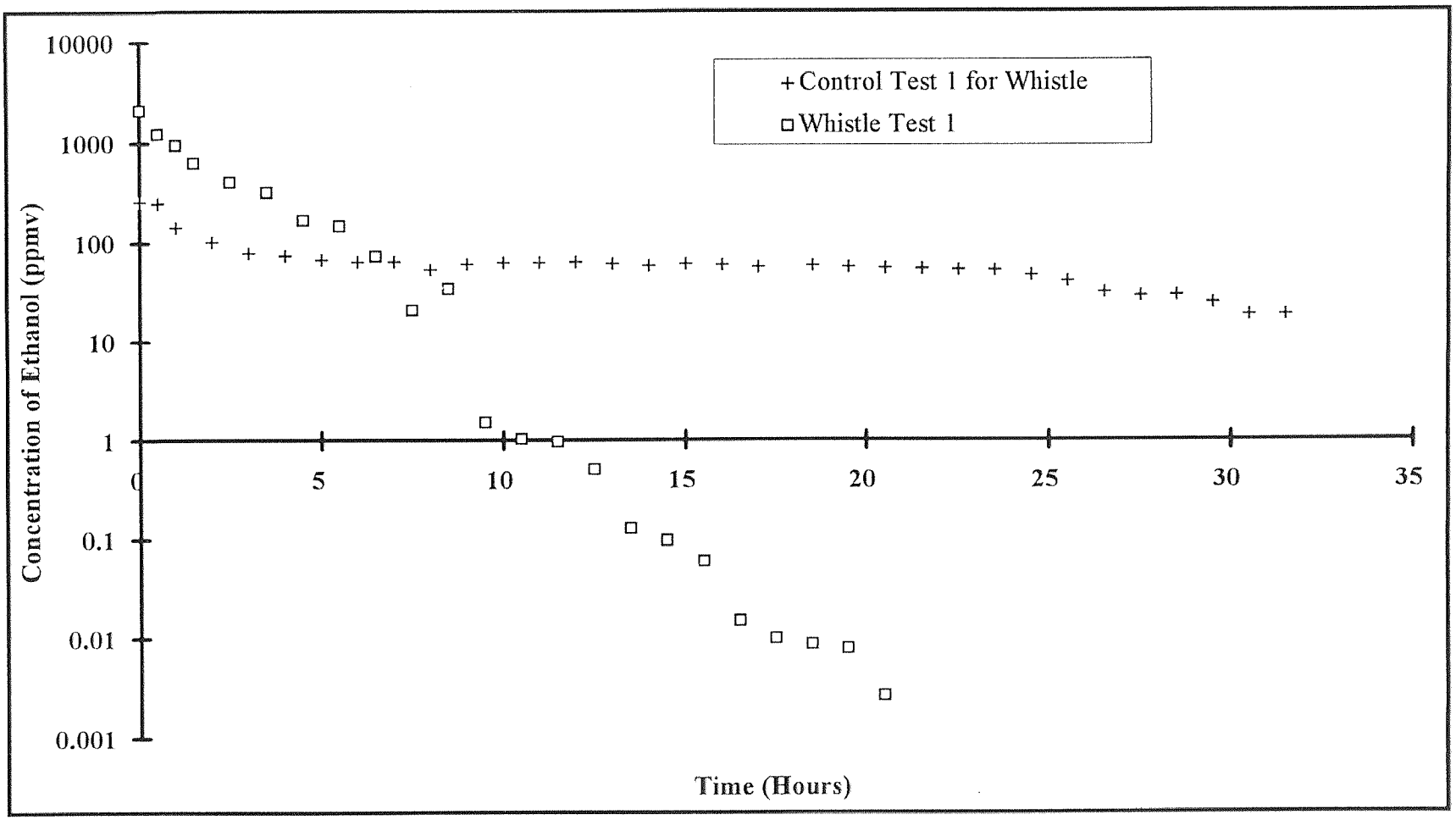

Figure 4.26 Semi Logarithmic Plot of Concentration Versus Time for Whistle Set 1

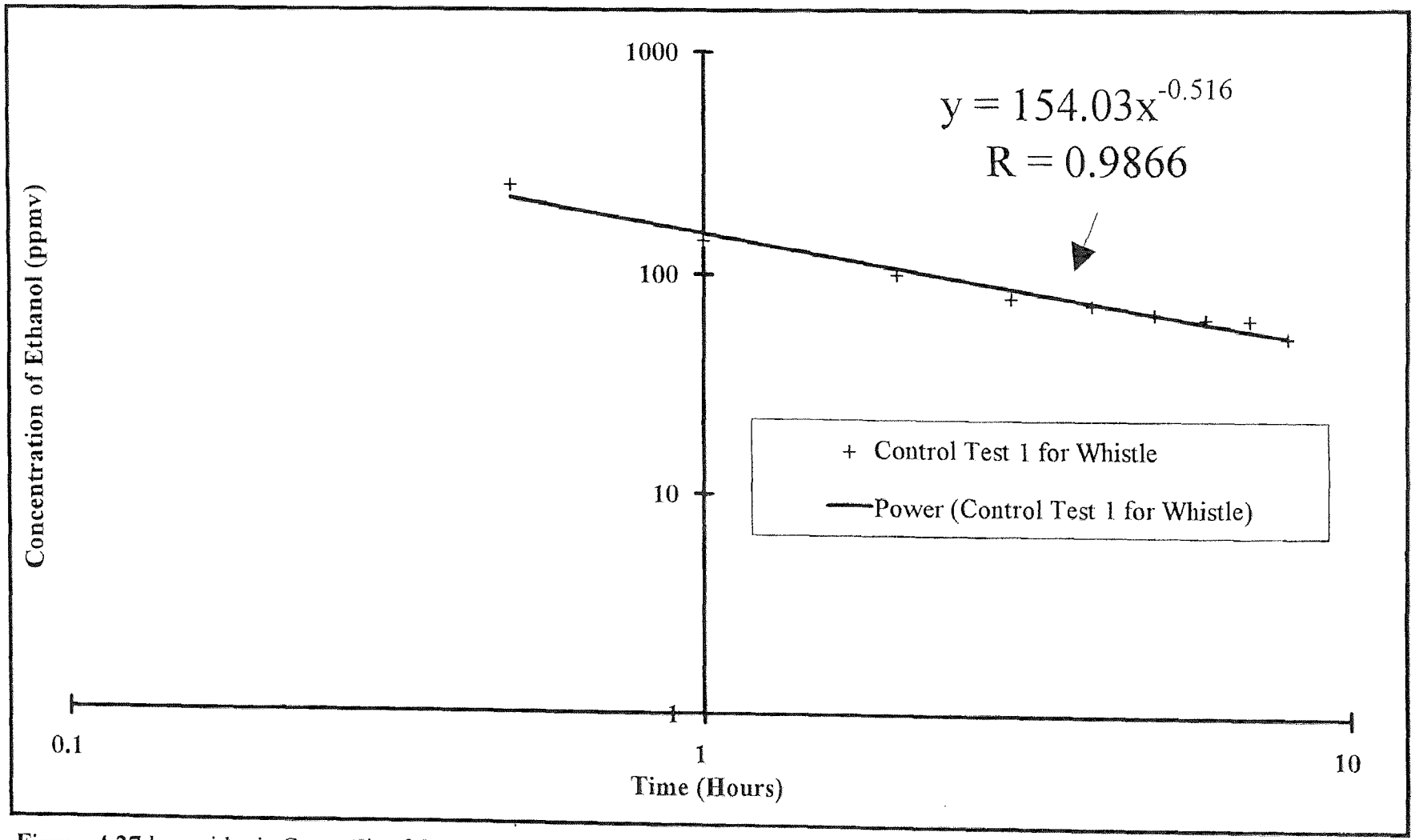

Figure 4.27 Logarithmic Curve Fit of Concentration Versus Time for Whistle Set 1 in the Transient Region

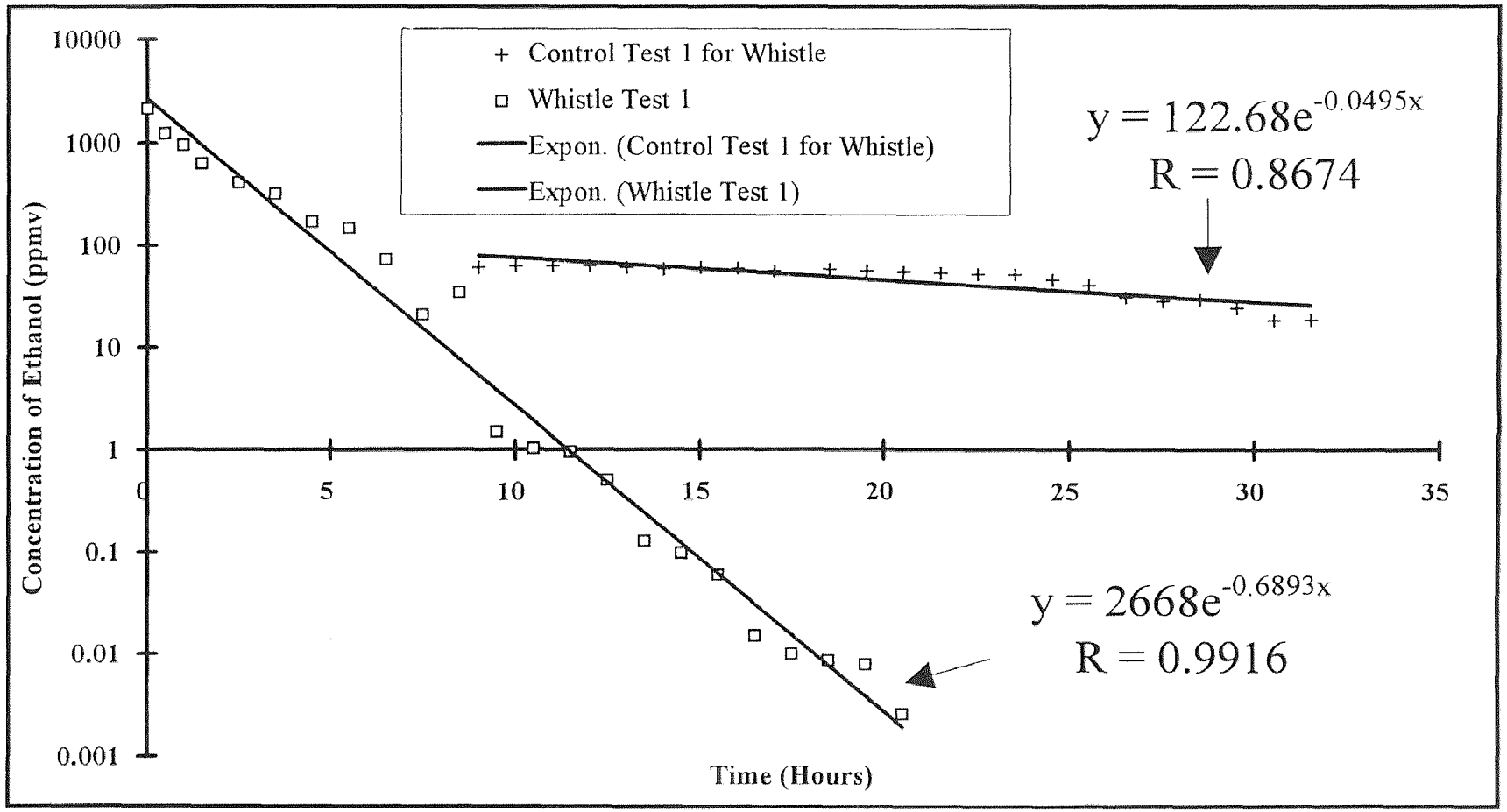

Figure 4.28 Semi Logarithmic Curve Fit of Concentration Versus Time for Whistle Set 1 in the Falling Rate Region

control test 1 are shown with their corresponding correlation equations and correlation coefficients in **Figure 4.28**.

Analysis of the Whistle Set 2 was performed similarly to the set 1 whistle data. **Figure 4.29** represents the complete data collected by the laboratory scale system for the Whistle Test 2 and the corresponding control test or baseline test for free moisture in the test cell versus time. The data in **Figure 4.29** were averaged in five minute intervals and the average was plotted in **Figure 4.30**. **Figure 4.30** is plotted on semi logarithmic coordinates and represents the five minute average of free moisture in the test cell versus the five minute average time in **Figure 4.29**. **Figure 4.30** was divided into two figures, **Figure 4.31** and **Figure 4.32**. **Figure 4.31** is the transient behavior of free moisture in the tank versus time with its corresponding control test. The data in **Figure 4.31** were plotted on logarithmic coordinates and correlated with a logarithmic curve fit. The transient region in **Figure 4.31** is shown and correlated well by a logarithmic curve fit between the time range of .05 hours to 7 hours for both the control test 2 and the whistle test 2 in the transient region. **Figure 4.32** represents the falling rate region of whistle test 2 and the control test 2 where the free moisture versus time is correlated with an exponential curve fit on semi logarithmic coordinates for both test (whistle test 2 and control test 2). The correlated equations and the correlation coefficients are shown in **Figure 4.32**

. **Figures 4.33** represents the concentration of ethanol obtained for whistle test 2 and control test 2 versus time. The data are once again divided into two regions, the transient region and the falling rate region (**Figure 4.34** and **Figure 4.35** respectively) and these two regions are correlated on logarithmic coordinates and on semi logarithmic

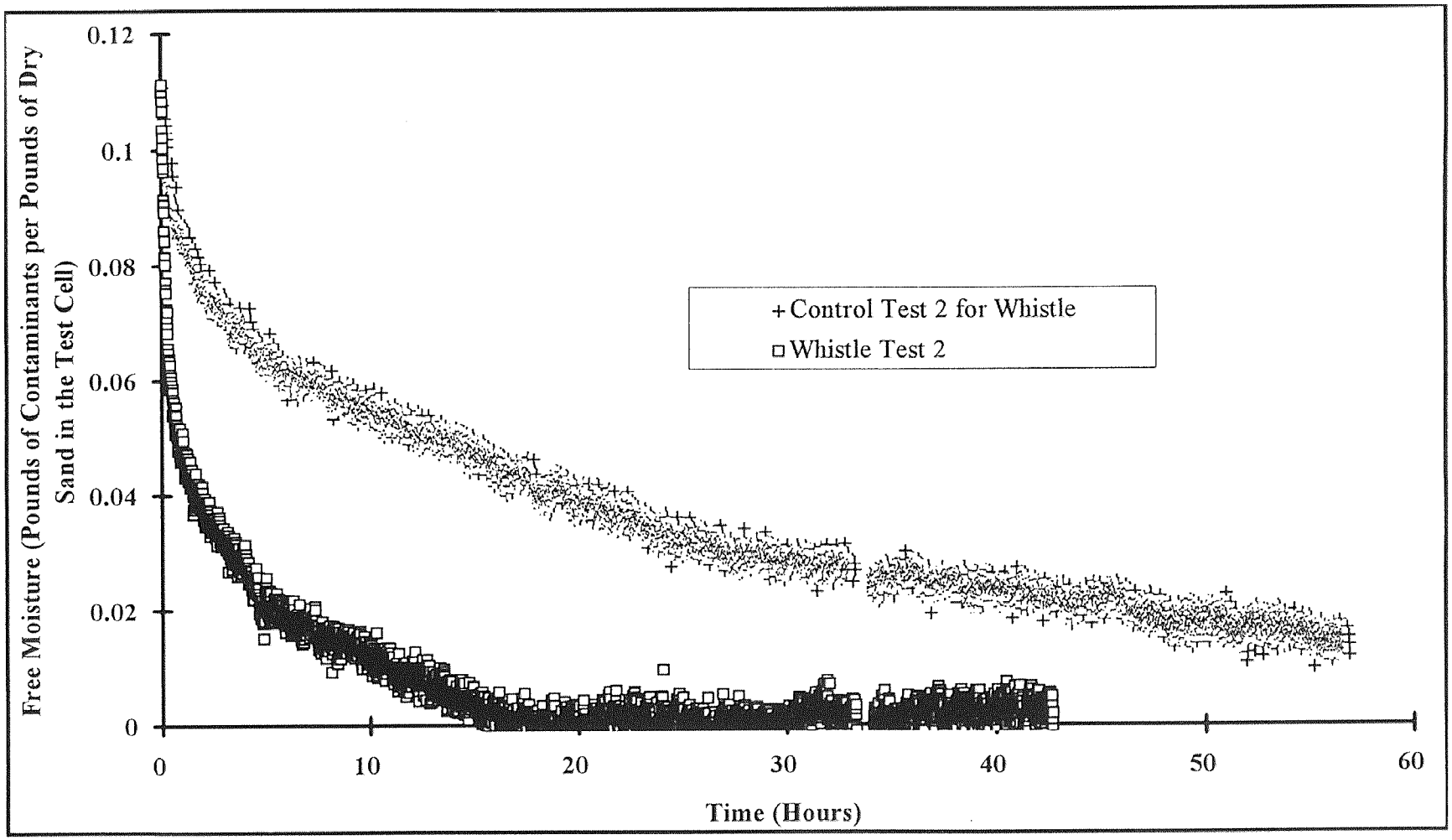

Figure 4.29 Measured Data of Free Moisture Versus Time for Whistle Set 2

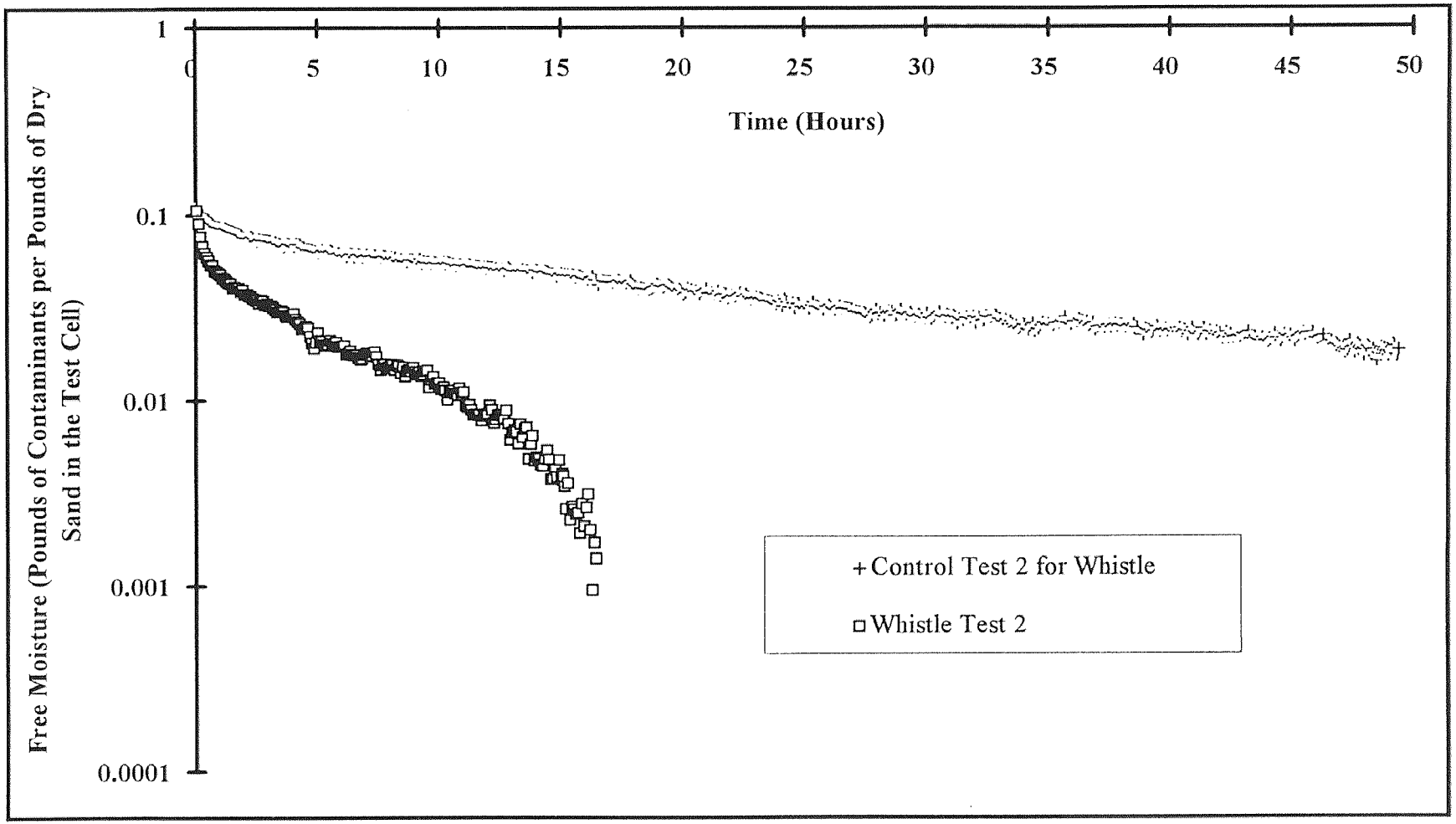

Figure 4.30 Average Semi Logarithmic Plot of Free Moisture Versus Time for Whistle Set 2

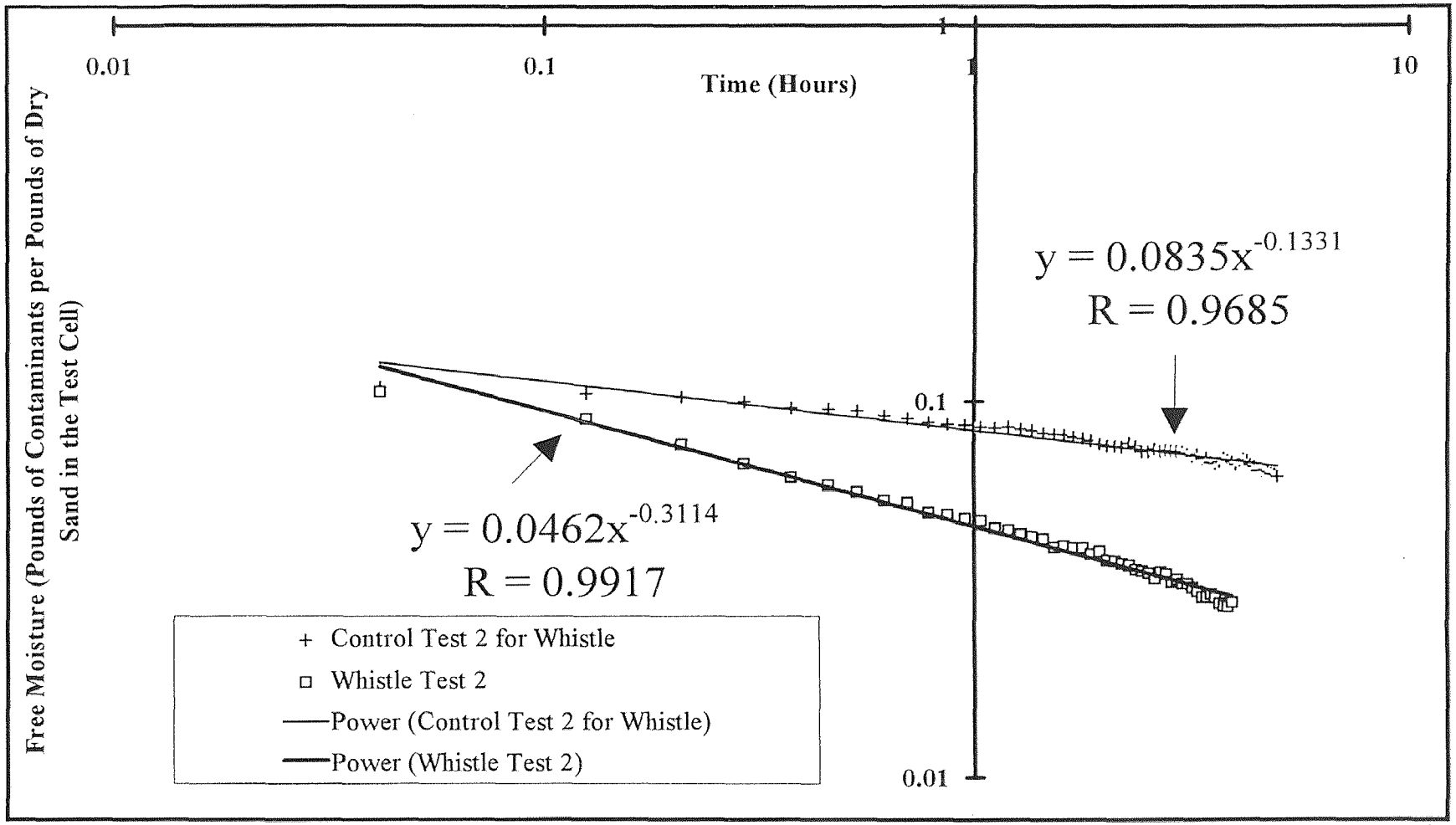

Figure 4.31 Average Logarithmic Curve Fit of Free Moisture Versus Time for Whistle Set 2 in the Transient Region

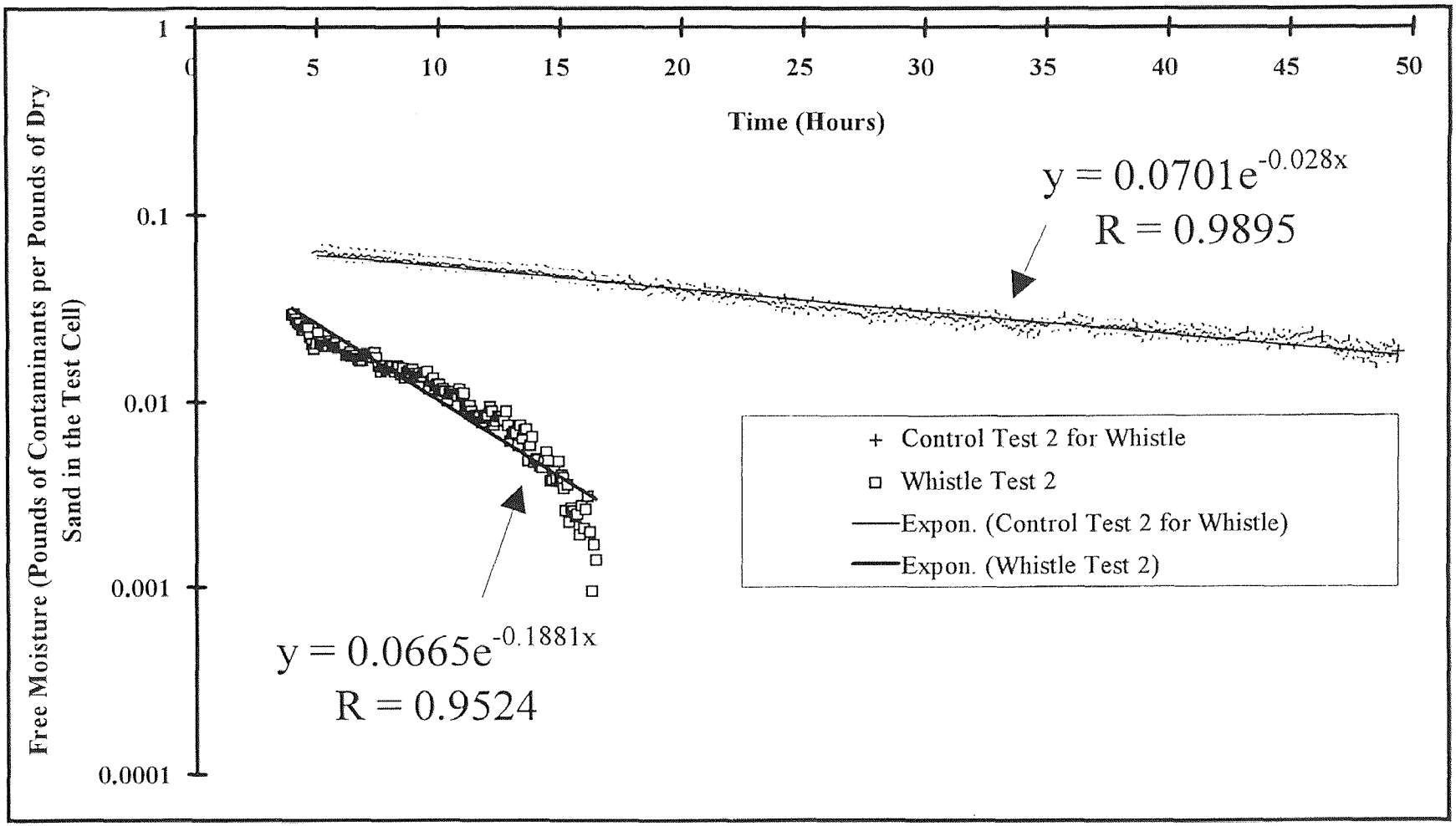

Figure 4.32 Average Semi Logorithmic Curve Fit of Free Moisture Versus Time for Whistle Set 2 in the Falling Rate Region

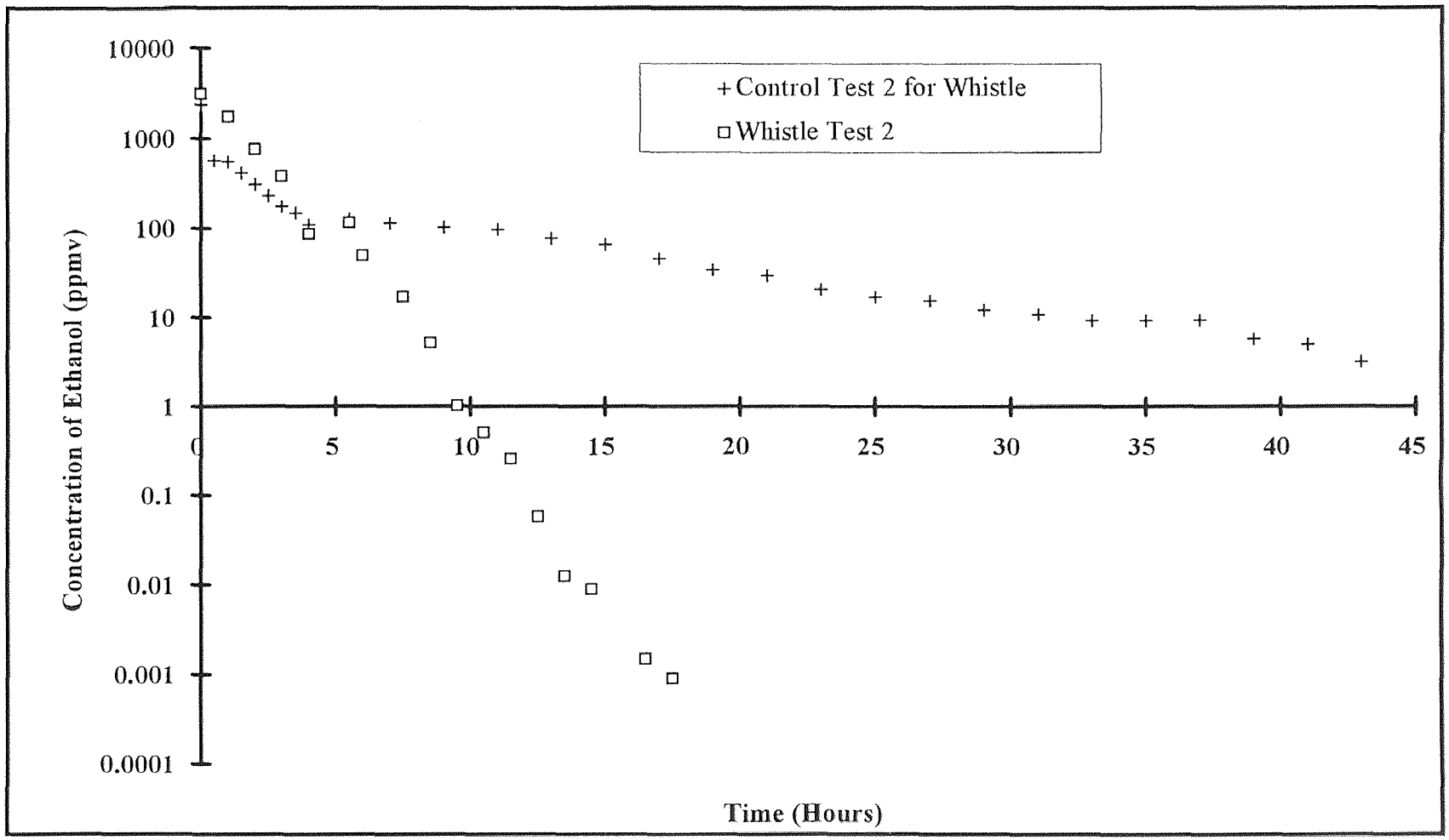

Figure 4.33 Semi Logarithmic Plot of Concentration Versus Time for Whistle Set 2

Removal Rate of Ethanol Versus Soil Ethanol Content For Whistle Test 1 and Control Run for Whistle Test 3

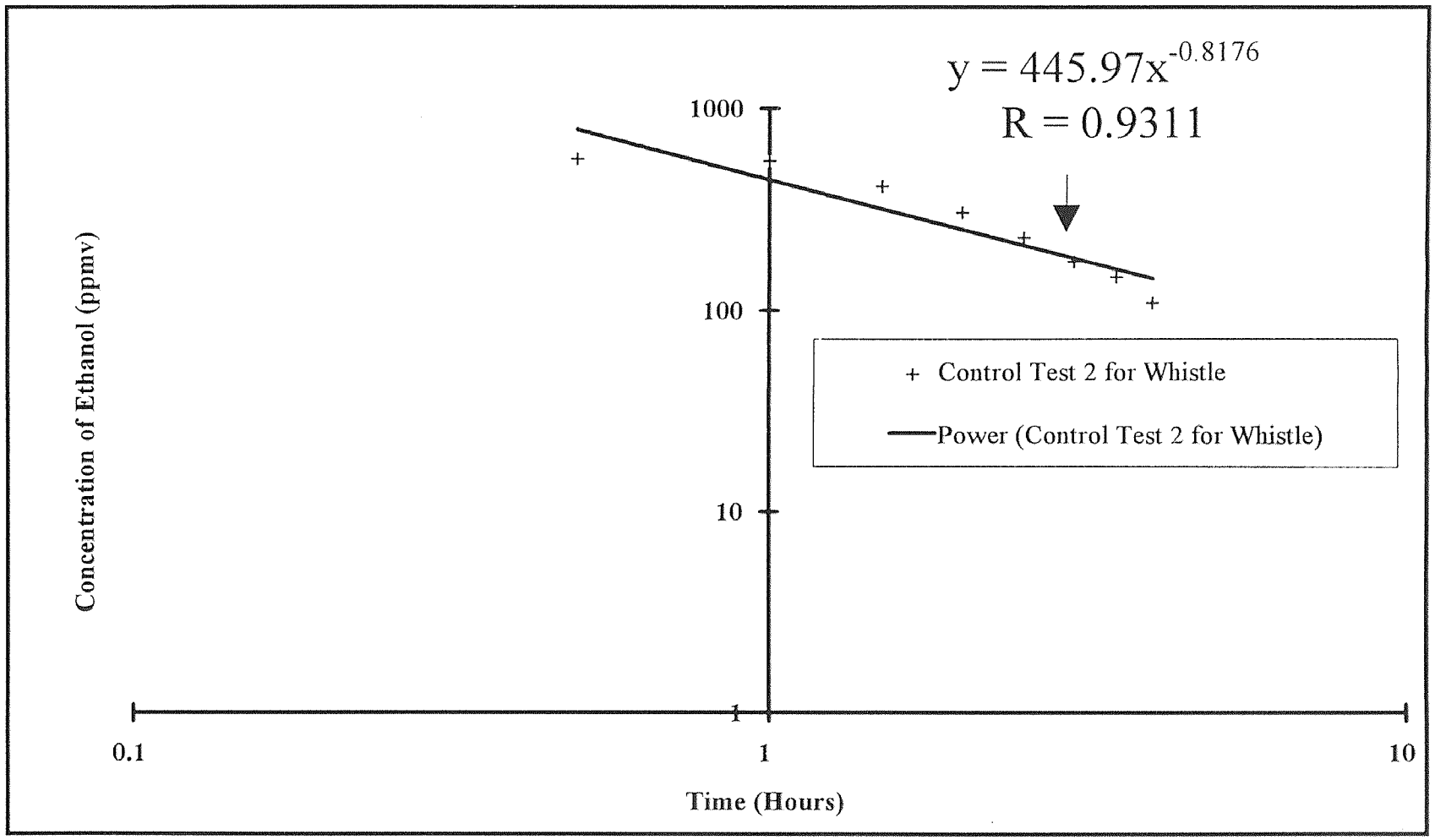

Figure 4.34 Logarithmic Curve Fit of Concentration Versus Time for Whistle Set 2 in theTransient Region

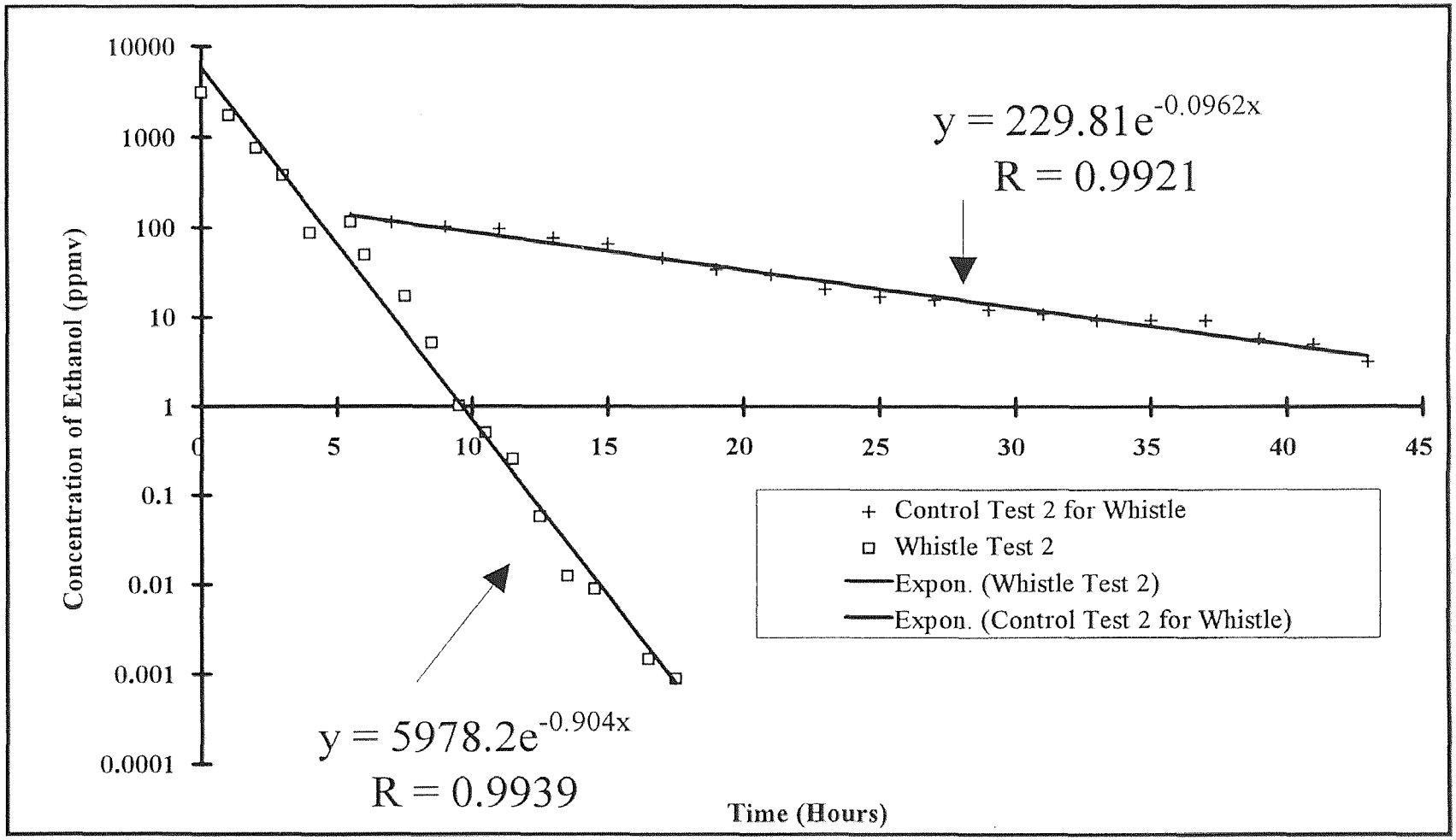

Figure 4.35 Semi Logarithmic Curve Fit of Concentration Versus Time for Whistle Set 2 in the Falling Rate Region

coordinates respectively. There was no transient region observed in the concentration decay versus time with the whistle in the whistle test 2. However a transient region was observed for the control test and is plotted in **Figure 4-34** with its correlation equation and correlation coefficient. The falling rate period for both the whistle test 2 and the control test 2 is shown with its corresponding correlated equations and correlation coefficients in **Figure 4-35**.

Set 3 of the whistle test was also divided into seven figures. **Figure 4.36** represents the complete data collected by the laboratory scale system for the whistle test 3 and the corresponding control test or baseline test for free moisture in the test cell versus time. The data in **Figure 4.36** were averaged in five minute intervals and the average was plotted in **Figure 4.37**. **Figure 4.37** is plotted on semi logarithmic coordinates and represents the five minute average of free moisture in the test cell versus the five minute average time in **Figure 4.36**. **Figure 4.37** was divided into two figures, **Figure 4.38** and **Figure 4.39**. **Figure 4.38** is the transient behavior of free moisture in the tank versus time with its corresponding control test. The data in **Figure 4.38** were plotted on logarithmic coordinates and correlated with a logarithmic curve fit. The transient region in **Figure 4.38** is shown and correlated well by a logarithmic curve fit between the time range of .05 hours to 7 hours for both the control test 3 and the whistle test 3 in the transient region. **Figure 4.39** represents the falling rate region of whistle test 3 and the control test 3 where the free moisture versus time is correlated with an exponential curve fit on semi logarithmic coordinates for both test (whistle test 3 and control test 3)

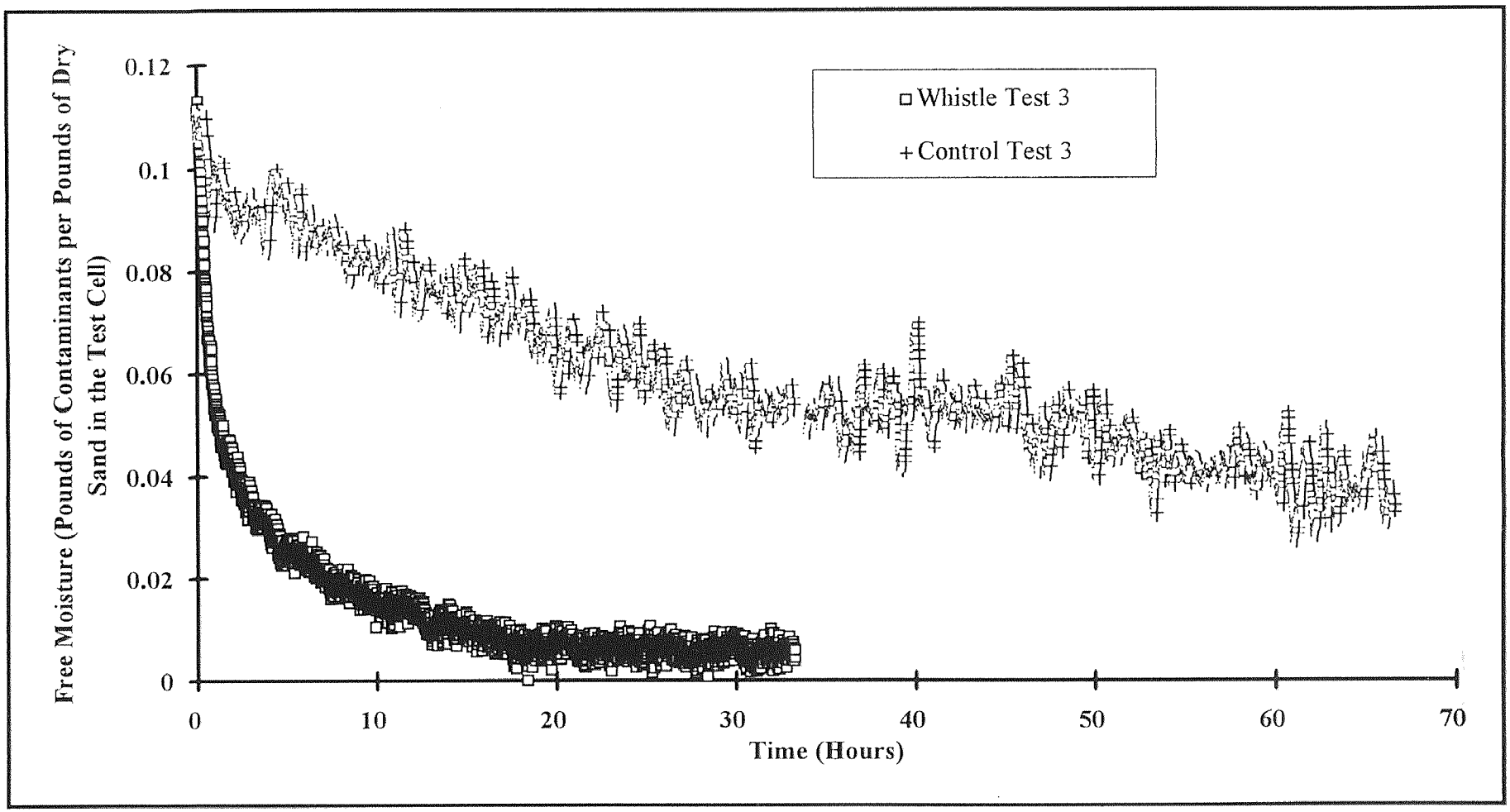

Figure 4.36 Measured Data of Free Moisture Versus Time for Whistle Set 3

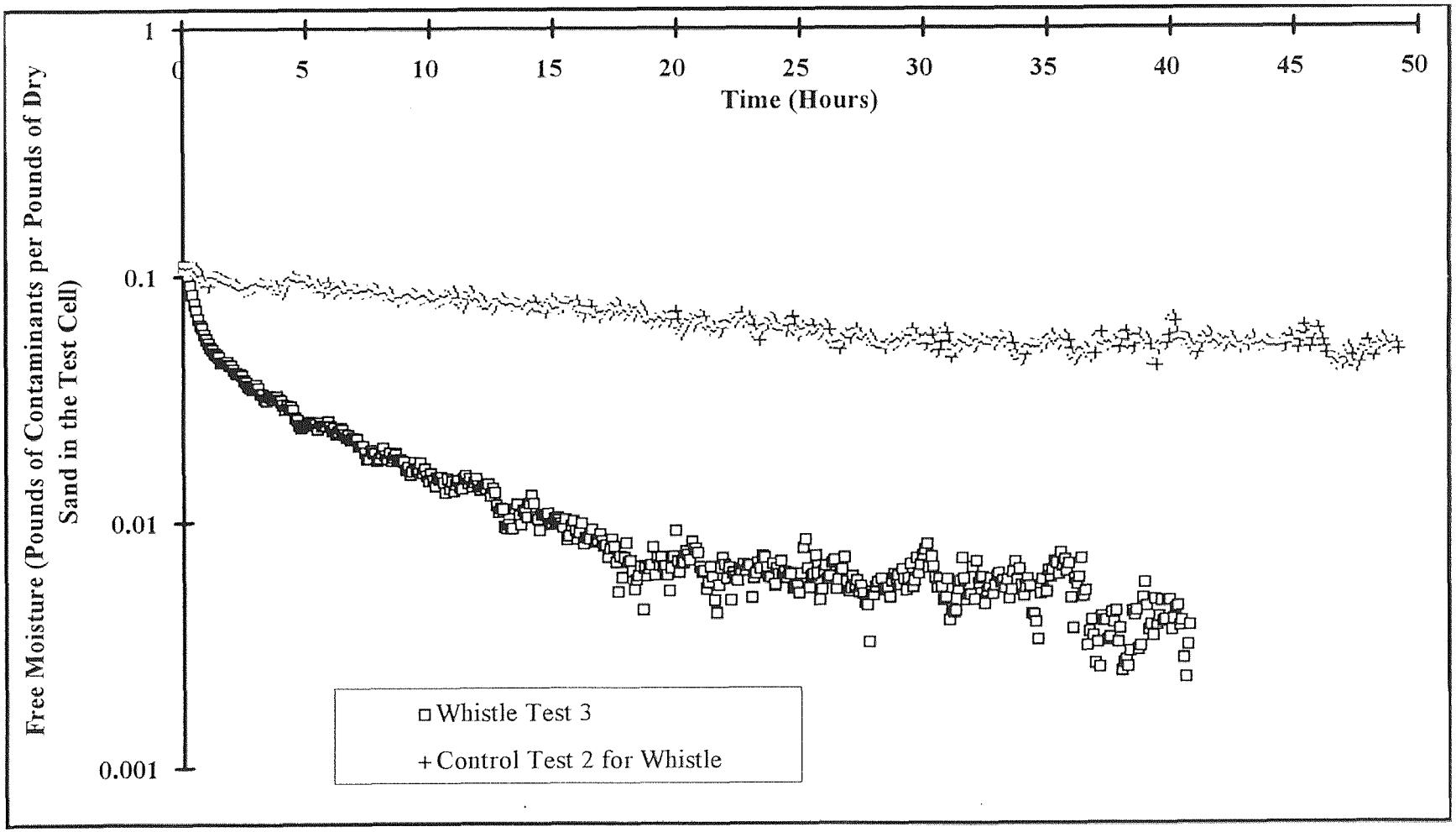

Figure 4.37 Average Semi Logarithmic Plot of Free Moisture Versus Time for Whistle Set 3

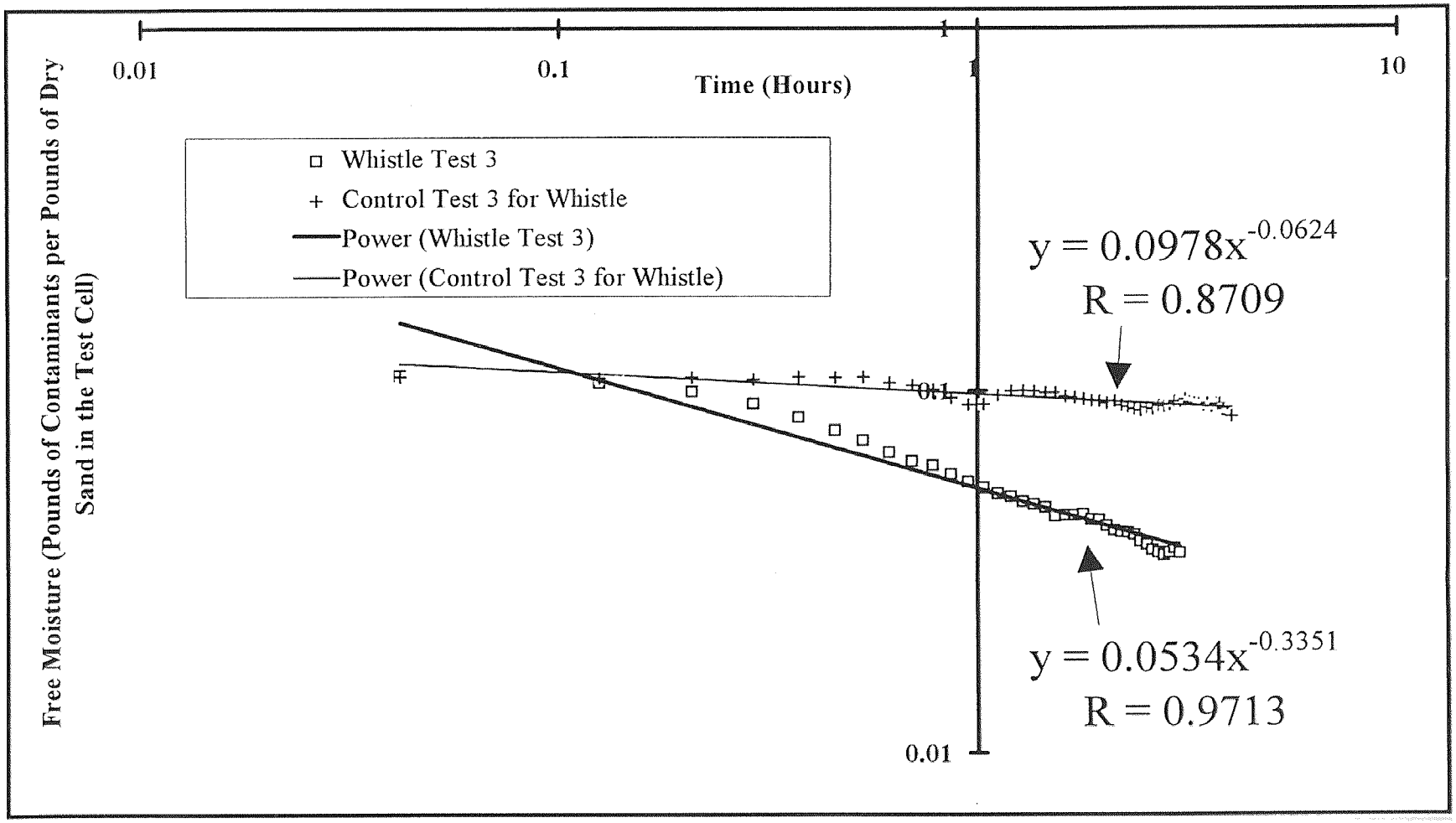

Figure 4.38 Average Logarithmic Curve Fit of Free Moisture Versus Time for Whistle Set 3 in the Transient Region

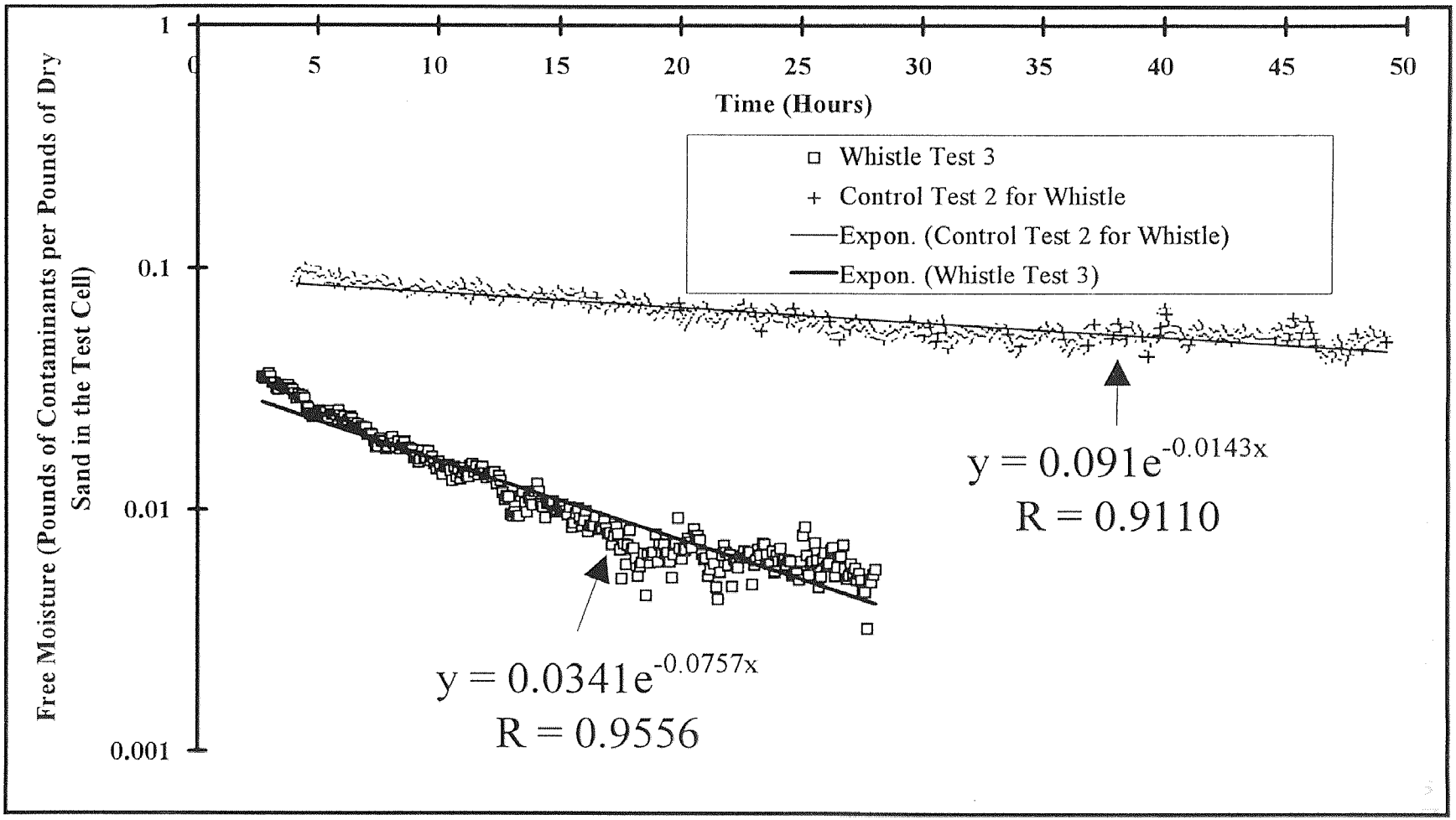

Figure 4.39 Average Semi Logarithmic Curve Fit of Free Moisture Versus Time for Whistle Set 3 in the Falling Rate Region

The correlated equations as well as the correlation coefficients are shown in **Figure 4.39**.

Figures 4.40 represents the concentration of ethanol obtained for whistle test 3 and control test 3 versus time. The data are divided into two regions, the transient region and the falling rate region (**Figure 4.41** and **Figure 4.42** respectively) and these two regions are correlated with a logarithmic curve fit and a semi logarithmic curve fit respectively. There was no transient region observed in the concentration decay versus time with the whistle in whistle test 3. However a transient region was observed for the control test 3 which corresponds to whistle test 3 and is plotted in **Figure 4-41** with its correlation equation and correlation coefficient. The falling rate period for both the whistle test 3 and the control test 3 is shown with its corresponding correlation equations and correlation coefficients in **Figure 4-42**.

A comparison of the complete data in **Figures 4.22**, **4.29**, and **4.36** shows in every test that the curves for the whistle lie below the curves for the control. This fact indicates that for each set of data the whistle enhanced the removal rate. Furthermore, the average time to reach a low asymptotic value of 0.01 moisture content or 91 percent removal was reduced using the whistle from greater than 60 hours to 16 hours. This change represents a percent reduction in time of greater than 74% when compared to the averages obtain in the control tests. These data are summarized in **Table 4.5**. These shorter remediation times can reduce the clean up cost. These times can also be estimated from **Figures 4.25**, **4.32** and **4.39**. Furthermore, the data in **Figure 4.22**, **4.29** and **4.36** show a greater effect

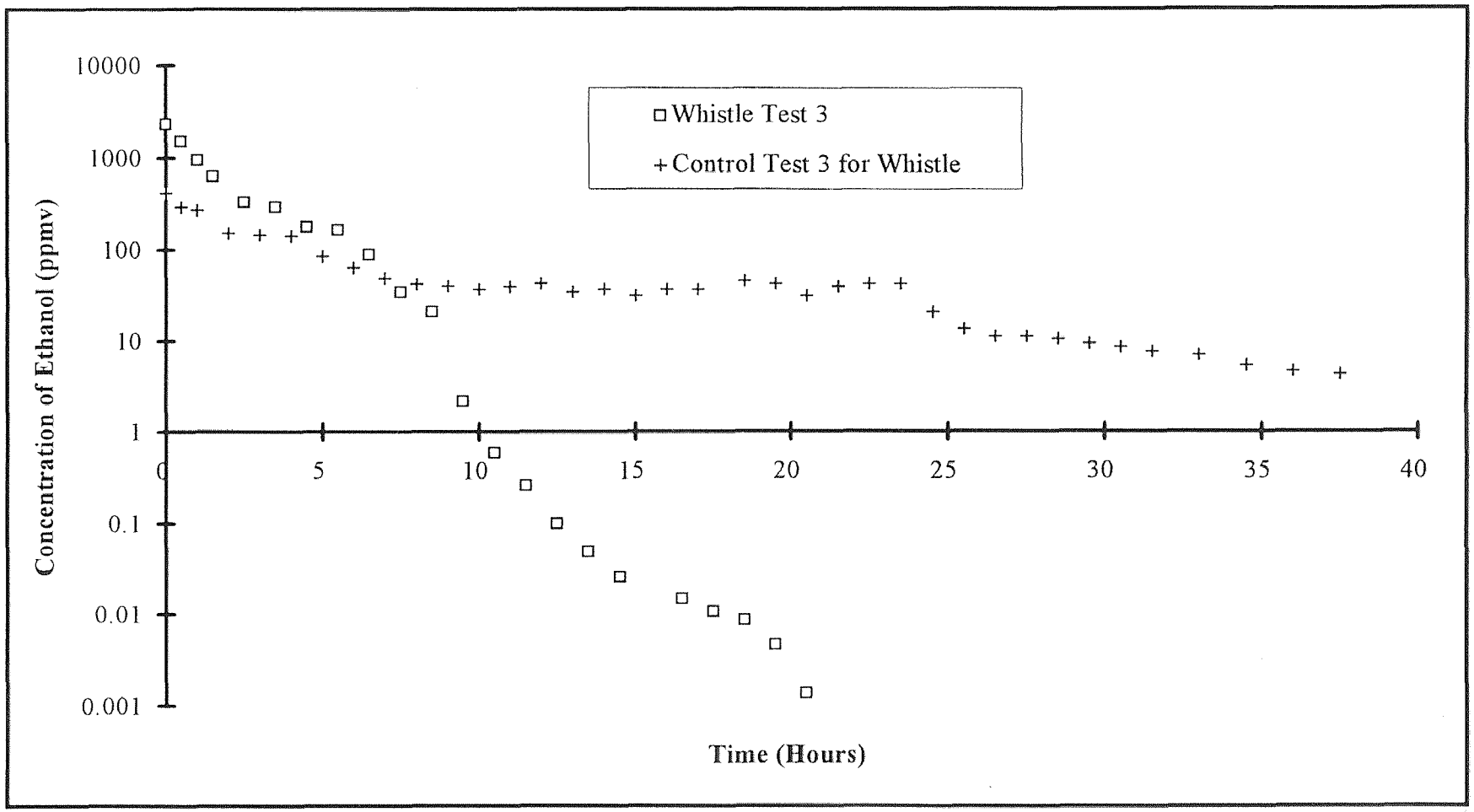

Figure 4.40 Semi Logarithmic Plot of Concentration Versus Time for Whistle Set 3

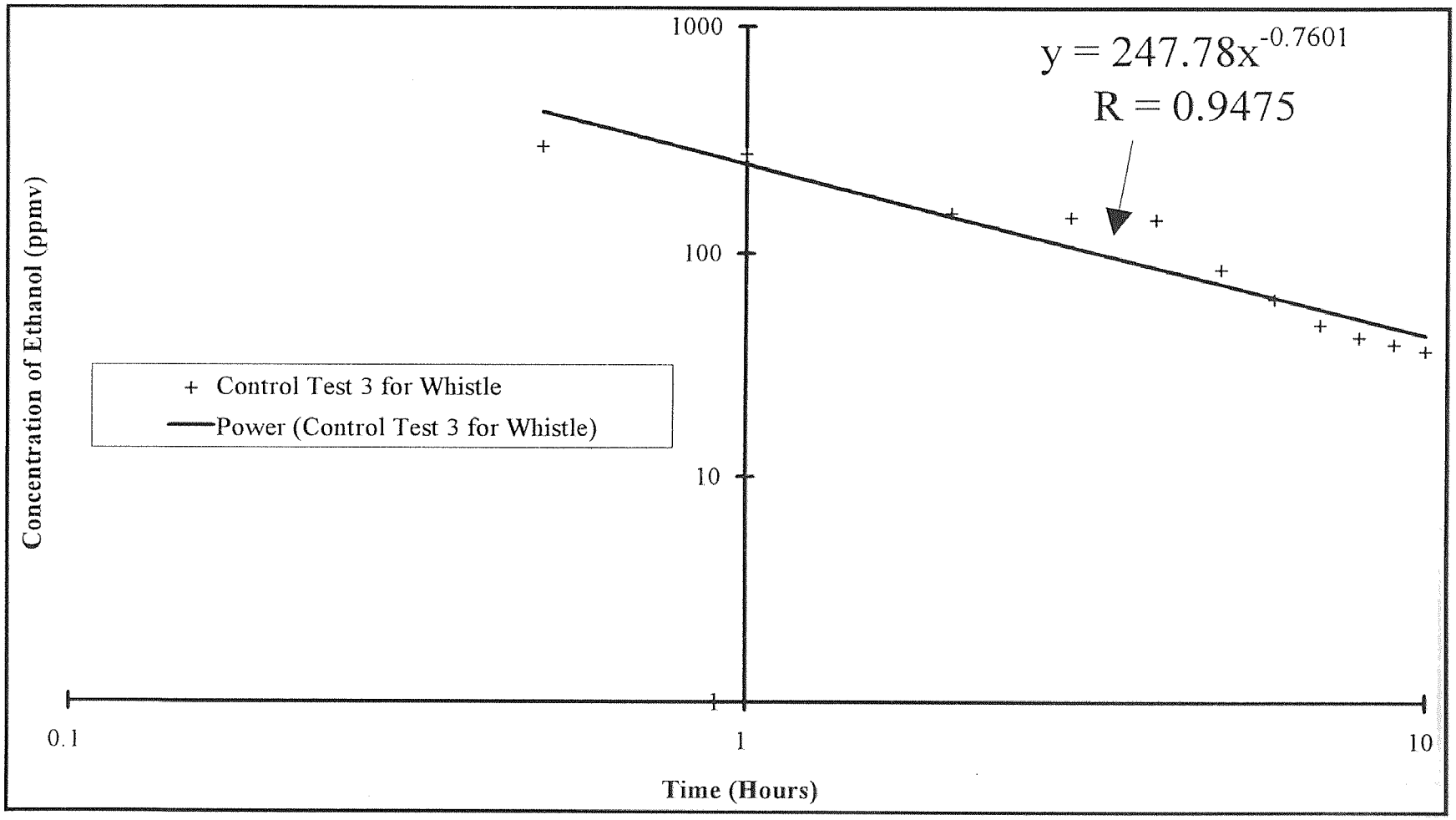

Figure 4.41 Logarithmic Curve Fit of Concentration Versus Time for Whistle Set 3 in the Transient Region

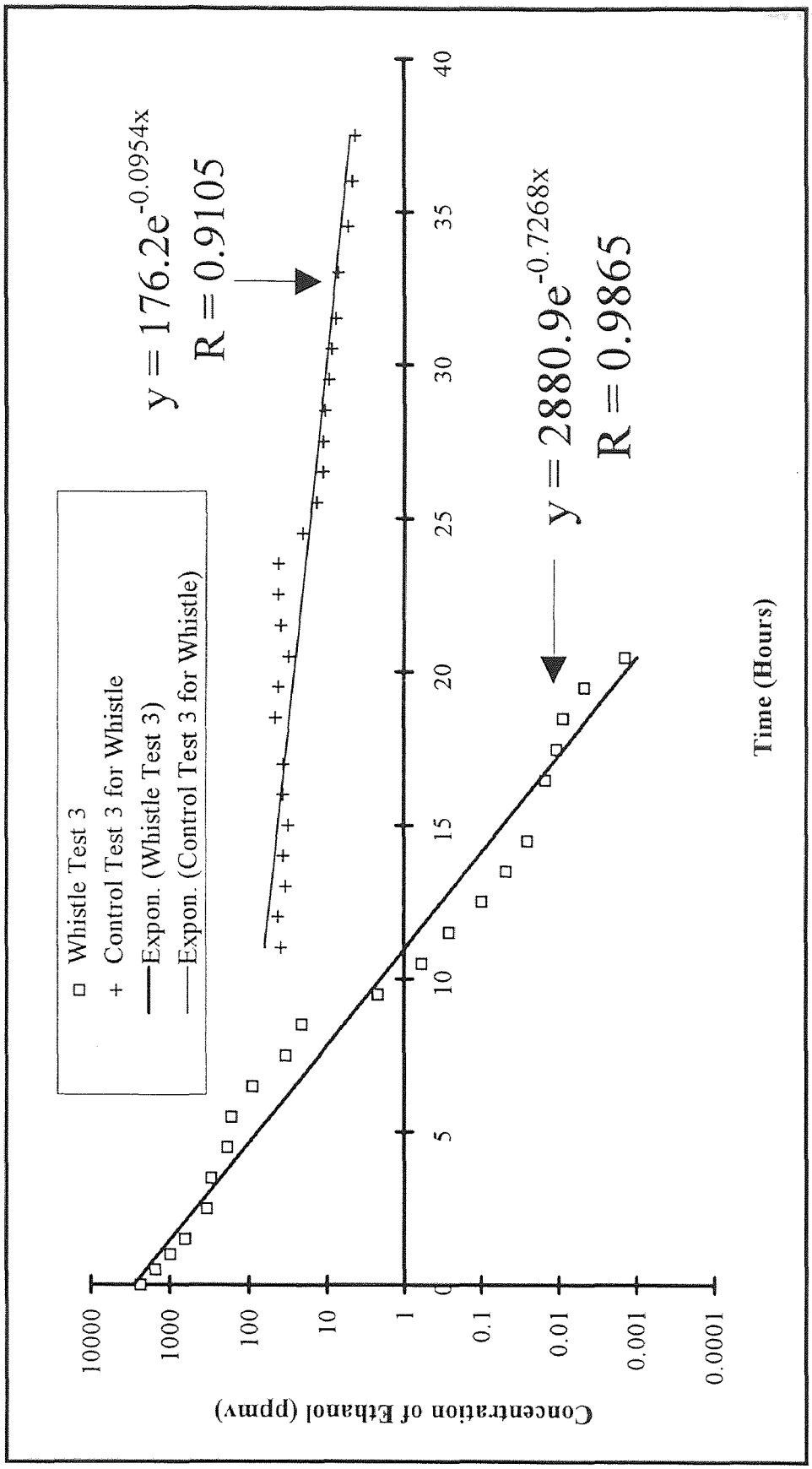

Figure 4.42 Semi Logarithmic Curve Fit of Concentration Versus Time for Siren Set 3 in the Falling Rate Region

of ultrasound with the whistle during the transient period and also significant effects during the falling rate period.

Table 4-5 Estimated Time to Reach an Asymptotic Value of 0.01 Free Moisture per Pounds of Solids for the Whistle from Figures 4.23, 4.30 and 4.37

Whistle Set Number	Time for Control Run	Time for Actual Run	Percent Reduction
	Hours	Hours	Percentage
1	>66	20	>70
2	>55	11	>80
3	>60	16	>73
Average	>60	16	>74
Range	----------	20-44	----------

An examination of the total data for concentration versus time in **Figure 4.26, 4.33** and **4.40** show that the removal of ethanol with the whistle is greater than the control case for all three runs.

A comparison of the times to reach a low concentration of 1 ppmv ethanol with the whistle are shown in **Table 4.6**. The data revealed that the whistle reduced the average

Table 4-6 Estimated Time to Reach an Concentration of 1 ppmv of Ethanol in the Vapor for the Whistle from Figures 4.27, 4.34 and 4.41

Whistle Set Number	Time for Control Run	Time for Actual Run	Percent Reduction
	Hours	Hours	Percentage
1	>33	11	>67
2	>45	9	>80
3	>40	10	>75
Average	>39	10	>74
Range	----------	9-11	----------

time to reach 1 ppmv of ethanol from greater than 39 hours to 10 hours. This difference represents a percent improvement greater than 74%. These data corroborate more rapid removal of ethanol using ultrasound with the whistle and hence potentially reducing site remediation times and cost. A similar comparison of the estimated time reduction to reach level of 1 ppmv can be obtained from **Figure 4.28**, **4.35** and **4.42**.

Table 4.7 is a summary of the slopes obtained for **Figures 4.22** through **4.42**. The first portion of the table represents the slopes of the transient region for Whistle Set 1 through 3 for the free moisture versus time curve. These slopes are averaged at the bottom of the set and the mean is compared statistically using a student t test with the control mean or baseline.

The Student's t test revealed that in the free moisture versus time curve in the transient region of the whistle sets 1 through 3 there is a significant difference between the three control Tests and the three whistle tests. The Student's t test shows that there is a 99.5% certainty that there is a statistically significant difference between whistle sets 1 through 3 and its corresponding control test in the transient part of the free moisture versus time slopes. The slopes were averaged and an average percent enhancement of 412.4% with a range of 134 to 666.3% was obtained. These results are also shown in **Table 4.7**.

The slopes in whistle set 1 through 3 in **Table 4.7** were averaged and compared in the falling rate region using a student t test. The Student's t test revealed that there is a significant difference between the slopes of the whistle sets 1-3 and their corresponding baseline in the falling rate region. The Student's t test shows that there is a 97.5% certainty that there is a difference between the mean of whistle sets 1 through 3 and the

Table 4-7 Slopes of Free Moisture Removal With Time in the Transient Region and in the Falling Rate Region for the Whistle

Transient Region				Falling Rate Region			
Siren Set Number	Slope for Control Run	Slope for Actual Run	Percent Enhancement	Siren Set Number	Slope for Control Run	Slope for Actual Run	Percent Enhancement
	Dimensionless	Dimensionless	Percentage		1/Hour	1/Hour	Percentage
1	-0.041	-0.311	666.26	1	-0.020	-0.127	534.00
2	-0.133	-0.311	133.96	2	-0.028	-0.188	572.86
3	-0.062	-0.335	437.02	3	-0.014	-0.051	258.04
Mean	-0.079	-0.319	412.41	Mean	-0.021	-0.122	454.97
Transient Region				Falling Rate Region			
Student t Calulated	Student t Published 2 tailed	Significance Level with 4 Degrees of Freedom	Significant Difference (Yes or No)	Student t Calulated	Student t Published 2 tailed	Significance Level with 4 Degrees of Freedom	Significant Difference (Yes or No)
8.285	4.604	99.500	Yes	3.649	2.776	97.500	Yes

mean of the corresponding control tests in the falling rate region for the free moisture versus time slopes. The slopes were averaged and a percent enhancement of 455.0% with a range of 258 to 572.9% was obtained. These results are also shown in **Table 4.7**

The slope of the concentration versus time for Whistle Set 1 through 3 in the transient region is presented in **Table 4.8**. A Student's t test could not be performed in this region because no transient behavior was observed for the whistle set.

The slope of the concentration versus time for whistle set 1 through 3 in the falling rate region is presented in **Table 4.8**. A Student's t test was performed on the mean slope of these 3 tests with their corresponding control tests. The Student's t test revealed that there is a 99.5% certainty that there is significant difference between the mean slopes of the whistle concentration decay versus time in the falling rate region and its corresponding control tests.

The data in **Table 4.8** show a similar analysis based upon the concentration of ethanol in the vapor. For the transient region shown in the **Figure 4.27**, **4.34** and **4.41** no comparison was made because no transient behavior was observed in the transient region for the all the whistle tests. For the falling rate shown in the **Figure 4.28**, **4.35** and **4.42** the percent enhancement based upon ethanol concentration in the effluent averaged 931.4% with a range of 661.8% to 1292.5% for the three tests.

Based upon these analyses the inclinations are that the whistle greatly improves the removal rate and reduces remediation times. The whistle also appears to be more effective than the siren under these test conditions.

Table 4-8 Slopes of Ethanol Concentration Decay With Time in the Transient Region and in the Falling Rate Region for the Whistle

Transient Region				Falling Rate Region			
Siren Set Number	Slope for Control Run	Slope for Actual Run	Percent Enhancement	Siren Set Number	Slope for Control Run	Slope for Actual Run	Percent Enhancement
	Dimensionless	Dimensionless	Percentage		1/Hour	1/Hour	Percentage
1	----------	-0.516	----------	1.00	-0.050	-0.689	1292.53
2	----------	-0.818	----------	2.00	-0.096	-0.904	839.71
3	----------	-0.760	----------	3.00	-0.095	-0.727	661.84
Mean	----------	----------	----------	Mean	-0.080	-0.773	931.36
Transient Region				Falling Rate Region			
Student t Calulated	Student t Published 2 tailed	Significance Level with 4 Degrees of Freedom	Significant Difference (Yes or No)	Student t Calulated	Student t Published 2 tailed	Significance Level with 4 Degrees of Freedom	Significant Difference (Yes or No)
----------	----------	----------	----------	10.194	4.604	99.500	Yes

4.4 Heat and Humidity Effects

To ensure that the sonic effects produced by the siren were not caused by heat generated by the siren, thermocouples were inserted in the fracture to measured the temperature of the air stream in the fracture. As described in Section 3.2, thermocouples were placed at; (1) the sound source in the fracture;(2) half way between the extraction pipe and the sound source in the fracture; and (3) either next to the extraction pipe or inside one of the extraction pipes. Temperature was not monitored in the whistle runs because there are no moving parts which can generate heat (Boucher 1958). Furthermore, the humidity of the air fed to the test cell and ultrasonic devices was monitored and found to remain constant at 28% relative humidity and room temperature.

In **Figure 4.43** the temperature versus time is presented for Siren Set 1 and the corresponding control tests at the siren sound source in the fracture. Similar data were obtained for siren set 2 and set 3. The data show that in the beginning, the temperature in the fracture is slightly lowered in the control test then it is in the siren test, but as time increases, the temperature of the two runs approach each other. This small temperature variation is possibly due to the wet bulb dry bulb effects. When the sand is wet, the temperature registered by the thermocouple is that of the liquid which is present in the fracture of the tank. As the soil at the fracture dries up, the temperature measured by the thermocouple is the dry bulb temperature, or the actual air temperature. Based on these data it was determined that for all experiments to follow, isothermal operation was a valid assumption.

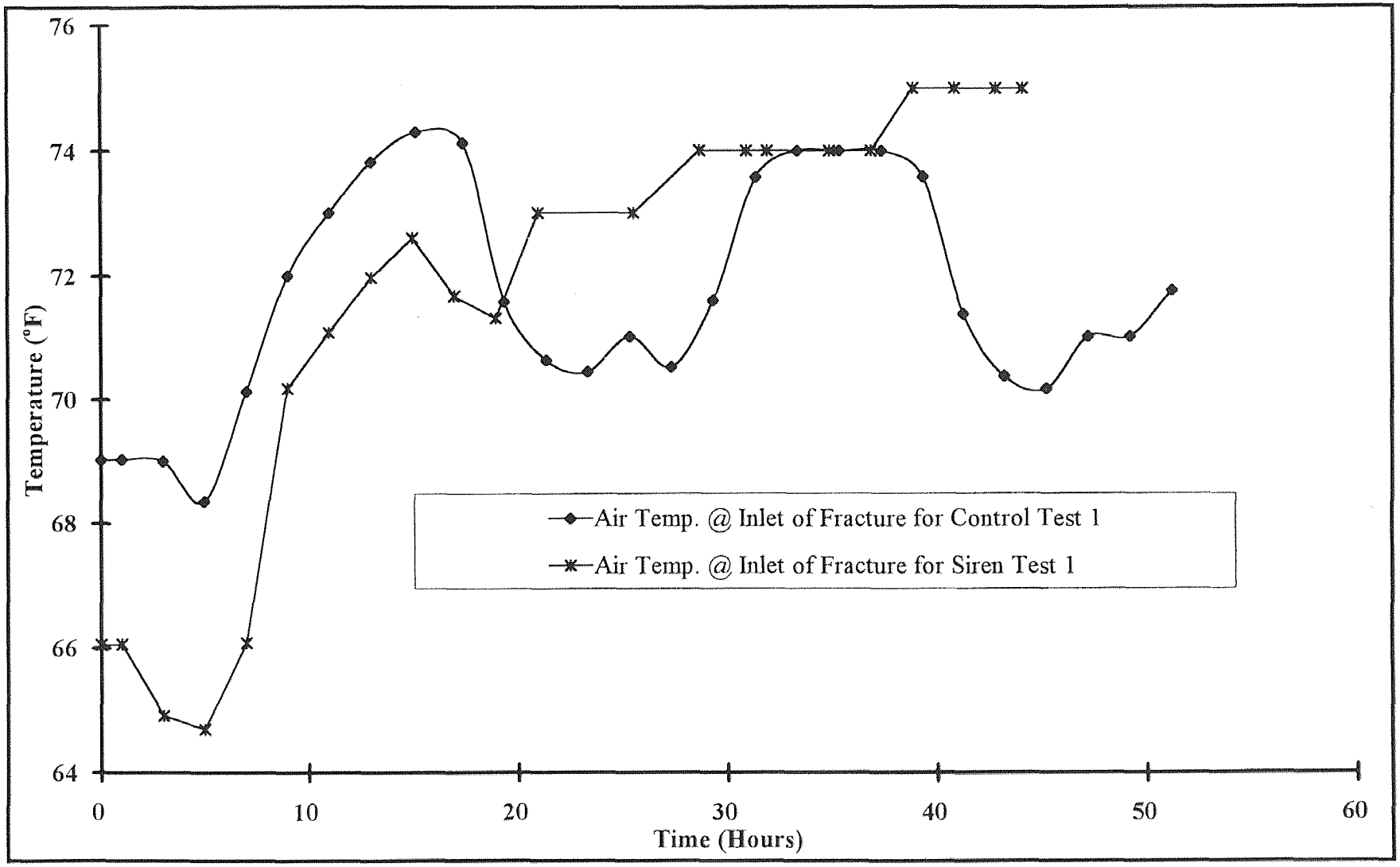

Figure 4.43 Air Temperature at Inlet of Fracture for Siren Test 1 and Control Test 1 Versus Time

CHAPTER 5

5. CONCLUSIONS AND RECOMMENDATIONS

The investigation into air coupled sonic energy in a soil fracture with a siren and a whistle has revealed that overall, sonic energy enhances the removal of volatile organic contaminants, in our case ethanol, as well as water out of fractures.

5.1 Conclusions for the Siren Type Device

The conclusions for the siren are:

1. In every case the siren showed a faster removal rate and shorter remediation time to reach asymptotic levels.
2. Data showing the removal of ethanol corroborate a faster removal rate and shorter remediation time using the siren.
3. The free moisture versus time data show a 39.1% improvement in the transient region and a 69% improvement in the falling rate region.
4. The concentration of ethanol versus time data show a 62.9% improvement for the transient region and a 192% improvement in the falling rate region.
5. However, a comparison of means of the free moisture content of the bed for a sample size of three shows no significant difference at 90% confidence level.
6. A comparison of means using the concentration of ethanol versus time data shows a significant difference at 98.75% confidence level that the siren improved the removal rate of ethanol.
7. The data show that the siren reduces the time required to reach asymptotic value of about 0.01 moisture free moisture or about 91% removal from an average of 50 hours

(range of 43 to 56 hours) for the control tests down to 32 hours (range of 21 to 53 hours) for the siren tests. This represents a 37% improvement.

8. The data also show that the siren reduces the time required to reach a value of 1 ppmv ethanol from an average greater than 42 hours for the control tests down to 24 hours (range of 18 to 25 hours) for the siren tests. This represents greater than 41% improvement.

5.2 Conclusions for the Whistle Type Device

The conclusion for the whistle are:

1. In every case the whistle showed a faster removal rate and shorter remediation time to reach asymptotic levels.
2. Data showing the removal of ethanol corroborate a faster removal rate and shorter remediation time using the siren.
3. The free moisture versus time data show a 412.4% improvement in the transient region and a 455% improvement in the falling rate region.
4. The concentration of ethanol versus time data show a 931.4% improvement for the falling rate period. No calculation was made for the transient region
5. A comparison of means of the free moisture content of the bed for a sample size of three shows a significant difference at 99.5% confidence for the transient region and at 95% confidence for the falling rate region.
6. A comparison of means using the concentration of ethanol versus time data shows a significant difference at 99.5% confidence level that the siren improved the removal rate of ethanol.

7. The data show that the whistle reduces the time required to reach asymptotic value of about 0.01 moisture free moisture or about 91% removal from an average greater than 60 hours for the control tests down to 16 hours (range of 20 to 44 hours) for the whistle tests. This represents greater than 74% improvement.
8. The data also show that the whistle reduces the time required to reach a value of 1 ppmv ethanol from an average greater than 39 hours for the control tests down to 10 hours (range of 9 to 11 hours) for the whistle tests. This also represents greater than 74% improvement.

5.3 Recommendations

It is recommended that more tests should be made to compare the control test for the siren with the siren test to establish a statistical difference. Tests should be run to find the attenuation coefficients in different types of soils and also to establish the radius of influence of both the siren type device and the whistle type device. Based upon the attenuation coefficient obtained and the removal enhancement recorded the optimum power levels should be obtained at which the siren or whistle should operate.

Most researchers have focused on enhancing the removal rate of water in an airborne sonic field when drying solids. Thus far, little work has been perforemed enhancing the removal rate using airborne sonic energy in tight soils and bedrock. It is recommended that this process should be studied more closely.

It is also known that sonic and ultrasonic energy are capable of enhancing the reaction rate of chemical reaction in an aqueous phase by a phenomenon known as cavitation. Based upon this fact, it is recommended that reaction rates of aqueous chemical reactions capable of changing toxic chemicals that are trapped in soils into non-

toxic forms should be studied in a fracture. This study could first be accomplished in test cells containing an artificial fracture in saturated contaminated soil. Ultrasonic energy should be applied in the immediate fracture region and changes monitored with the proper instrumentation.

Eventually, an extensive field test should be performed with a scaled up version of the two devices to show whether the process will work at a field level.. During these extensive field tests, attenuation coefficients should be measured both in the laboratory test cells and in the field. Presently, as a result of this study, preliminary field tests have been planned using these sonic devices to remove trichloroethylene from a toxic site located in Hillsborough, New Jersey.

All the above recommendations should be incorporated into a mathematical model which is able to predict the expected amount of enhancement and the effective range of the sonic field for a sonic device. The model must take into account the soil type, the contaminant type, the distribution of the contaminant and the fracture aperture.

APPENDIX A

SAMPLE CALCULATIONS AND TABLES FOR MOISTURE VERSUS TIME FOR SIREN TESTS

In this appendix, the data for the siren test and the corresponding control test are presented. First, the experimental condition is given, followed by a sample calculation on how the packing height was obtained. Finally, all the moisture versus time data is tabulated in a 2 hour average and sample calculation will be made on how the data were converted to moisture content in the bed.

A.1 Experimental Conditions for Siren Tests and Control Tests

In the following table, the experimental conditions for the siren as well as the experimental conditions for the the control run will be described. The first table, **Table A.1**, describes the experimental conditions in which the siren and the control run were operated.

Table A.1 Experimental Conditions for the Siren Runs and Control Runs

Experimental Parameter	Experimental Conditions for Siren Tests	Experimental Conditions for Siren Control Tests
Inlet Air Volumetric Flow	7 SCFM @ 40-50 PSIG	7 SCFM @ 40-50 PSIG
Inlet Outlet Volumetric Flow	7 SCFM @ 80 Inches of Water	7 SCFM @ 80 Inches of Water
Fracture Material	Geotextile 1/2 inch Thick	Geotextile 1/2 inch Thick
Fracture Approximate Area	1.68 ft^2	1.68 Ft^2
Packing Density	100 lbs/ ft^3	100 lbs/ ft^3
Liquid Content of Soil	10% by Weight	10% by Weight
Contaminants	10 % Ethanol and 90% Water	10 % Ethanol and 90% Water
Siren Frequency	18 kHz	No Sound Applied
Siren Sound Level	125 Db	No Sound Applied

A.2 Experimental Packing Calculations

The tanks were packed to a packing density of 100 pounds per cubic foot and 10% moisture content. This was accomplished by first fixing the amount of dry sand to 100 pounds and then calculating the total mass of the bed with the moisture. The total mass of the bed with the moisture is calculated by dividing the mass of the dry sand by .9 which is the fraction of the dry sand:

$$\frac{100\text{lbs of Dry Sand}}{.90} = 111.11\text{lbs Total Mass of Bed} \qquad \text{(A.1).}$$

From Equation A.1,100 pounds of dry sand is used and the balance is 11.11 pounds of moisture. The moisture is broken down into 90% water and 10% ethanol by weight.

To obtain the bed volume, the total weight of the bed was divided by the target density which was 100 pounds per cubic foot.

$$\frac{111.11\text{ lb of Total Bed}}{100\text{ lb of Total Bed / ft}^3} = 1.11\text{ ft}^3 \qquad \text{(A.2).}$$

Since the siren, the 1/2 inch geotextile fracture and the two extraction pipes were buried in the bed, the volume of these devices were calculated and added to the volume calculated in Equation A.2. The volume of the siren is 0.065 ft^3, the volume of the two extraction pipes is 0.00920 ft^3 and the volume of the fracture is 0.035 ft^3. Therefore, the total volume of the bed is the sum of all these volumes:

Total Volume of Bed = 1.11 ft^3 + 0.065 ft^3 + 0.00920 ft^3 + 0.035 ft^3 = 1.23 ft^3 (A.3).

By dividing the total volume of the bed by the cross sectional area of the bed which is 0.84 ft^2, the bed height is obtained. Therefore, in our case, the bed height is,

$$\frac{1.23\ \text{ft}^3\ \text{Total Bed Volume}}{0.84\ \text{ft}^3\ \text{of Cross Sectional Area}} = 1.46\ \text{ft} = 17.6\ \text{inches} \qquad \text{(A.4)}.$$

The bed height was measured and was 18.0 inches.

A.3 Moisture in the bed Versus Time Sample Calculations and Tables

In **Tables A.2** to **A.4** the laboratory data are presented for Siren Sets 1 to 3, respectively, in a 238 point average which is approximately a two hour interval. In the fisrt column and in the fourth column of Siren Set 1, the elapsed times for the control run and siren run are presented in a two hour interval. In column 2 for the control run and column 5 for the siren run the total weight of moisture in the test cell is presented in a 238 point average, which corresponds with the time presented. In column 3 and column 6, the moisture in the tank per pound of sand is presented for the control run and the siren run respectively. These ratios are obtained by dividing the moisture in column 2 and column 4 by the amount of sand in the bed which is held constant at 100 pounds. The following is a sample calculation of the sand to moisture content presented in column 3 for the first point in the control run:

$$\frac{11.11\ \text{lbs of Moisture}}{100\ \text{lbs of Sand}} = 0.11 \qquad \text{(A.5)}$$

Table A.2 Results of Test 1: Total Weight of Moisture in Tank for Control Run and Siren Run
Note: Data was Averaged 0n a 238 Point Interval for Time and Moisture Weight.

Control Test 1			Siren Test 1		
Elapsed Time	Total Weight of Moisture in Tank	Sand to Moisture Content	Elapsed Time	Total Weight of Moisture in Tank	Sand to Moisture Content
Hours	Lbs	Lbs Moisture / Lbs Sand	Hours	Lbs	Lbs Moisture / Lbs Sand
0	11.11	1.11E-01	0	11.11	1.11E-01
1	8.60	8.60E-02	1	8.20	8.20E-02
3	7.31	7.31E-02	3	6.49	6.49E-02
5	6.81	6.81E-02	5	5.84	5.84E-02
7	6.39	6.39E-02	7	5.46	5.46E-02
9	5.93	5.93E-02	9	5.02	5.02E-02
11	5.56	5.56E-02	11	4.53	4.53E-02
13	5.47	5.47E-02	13	3.74	3.74E-02
15	5.05	5.05E-02	15	2.66	2.66E-02
17	4.65	4.65E-02	17	1.93	1.93E-02
19	4.20	4.20E-02	19	1.17	1.17E-02
21	3.74	3.74E-02	21	0.77	7.74E-03
23	3.02	3.02E-02	26	0.49	4.95E-03
25	2.37	2.37E-02	29	0.45	4.49E-03
27	1.87	1.87E-02	31	0.46	4.58E-03
29	1.66	1.66E-02	32	0.66	6.60E-03
31	1.35	1.35E-02	35	0.74	7.39E-03
33	1.26	1.26E-02	37	0.64	6.41E-03
35	1.35	1.35E-02	39	0.58	5.82E-03
37	1.31	1.31E-02	41	0.36	3.64E-03
39	1.22	1.22E-02	43	0.11	1.06E-03
41	1.00	9.97E-03	44	-0.07	-7.35E-04
43	0.87	8.70E-03	--------	--------	--------
45	0.41	4.13E-03	--------	--------	--------
47	0.05	5.05E-04	--------	--------	--------
49	0.00	0.00E+00	--------	--------	--------
51	0.00	0.00E+00	--------	--------	--------

Table A.3 Results of Test 2: Total Weight of Moisture in Tank for Control Run and Siren Run

Note: Data was Averaged 0n a 238 Point Interval for Time and Moisture Weight.

Control Test 2			Siren Test 2		
Elapsed Time	Weight of Moisture in Tank	Sand to Moisture Content	Elapsed Time	Weight of Moisture in Tank	Sand to Moisture Content
Hours	Lbs	Lbs Moisture / Lbs Sand	Hours	Lbs	Lbs Moisture / Lbs Sand
0	11.11	1.11E-01	0	11.11	1.11E-01
1	9.04	9.04E-02	1	8.20	8.20E-02
3	8.13	8.13E-02	3	6.49	6.49E-02
5	7.51	7.51E-02	5	5.84	5.84E-02
7	7.13	7.13E-02	7	5.46	5.46E-02
9	6.67	6.67E-02	9	5.02	5.02E-02
11	6.45	6.45E-02	11	4.53	4.53E-02
13	6.08	6.08E-02	13	3.74	3.74E-02
15	5.69	5.69E-02	15	2.66	2.66E-02
17	5.31	5.31E-02	17	1.93	1.93E-02
19	4.92	4.92E-02	19	1.17	1.17E-02
21	4.55	4.55E-02	21	0.77	7.74E-03
23	4.12	4.12E-02	26	0.49	4.95E-03
25	3.76	3.76E-02	29	0.45	4.49E-03
27	3.49	3.49E-02	31	0.46	4.58E-03
29	3.25	3.25E-02	32	0.66	6.60E-03
31	2.88	2.88E-02	35	0.74	7.39E-03
33	2.68	2.68E-02	37	0.64	6.41E-03
35	2.53	2.53E-02	39	0.58	5.82E-03
37	2.46	2.46E-02	41	0.36	3.64E-03
39	2.34	2.34E-02	43	0.11	1.06E-03
41	2.15	2.15E-02	44	0.00	0.00E+00
43	2.05	2.05E-02	--------	--------	--------
45	1.91	1.91E-02	--------	--------	--------
47	1.78	1.78E-02	--------	--------	--------
49	1.55	1.55E-02	--------	--------	--------
51	1.47	1.47E-02	--------	--------	--------
53	1.28	1.28E-02	--------	--------	--------
53	1.28	1.28E-02	--------	--------	--------

Table A.4 Results of Test 3: Total Weight of Moisture in Tank for Control Run and Siren Run
Note: Data was Averaged 0n a 238 Point Interval for Time and Moisture Weight.

Control Test 3			Siren Run Test 3		
Elapsed Time	Weight of Moisture in Tank	Sand to Moisture Content	Elapsed Time	Weight of Moisture in Tank	Sand to Moisture Content
Hours	Lbs	Lbs Moisture / Lbs Sand	Hours	Lbs	Lbs Moisture / Lbs Sand
0	11.11	1.11E-01	0	11.11	1.11E-01
1	10.36	1.04E-01	1	10.05	1.01E-01
3	9.75	9.75E-02	3	9.20	9.20E-02
5	9.38	9.38E-02	5	8.68	8.68E-02
7	8.97	8.97E-02	7	7.99	7.99E-02
9	8.64	8.64E-02	9	7.58	7.58E-02
11	8.30	8.30E-02	11	7.07	7.07E-02
13	7.92	7.92E-02	13	6.46	6.46E-02
15	7.61	7.61E-02	15	5.92	5.92E-02
17	7.24	7.24E-02	17	5.27	5.27E-02
19	6.90	6.90E-02	19	4.69	4.69E-02
21	6.50	6.50E-02	21	4.09	4.09E-02
23	6.06	6.06E-02	23	3.66	3.66E-02
25	5.87	5.87E-02	25	3.33	3.33E-02
27	5.64	5.64E-02	27	3.11	3.11E-02
29	5.29	5.29E-02	29	2.88	2.88E-02
31	5.04	5.04E-02	31	2.73	2.73E-02
33	4.88	4.88E-02	33	2.91	2.91E-02
35	4.78	4.78E-02	35	2.79	2.79E-02
37	4.65	4.65E-02	37	2.66	2.66E-02
39	4.54	4.54E-02	39	2.51	2.51E-02
41	4.26	4.26E-02	41	2.52	2.52E-02
43	4.00	4.00E-02	43	2.46	2.46E-02
45	3.88	3.88E-02	45	2.30	2.30E-02
47	3.74	3.74E-02	50	2.05	--------
49	3.65	3.65E-02	52	1.91	--------
51	3.50	3.50E-02	54	1.93	--------
53	3.36	3.36E-02	56	1.86	--------
55	3.29	3.29E-02	58	1.85	--------
57	3.28	3.28E-02	58	1.85	--------

APPENDIX B

TABLES FOR ETHANOL CONCENTRATION VERSUS TIME FOR SIREN TESTS

In **Tables B.1** to **B.3** the concentration of ethanol in parts per million volume is reported for the siren sets 1 to 3. In columns 1 and 4 are the elapsed times at which the gas chromatograph samples were taken during the course of the run for the control and siren s runs respectively. The integrated data are shown in columns 2 and 5 for the control run and the siren run data respectively. The integrated data in columns 2 and 5 for the control runs and the siren run data are converted to concentration through the use of the correlation equation which appears in **Figure 3.5** and the data are converted into parts per million volume and presented in columns 3 and 6.

Table B.1 Results of Gas Chromatograph Analysis of Test 1 for the Control and Siren Runs

	Control Test 1		Siren Test 1		
Elapsed Time	Integrated Area of Ethanol	Outlet Conc. of Ethanol	Elapsed Time	Integrated Area of Ethanol	Outlet Conc. of Ethanol
Hours	Volt*Second	ppmv	Hours	Volt*Second	ppmv
0.15	1.57E+04	2.25E+03	0.1	2.59E+04	4.11E+03
0.25	7.74E+03	9.56E+02	0.333	1.34E+04	1.85E+03
0.5	3.84E+03	4.10E+02	0.5	7.38E+03	9.03E+02
0.75	2.79E+03	2.78E+02	0.75	5.88E+03	6.86E+02
1	2.15E+03	2.03E+02	1	4.24E+03	4.62E+02
1.25	1.81E+03	1.65E+02	1.25	3.20E+03	3.28E+02
1.5	1.57E+03	1.39E+02	1.5	2.48E+03	2.42E+02
1.75	1.40E+03	1.21E+02	1.75	1.92E+03	1.77E+02
2	1.24E+03	1.04E+02	2	1.83E+03	1.68E+02
2.25	1.17E+03	9.77E+01	2.25	1.43E+03	1.25E+02
2.5	1.12E+03	9.30E+01	2.5	1.16E+03	9.70E+01
2.75	1.18E+03	9.84E+01	2.75	9.58E+02	7.67E+01
3.25	1.15E+03	9.53E+01	3	8.07E+02	6.23E+01
4.25	1.09E+03	8.97E+01	3.25	7.30E+02	5.52E+01
5.25	9.99E+02	8.06E+01	3.75	6.18E+02	4.51E+01
6.25	8.98E+02	7.09E+01	4	5.49E+02	3.92E+01
7.25	8.30E+02	6.45E+01	4.25	5.29E+02	3.74E+01
9.25	8.15E+02	6.31E+01	4.5	4.87E+02	3.39E+01
9.75	7.99E+02	6.16E+01	4.75	4.86E+02	3.38E+01
10	7.84E+02	6.02E+01	5	5.02E+02	3.52E+01
14	6.99E+02	5.24E+01	5.25	4.99E+02	3.49E+01
15.25	7.06E+02	5.30E+01	9.33	3.61E+02	2.36E+01
16.25	7.05E+02	5.29E+01	9.5	3.50E+02	2.27E+01
17.25	6.82E+02	5.08E+01	10.5	3.20E+02	2.04E+01
18.25	6.31E+02	4.63E+01	11.5	2.87E+02	1.79E+01
21.25	5.32E+02	3.76E+01	12.5	3.06E+02	1.93E+01
23.25	4.03E+02	2.69E+01	13.5	3.33E+02	2.14E+01
25.25	3.19E+02	2.03E+01	13.75	3.44E+02	2.22E+01
28.5	1.99E+02	1.15E+01	15.75	1.99E+02	1.15E+01
30.25	1.58E+02	8.69E+00	18.5	9.12E+00	2.78E-01
32.25	1.12E+02	5.74E+00	23	1.60E+00	3.40E-02

Table B.1 Results of Gas Chromatograph Analysis of Test 1 for the Control and Siren Runs (Continued)

	Control Test 1		Siren Test 1		
Elapsed Time	Integrated Area of Ethanol	Outlet Conc. of Ethanol	Elapsed Time	Integrated Area of Ethanol	Outlet Conc. of Ethanol
Hours	Volt*Second	ppmv	Hours	Volt*Second	ppmv
44.25	5.32E+02	3.76E+01	29.5	1.68E-01	2.23E-03
46.25	4.03E+02	2.69E+01	33	1.04E-01	1.25E-03
48.25	3.19E+02	2.03E+01	33.5	5.76E-02	6.13E-04
51.25	1.99E+02	1.15E+01	34.5	4.83E-02	4.95E-04
53.25	1.58E+02	8.69E+00	35.5	4.38E-02	4.40E-04
55.25	1.12E+02	5.74E+00	36.5	4.88E-02	5.01E-04
56.5	9.42E+01	4.66E+00	37.5	2.30E-02	2.03E-04
57.25	8.65E+01	4.20E+00	40.5	3.71E-02	3.61E-04
60.25	5.52E+01	2.44E+00	42.5	1.77E-02	1.47E-04
62.25	3.90E+01	1.60E+00	44.5	1.96E-02	1.67E-04
67.25	1.78E+01	6.25E-01	47.25	3.77E-03	2.28E-05
72.25	3.90E+00	9.95E-02	48.5	2.73E-03	1.55E-05
----------	----------	----------	49.5	5.83E-03	3.86E-05
----------	----------	----------	52.25	1.92E-03	1.01E-05

Table B.2 Results of Gas Chromatograph Analysis of Test 2 for the Control and Siren Runs

Control Test 2			Siren Test 2		
Elapsed Time	Integrated Area of Ethanol	Outlet Conc. of Ethanol	Elapsed Time	Integrated Area of Ethanol	Outlet Conc. of Ethanol
Hours	Volt*Seconds	ppmv	Hours	Volt*Seconds	ppmv
0	3.01E+06	5.09E+02	0	6.92E+02	3.45E+03
0.5	5.08E+05	1.20E+02	0.33	1.98E+02	7.61E+02
1	4.65E+05	1.12E+02	0.67	1.38E+02	4.93E+02
1.5	2.96E+05	7.73E+01	1	1.04E+02	3.51E+02
2.5	2.85E+05	7.49E+01	1.33	8.28E+01	2.66E+02
4	2.89E+05	7.57E+01	1.67	7.06E+01	2.19E+02
5.5	2.48E+05	6.69E+01	2	6.36E+01	1.93E+02
7	2.54E+05	6.81E+01	2.33	5.68E+01	1.69E+02
8.5	2.08E+05	5.81E+01	2.67	5.27E+01	1.54E+02
10	2.04E+05	5.72E+01	3	4.87E+01	1.40E+02
11.5	2.09E+05	5.81E+01	3.33	4.74E+01	1.35E+02
13	1.51E+05	4.47E+01	5.33	3.73E+01	1.01E+02
14.5	1.54E+05	4.54E+01	7.33	3.00E+01	7.81E+01
16	1.30E+05	3.95E+01	9.33	2.67E+01	6.76E+01
17.5	1.15E+05	3.59E+01	11.33	2.99E+01	7.76E+01
19	1.03E+05	3.27E+01	13.33	2.32E+01	5.70E+01
20.5	1.03E+05	3.29E+01	15.33	2.16E+01	5.24E+01
22	8.46E+04	2.79E+01	17.33	1.68E+01	3.87E+01
23.5	1.02E+05	3.24E+01	19.33	1.68E+01	3.87E+01
25	7.28E+04	2.47E+01	21.33	1.20E+01	2.58E+01
26.5	8.41E+04	2.78E+01	23.33	8.04E+00	1.59E+01
28	5.43E+04	1.95E+01	25.33	3.71E+00	6.25E+00
29.5	2.30E+04	9.69E+00	27.33	5.74E-01	3.26E+00
31	2.80E+04	1.14E+01	29.33	1.21E-01	1.03E+00
32.5	1.15E+04	5.53E+00	31.11	1.72E-01	9.21E-01
34	1.14E+04	5.48E+00	33.333	1.53E-01	8.13E-01
35.5	1.24E+04	5.84E+00	41.33	1.38E-01	6.56E-01
37	1.19E+04	5.67E+00	43.33	7.44E-02	1.00E-01
38.5	1.27E+04	5.97E+00	45.33	2.40E-03	1.54E-01
40	1.10E+04	5.31E+00	47.33	0.00E+00	1.33E-01
41.5	1.99E+04	8.59E+00	49.33	0.00E+00	1.17E-01

Table B.3 Results of Gas Chromatograph Analysis of Test 3 for the Control and Siren Runs

Control Test 3			Siren Test 3		
Elapsed Time	Integrated Area of Ethanol	Outlet Conc. of Ethanol	Elapsed Time	Integrated Area of Ethanol	Outlet Conc. of Ethanol
Hours	Volt*Second	ppmv	Hours	Volt*Second	ppmv
0	1.03E+02	3.47E+02	0	5.75E+02	2.76E+03
0.33	9.87E+01	3.28E+02	1.5	7.46E+01	2.34E+02
0.67	8.68E+01	2.81E+02	3	4.66E+01	1.33E+02
1	7.40E+01	2.32E+02	4.5	4.14E+01	1.15E+02
1.33	6.86E+01	2.12E+02	6	2.59E+01	1.02E+02
2.33	4.56E+01	1.29E+02	7.5	2.29E+01	9.01E+01
3.33	3.52E+01	9.47E+01	9	2.16E+01	8.50E+01
4.33	3.18E+01	8.35E+01	10.5	2.09E+01	8.21E+01
6.33	2.36E+01	5.84E+01	12	2.01E+01	7.91E+01
8.33	2.19E+01	5.32E+01	14.5	2.99E+01	7.76E+01
10.33	2.11E+01	5.09E+01	15.5	6.50E+00	1.23E+01
12.33	2.00E+01	4.78E+01	17.5	3.91E+00	6.66E+00
14.33	1.74E+01	4.05E+01	19.5	4.85E+00	8.64E+00
16.33	1.35E+01	2.98E+01	21.5	3.45E+00	5.71E+00
18.33	8.99E+00	1.82E+01	23.5	1.47E+00	2.04E+00
20.33	4.18E+00	7.22E+00	25.5	2.61E-01	1.025
22.33	3.93E+00	6.71E+00	27.5	1.40E-01	0.5514
24.33	4.65E+00	8.21E+00	29.5	4.01E-02	0.1578
26.33	4.53E+00	7.96E+00	----------	----------	----------
28.33	3.18E+00	5.19E+00	----------	----------	----------
30.33	2.89E+00	4.62E+00	----------	----------	----------
32.33	2.94E+00	4.72E+00	----------	----------	----------
34.33	2.47E+00	3.83E+00	----------	----------	----------
36.33	1.83E+00	2.67E+00	----------	----------	----------
38.33	1.80E+00	2.61E+00	----------	----------	----------
40.33	1.12E+00	1.47E+00	----------	----------	----------
44.33	1.81E-01	8.81E-01	----------	----------	----------
46.33	7.32E-01	8.33E-01	----------	----------	----------
48.33	7.00E-01	3.46E-01	----------	----------	----------
50.33	3.38E-01	#NUM!	----------	----------	----------

APPENDIX C

SAMPLE CALCULATIONS AND TABLES FOR MOISTURE VERSUS TIME FOR WHISTLE TESTS

In this appendix, the data for the whistle test and the corresponding control test is presented. First, the experimental condition is given, followed by a sample calculation on how the packing height was obtained. Finally, all the moisture versus time data is tabulated in a 2 hour average and sample calculation will be made on how the data were converted to moisture content in the bed.

C.1 Experimental Conditions for Whistle Tests and Control Tests

In the following table, the experimental conditions for the whistle as well as the experimental conditions for the control run will be described. The first table, **Table C.1**, describes the experimental conditions in which the whistle and the control run were operated.

Table C.1 Experimental Conditions for the Whistle Runs and Control Runs

Experimental Parameter	Experimental Conditions for Whistle Test	Experimental Conditions for Whistle Control Test
Inlet Air Volumetric Flow	7 SCFM @ 35 PSIG	7 SCFM @ 35 PSIG
Inlet Outlet Volumetric Flow	12.5 SCFM @ 80 Inches of Water	12.5 SCFM @ 80 Inches of Water
Fracture Material	Geotextile 1/2 inch Thick	Geotextile 1/2 inch Thick
Fracture Approximate Area	1.68 ft^2	1.68 Ft^2
Packing Density	100 lbs/ ft^3	100 lbs/ ft^3
Liquid Content of Soil	10% by Weight	10% by Weight
Contaminants	10 % Ethanol and 90% Water	10 % Ethanol and 90% Water
Whistle Frequency	11 kHz	No Sound Applied
Whistle Sound Level	160 Db	No Sound Applied

C.2 Experimental Packing Calculations

The tanks were packed to a packing density of 100 pounds per square inch and 10% moisture content. This was accomplished by first fixing the amount of dry sand to 100 pounds and then calculating the total mass of the bed with the moisture. The total mass of the bed with the moisture is calculated by dividing the mass of the dry sand by .9 which is the fraction of the dry sand:

$$\frac{100\text{lbs of Dry Sand}}{.90} = 111.11\text{lbs Total Mass of Bed} \qquad \text{(C.1)}$$

From Equation A.1 100 pounds of dry sand is used and the balance is 11.11 pounds of moisture. The moisture is broken down into 90% water and 10% ethanol by weight.

To obtain the bed volume, the total weight of the bed was divided by the target density which was 100 pounds per cubic foot.

$$\frac{111.11\text{ lb of Total Bed}}{100\text{ lb of Total Bed / ft}^3} * = 1.11\text{ ft}^3 \qquad \text{(C.2)}$$

Since the whistle, the 1/2 inch geotextile fracture, the extraction pipe and the feed hose were buried in the bed, the volume of these pieces of equipment were calculated and added to the volume calculated in Equation C.2. The volume of the whistle was not calculated because it is relatively small. The volume of the extraction pipe and the feed hose is 0.00920 ft^3 and the volume of the fracture is 0.035 ft^3. Therefore the total volume of the bed is the sum of all these volumes:

$$\text{Total Volume of Bed} = 1.11\text{ ft}^3 + + 0.00920\text{ ft}^3 + 0.035\text{ ft}^3 = 1.15\text{ ft}^3 \qquad \text{(C.3)}$$

By divide the total volume of the bed by the cross sectional area of the bed which is 0.84 ft^2, the bed height is obtained. There for in our case, the bed height is,

$$\frac{1.15\ ft^3\ \text{Total Bed Volume}}{0.84\ ft^3\ \text{of Cross Sectional Area}} = 1.36\ ft = 16.4\ in. \qquad (C.4)$$

The bed height was measured and was 16.0 inches.

C.3 Moisture in the bed Versus Time Sample Calculations and Tables

In **Tables C.2** to **C.4** the laboratory data is presented for siren sets 1 to3, respectively, in a 238 point average which is approximately a two hour interval. In the first column and in the fourth column of whistle set 1, the elapsed times for the control run and whistle run is present in a two hour interval. In column 2 for the control run and column 5 for the whistle run the total weight of moisture in the test cell is presented in a 238 point average, which corresponds with the time presented. In column 3 and column 6, the moisture in the tank per sand content is presented for the control run and the whistle run respectively. This ratios are obtained by dividing the moisture in column 2 and column 3 by the amount of sand in the bed which is held constant at 100 pounds. The following is a sample calculation of the sand to moisture content presented in column 3 for the first point in the control run:

$$\frac{11.11\ \text{lbs of Moisture}}{100\ \text{lbs of Sand}} = 0.11 \qquad (C.5)$$

Table C.2 Results of Test 1: Total Weight of Moisture in Tank for Control Run and Whistle Run
Note: Data was Averaged 0n a 238 Point Interval for Time and Moisture Weight.

Control Test 1			Whistle Test 1		
Elapsed Time	Weight of Moisture in Tank	Sand to Moisture Content	Elapsed Time	Weight of Moisture in Tank	Sand to Moisture Content
Hours	Lbs	Lbs Moisture / Lbs Sand	Hours	Lbs	Lbs Moisture / Lbs Sand
0	11.11	1.11E-01	0	11.11	1.11E-01
1	10.31	1.03E-01	1	7.06	7.06E-02
3	9.78	9.78E-02	3	4.55	4.55E-02
5	9.45	9.45E-02	5	3.58	3.58E-02
7	9.11	9.11E-02	7	2.53	2.53E-02
9	8.89	8.89E-02	9	2.04	2.04E-02
11	8.73	8.73E-02	11	1.65	1.65E-02
13	8.29	8.29E-02	13	1.51	1.51E-02
15	7.90	7.90E-02	15	1.35	1.35E-02
17	7.71	7.71E-02	17	1.18	1.18E-02
19	7.62	7.62E-02	19	0.99	9.94E-03
21	6.97	6.97E-02	21	0.77	7.69E-03
23	6.71	6.71E-02	23	0.71	7.09E-03
25	6.38	6.38E-02	25	0.64	6.43E-03
27	6.27	6.27E-02	27	0.71	7.12E-03
29	6.09	6.09E-02	29	0.39	3.91E-03
31	5.86	5.86E-02	31	0.19	1.89E-03
33	5.63	5.63E-02	33	0.18	1.78E-03
35	5.40	5.40E-02	34	0.17	1.66E-03
37	5.14	5.14E-02	36	0.26	2.58E-03
39	4.78	4.78E-02	38	0.15	1.51E-03
41	4.43	4.43E-02	40	0.00	0.00E+00
50	3.33	3.33E-02	42	0.00	0.00E+00
52	3.10	3.10E-02	--------	--------	--------
54	2.93	2.93E-02	--------	--------	--------
54	2.93	2.93E-02	--------	--------	--------
56	2.73	2.73E-02	--------	--------	--------
58	2.49	2.49E-02	--------	--------	--------
60	2.41	2.41E-02	--------	--------	--------
62	2.17	2.17E-02	--------	--------	--------
64	2.07	2.07E-02	--------	--------	--------

Table C.3 Results of Test 2: Total Weight of Moisture in Tank for Control Run and Whistle Run
Note: Data was Averaged 0n a 238 Point Interval for Time and Moisture Weight.

Control Test 2			Whistle Test 2		
Elapsed Time	Weight of Moisture in Tank	Sand to Moisture Content	Elapsed Time	Weight of Moisture in Tank	Sand to Moisture Content
Hours	Lbs	Lbs Moisture / Lbs Sand	Hours	Lbs	Lbs Moisture / Lbs Sand
0	11.11	1.11E-01	0	11.11	1.11E-01
1	8.83	8.83E-02	1	5.30	5.30E-02
3	7.23	7.23E-02	3	3.25	3.25E-02
5	6.49	6.49E-02	5	2.21	2.21E-02
7	6.03	6.03E-02	7	1.71	1.71E-02
9	5.65	5.65E-02	9	1.40	1.40E-02
11	5.35	5.35E-02	11	1.00	9.98E-03
13	5.04	5.04E-02	13	0.72	7.20E-03
15	4.77	4.77E-02	15	0.36	3.63E-03
17	4.38	4.38E-02	17	0.11	1.14E-03
19	4.05	4.05E-02	19	0.00	-2.10E-05
21	3.79	3.79E-02	--------	--------	--------
23	3.54	3.54E-02	--------	--------	--------
25	3.22	3.22E-02	--------	--------	--------
27	3.04	3.04E-02	--------	--------	--------
29	2.93	2.93E-02	--------	--------	--------
31	2.80	2.80E-02	--------	--------	--------
33	2.68	2.68E-02	--------	--------	--------
35	2.55	2.55E-02	--------	--------	--------
37	2.55	2.55E-02	--------	--------	--------
39	2.41	2.41E-02	--------	--------	--------
41	2.33	2.33E-02	--------	--------	--------
48	1.83	1.83E-02	--------	--------	--------
49	1.79	1.79E-02	--------	--------	--------
50	1.83	1.83E-02	--------	--------	--------
50	1.83	1.83E-02	--------	--------	--------
51	1.77	1.77E-02	--------	--------	--------
52	1.65	1.65E-02	--------	--------	--------
53	1.70	1.70E-02	--------	--------	--------
54	1.67	1.67E-02	--------	--------	--------
55	1.57	1.57E-02	--------	--------	--------

Table C.4 Results of Test 3: Total Weight of Moisture in Tank for Control Run and Whistle Run
Note:Data was Averaged 0n a 238 Point Interval for Time and Moisture Weight

Control Test 3			Whistle Test 3		
Elapsed Time	Weight of Moisture in Tank	Sand to Moisture Content	Elapsed Time	Weight of Moisture in Tank	Sand to Moisture Content
Hours	Lbs	Lbs Moisture / Lbs Sand	Hours	Lbs	Lbs Moisture / Lbs Sand
0	11.11	1.11E-01	0	11.11	1.11E-01
1	10.06	1.01E-01	1	6.26	6.26E-02
3	9.08	9.08E-02	3	3.51	3.51E-02
5	9.31	9.31E-02	5	2.61	2.61E-02
7	8.72	8.72E-02	7	2.11	2.11E-02
9	8.26	8.26E-02	9	1.73	1.73E-02
11	8.08	8.08E-02	11	1.45	1.45E-02
13	7.66	7.66E-02	13	1.16	1.16E-02
15	7.57	7.57E-02	15	1.02	1.02E-02
17	7.19	7.19E-02	17	0.79	7.95E-03
19	6.84	6.84E-02	19	0.63	6.32E-03
21	6.32	6.32E-02	21	0.66	6.58E-03
23	6.41	6.41E-02	23	0.62	6.19E-03
25	6.10	6.10E-02	25	0.61	6.05E-03
27	5.66	5.66E-02	27	0.57	5.67E-03
29	5.41	5.41E-02	29	0.57	5.74E-03
31	5.34	5.34E-02	31	0.56	5.61E-03
33	5.29	5.29E-02	33	0.56	5.64E-03
35	5.25	5.25E-02	35	0.56	5.63E-03
37	5.08	5.08E-02	37	0.41	4.11E-03
39	5.23	5.23E-02	39	0.38	3.75E-03
41	5.51	5.51E-02	41	0.38	3.77E-03
43	5.28	5.28E-02	43	0.42	4.23E-03
45	5.33	5.33E-02	45	0.37	3.70E-03
47	4.80	4.80E-02	47	0.48	4.81E-03
49	5.06	5.06E-02	--------	--------	--------
51	4.69	4.69E-02	--------	--------	--------
53	4.40	4.40E-02	--------	--------	--------
55	4.22	4.22E-02	--------	--------	--------
57	4.06	4.06E-02	--------	--------	--------
59	4.23	4.23E-02	--------	--------	--------

APPENDIX D

TABLES FOR ETHANOL CONCENTRATION VERSUS TIME FOR WHISTLE TESTS

In the **Tables D.1** to **D.3** the concentration of ethanol in part per million volume is reported for the whistle sets 1 to 3. In columns 1 and 3 are the elapsed times at which the gas chromatograph samples were taken during the course of the control and whistle runs respectively. The integrated data are shown in columns 2 and 5 for the control run and the whistle run data respectively. The integrated data in columns 2 and 5 for the control run and the whistle run data are converted to concentration through the use of the correlation equation which appears in **Figure 3.5** and the data are converted into parts per million volume and present in columns 3 and 6.

Table D.1 Results of Gas Chromatograph Analysis of Test 1 for the Control and Whistle Runs

Control Test 1			Whistle Test 1		
Elapsed Time	Integrated Area of Ethanol	Outlet Conc. of Ethanol	Elapsed Time	Integrated Area of Ethanol	Outlet Conc. of Ethanol
Hours	Volt*Seconds	ppmv	Hours	Volt*Seconds	ppmv
0	8.08E+01	2.58E+02	0	4.63E+02	2.12E+03
0.5	7.86E+01	2.50E+02	0.5	2.92E+02	1.22E+03
1	4.94E+01	1.42E+02	1	2.36E+02	9.40E+02
2	3.72E+01	1.01E+02	1.5	1.68E+02	6.22E+02
3	3.02E+01	7.87E+01	2.5	1.17E+02	4.03E+02
4	2.86E+01	7.35E+01	3.5	9.59E+01	3.17E+02
5	2.64E+01	6.70E+01	4.5	5.62E+01	1.66E+02
6	2.53E+01	6.36E+01	5.5	5.05E+01	1.46E+02
7	2.52E+01	6.31E+01	6.5	2.80E+01	7.18E+01
8	2.16E+01	5.25E+01	7.5	9.91E+00	2.05E+01
9	2.40E+01	5.94E+01	8.5	1.50E+01	3.38E+01
10	2.48E+01	6.19E+01	9.5	1.14E+00	1.50E+00
11	2.48E+01	6.21E+01	10.5	2.19E-01	1.03E+00
12	2.49E+01	6.22E+01	11.5	2.07E-01	9.59E-01
13	2.42E+01	6.00E+01	12.5	1.21E-01	5.03E-01
14	2.34E+01	5.77E+01	13.5	3.86E-02	1.26E-01
15	2.43E+01	6.03E+01	14.5	3.08E-02	9.59E-02
16	2.38E+01	5.89E+01	15.5	2.05E-02	5.87E-02
17	2.28E+01	5.59E+01	16.5	6.58E-03	1.49E-02
18.5	2.35E+01	5.81E+01	17.5	4.69E-03	9.88E-03
19.5	2.27E+01	5.56E+01	18.5	4.16E-03	8.55E-03
20.5	2.24E+01	5.48E+01	19.5	1.46E-02	7.78E-03
21.5	2.21E+01	5.40E+01	20.5	5.87E-03	2.59E-03
22.5	2.16E+01	5.26E+01	----------	----------	----------
23.5	2.14E+01	5.17E+01	----------	----------	----------
24.5	1.94E+01	4.62E+01	----------	----------	----------
25.5	1.75E+01	4.06E+01	----------	----------	----------
26.5	1.40E+01	3.10E+01	----------	----------	----------
27.5	1.30E+01	2.85E+01	----------	----------	----------
28.5	1.33E+01	2.91E+01	----------	----------	----------
29.5	1.14E+01	2.42E+01	----------	----------	----------
30.5	9.05E+00	1.83E+01	----------	----------	----------
31.5	9.03E+00	1.83E+01	----------	----------	----------

Table D.2 Results of Gas Chromatograph Analysis of Test 2 for the Control and Whistle Runs

Control Test 2			Whistle Test 2		
Elapsed Time	Integrated Area of Ethanol	Outlet Conc. of Ethanol	Elapsed Time	Integrated Area of Ethanol	Outlet Conc. of Ethanol
Hours	Volt*Seconds	ppmv	Hours	Volt*Seconds	ppmv
0	5.07E+02	2.37E+03	0	6.36E+02	3.11E+03
0.5	1.54E+02	5.62E+02	1	3.93E+02	1.74E+03
1	1.52E+02	5.53E+02	2	1.96E+02	7.52E+02
1.5	1.19E+02	4.13E+02	3	1.11E+02	3.77E+02
2	9.32E+01	3.06E+02	4	3.23E+01	8.53E+01
2.5	7.33E+01	2.29E+02	5.5	4.14E+01	1.15E+02
3	5.85E+01	1.75E+02	6	2.04E+01	4.89E+01
3.5	5.05E+01	1.46E+02	7.5	8.46E+00	1.69E+01
4	3.95E+01	1.09E+02	8.5	3.14E+00	5.11E+00
5.5	4.48E+01	1.26E+02	9.5	8.23E-01	1.01E+00
7	4.07E+01	1.13E+02	----------	----------	----------
25	8.43E+00	1.68E+01	----------	----------	----------
27	7.87E+00	1.55E+01	----------	----------	----------
29	6.41E+00	1.21E+01	----------	----------	----------
31	5.85E+00	1.08E+01	----------	----------	----------
33	5.08E+00	9.14E+00	----------	----------	----------
35	5.07E+00	9.11E+00	----------	----------	----------
37	5.07E+00	9.11E+00	----------	----------	----------
39	3.43E+00	5.68E+00	----------	----------	----------
41	3.05E+00	4.94E+00	----------	----------	----------
43	2.10E+00	3.14E+00	----------	----------	----------

Table D.3 Results of Gas Chromatograph Analysis of Test 3 for the Control and Whistle Runs

Control Test 3			Whistle Test 3		
Elapsed Time	Integrated Area of Ethanol	Outlet Conc. of Ethanol	Elapsed Time	Integrated Area of Ethanol	Outlet Conc. of Ethanol
Hours	Volt*Seconds	ppmv	Hours	Volt*Seconds	ppmv
0	1.20E+02	4.16E+02	0	5.00E+02	2.33E+03
0.5	9.00E+01	2.94E+02	0.5	3.50E+02	1.51E+03
1	8.50E+01	2.74E+02	1	2.40E+02	9.60E+02
2	5.20E+01	1.52E+02	1.5	1.70E+02	6.33E+02
3	5.00E+01	1.44E+02	2.5	1.00E+02	3.34E+02
4	4.90E+01	1.41E+02	3.5	9.00E+01	2.94E+02
5	3.20E+01	8.43E+01	4.5	6.00E+01	1.80E+02
6	2.50E+01	6.26E+01	5.5	5.50E+01	1.62E+02
7	2.00E+01	4.78E+01	6.5	3.30E+01	8.75E+01
8	1.80E+01	4.21E+01	7.5	1.50E+01	3.38E+01
9	1.70E+01	3.93E+01	8.5	1.00E+01	2.07E+01
10	1.60E+01	3.65E+01	9.5	1.53E+00	2.14E+00
11	1.68E+01	3.87E+01	19.5	1.47E-02	7.82E-03
12	1.80E+01	4.21E+01	20.5	4.64E-02	3.14E-02
13	1.50E+01	3.38E+01	----------	----------	----------
14	1.60E+01	3.65E+01	----------	----------	----------
15	1.40E+01	3.11E+01	----------	----------	----------
16	1.60E+01	3.65E+01	----------	----------	----------
17	1.60E+01	3.65E+01	----------	----------	----------
18.5	1.90E+01	4.49E+01	----------	----------	----------
19.5	1.80E+01	4.21E+01	----------	----------	----------
20.5	1.40E+01	3.11E+01	----------	----------	----------
21.5	1.70E+01	3.93E+01	----------	----------	----------
22.5	1.80E+01	4.21E+01	----------	----------	----------
23.5	1.80E+01	4.21E+01	----------	----------	----------
24.5	1.00E+01	2.07E+01	----------	----------	----------
25.5	7.00E+00	1.34E+01	----------	----------	----------
26.5	6.00E+00	1.12E+01	----------	----------	----------
27.5	6.00E+00	1.12E+01	----------	----------	----------
28.5	4.00E+00	6.84E+00	----------	----------	----------
29.5	3.00E+00	4.83E+00	----------	----------	----------
30.5	2.00E+00	2.96E+00	----------	----------	----------
31.5	9.00E-01	1.13E+00	----------	----------	----------

APPENDIX E

TABLE FOR TEMPERATURE VERSUS TIME FOR SIREN TEST

In **Table E.1**, are the tabulated data of temperature versus time obtained for siren test 1 and its corresponding control test. The data in the table represent the temperature obtained at the source of the siren in the fracture, midway between the fracture and one of the extraction pipes, outside the extraction pipe and inside the extraction pipe. The temperature reading was taken on a two hour interval.

Table E.1 Temperature Distribution in Fracture Vs. Time for Control Test 1 and Siren Test 1

Control Test 1					Siren Test 1				
Elapsed Time	Temp @ Source	Temp. @ Mid Point	Temp. Outside Pipe	Temp. Inside Pipe	Elapsed Time	Temp @ Source	Temp. @ Mid Point	Temp. Outside Pipe	Temp. Inside Pipe
Hours	°F	°F	°F	°F	Hours	°F	°F	°F	°F
0	69	65	58	62	0	66	70	63	64
1	69	65	58	62	1	66	70	63	64
3	69	64	56	63	3	65	69	62	66
5	68	64	56	63	5	65	68	61	65
7	70	65	56	65	7	66	69	62	66
9	72	67	58	67	9	70	71	63	67
11	73	67	59	68	11	71	73	63	68
13	74	68	59	69	13	72	74	64	68
15	74	68	59	69	15	73	74	64	69
17	74	68	60	70	17	72	74	64	69
19	72	67	58	68	19	71	73	63	68
21	71	67	58	68	21	73	75	64	69
23	70	68	59	68	26	73	75	64	72
25	71	70	61	69	29	74	75	65	72
27	71	70	65	69	31	74	75	75	72
29	72	72	69	70	32	74	75	75	72
31	74	74	72	72	35	74	75	75	72
33	74	74	74	73	37	74	75	75	72

Table E.1 Temperature Distribution in Fracture Vs. Time for Control Test 1 and Siren Test 1(Continued)

Control Test 1					Siren Test 1				
Elapsed Time	Temp @ Source	Temp. @ Mid Point	Temp. Outside Pipe	Temp. Inside Pipe	Elapsed Time	Temp @ Source	Temp. @ Mid Point	Temp. Outside Pipe	Temp. Inside Pipe
Hours	°F	°F	°F	°F	Hours	°F	°F	°F	°F
35	74	74	74	73	39	75	75	76	72
37	74	74	74	73	41	75	75	76	72
39	74	74	74	73	43	75	75	76	72
41	71	71	72	71	44	75	75	76	72
43	70	71	71	70	--------	--------	--------	--------	--------
45	70	71	71	70	--------	--------	--------	--------	--------
47	71	71	71	70	--------	--------	--------	--------	--------
49	71	71	71	71	--------	--------	--------	--------	--------
51	72	72	72	72	--------	--------	--------	--------	--------

REFERENCES

Allen, C. H., and B. G. Watters 1959 "Siren Design for Producing Controlled Wave Forms At High Intensities", *The Journal of the Acoustical Society of America*, **31**(2):177-185.

Allen, C. H., and J. Rudnick 1947 "A Powerful High Frequency Siren", *The Journal of the Acoustical Society of America*, 19(5):857:865.

Blangy, J.P., Strandenes, S. and A. Nur 1993 "Ultrasonic Velocities in Sands-Revisited", *Geophysics*, **58**(3):344-356.

Borisov, Yu Ya, Dolgopolov, N. N. and S. G. Simonyan 1966 "Comparison of Acoustical and Infrared Drying Methods", *Soviet Physics*, **11**(3):328-330.

Boucher, R.M.G. 1961 "Ultrasonics in Processing", *Chemical Engineering*, 40(10):84-99.

Boucher, R.M.G. 1958 "Industrial Application of Airborne Ultrasonics", *Ultrasonic News*, 4(8):8-13.

Boucher, R.M.G. 1957 "Research on the Acoustic Air-Jet Generator: A New Development", *The Journal of the Acoustical Society of America*, **29**(5):573-583.

Burger, F. J. and K. Sollner 1936, *Transaction of the Faraday Society,* **32**:1598-1603.

Chendke, P.K. and H.S. Fogler 1975, "Macrosonics in Industry: 4.0 Chemical Processing", *Ultrasonics*, **13**:31-37.

Crawford, Alan E. 1955, Ultrasonic Engineering With Particular Reference to High Power Applications, Butterworth Scientific Publishing, London, England.

Cracknell, A.P. 1980, Ultrasonics Wykeham Publications, London, England.

Cleaveland, Theodore G. and Sanjay Garg 1993, "Field Demonstration of Acoustically Enhanced Soil Washing System For *In Situ* Treatment of Low Permeable Soils", *Waste Management Journal*, **13**(5-7):519-520.

EPA (Environmental Protection Agency). 1991. "Prospect for *In Situ* Treatment for Contaminated Soil", EPA/600/D-91/285, Risk Reduction Engineering Laboratory, Environmental Protection Agency, Cincinnati, Ohio.

EPA (Environmental Protection Agency). 1990. "Handbook on *In Situ* Teatment of Hazardous Waste-Contaminated Soils", EPA/540/2-90/002, Risk Reduction Engineering Laboratory, Environmental Protection Agency, Cincinnati, Ohio.

REFERENCES
(Continued)

Gallego-Juarez, J.A. 1988 "High Power Ultrasonic Transducer for Use in Gases and Interphases", *Power Sonic and Ultrasonic Transducer Design*, (Berlin :Springer):175-184.

Geankoplis, Christie J. 1993 Transport Process and Unit Operations Fifth Edition, Simon and Schuster, Englewood Cliffs, New Jersey.

Graham, Ched 1970 Sound: Fom Communication to Noise Pollution, Doubleday & Company, Garden City, New York.

Greguss, P. 1961 "Drying by Airborne Ultrasonics", *Ultrasonic News*, 5:(3):7-12.

Greguss, P. 1963 "The Mechanism and Possible Applications of Sonic Drying by Ultrasonic Irradiation", *Ultrasonics*, April-June.

Han, De-hua, Nur, A., and Dale Morgan 1986 "Effects of Porosity and Clay Content on Wave Velocities in Sandstones", *Geophysics*, **51**(11):2093-2107.

Jadhav, S.V. and V.G. Pangarkar 1989 "Gas-Liquid and Solid-Liquid Mass Transfer in Three-Phase Sparge Reactors With and Without Ultrasound", *JAOCS*, **66**(3):362-364.

Johnson, R.F. and R.I. Starr 1970, "Ultrasonic Extraction of Insecticides in Soil II: Refinement and treatment, *Journal of Economic Entomology*, **63**(1):165-168.

Kleppe, J.A. 1989 Engineering Applications of Acoustic, Scientific Engineering Instruments, Sparks, Nevada.

Manthey, W., Kroemer, N. and V. Mágori 1992 "Instrument Science and Technology, Ultrasonic Transducer Arrays for Application in Air", *Measurement Science and Technology*, 3:249-261.

Marks, Peter J., Wujcik, Water J., and Amy F. Loncar 1994 "Remediation Technologies Screening Matrix and Reference Guide", Second Edition, EPA/542/B-94/013, NTIS PB95-104782, Aberdeen Proving Ground, Maryland.

McCabe, Warren L., Smith, Julian C. and Peter Harriot 1985 Unit Operations of Chemical Engineering, McGraw-Hill, New York, New York.

Meyer, Erwin and Ernst-Georg Neumann 1972 Physical and Applied Acoustics,. Academic Press, New York, New York.

Muralidhara, H.S. and D. Ensminger 1984 "Acoustic Dewatering and Drying: State of the Art Review", *Proceedings of the 4th International Drying Symposium*, 1:304-315.

REFERENCES
(Continued)

Purdy, Kenneth R., Simmons, Gary W., Hribar, Allan E., and Edwin Griggs 1971 "Acoustically Augmented Convective Drying", *Chemical Engineering Progress* Symposium Series No. 109, 67(109):55-67.

Reddi, Lakshmi N., Berliner III, S., and K.Y. Lee 1993 "Feasibility of Ultrasonic Enhancement of Flow in Clayey Sands", *Journal of Environmental Engineering*, 119(4):746:752.

Sears, Francis W., Zemansky, Mark W. and Hugh D. Young 1986 University Physics, Seventh Edition, Addison-Wesley Publishing Company, Menlo Park, California.

Shah, N.P. 1991 "Study of Pneumatic Fracturing to Enhance Vapor Extraction of the Vadose Zone", M.S. Thesis, Department of Civil and Environmental Engineering, New Jersey Institute of Technology, Newark, New Jersey.

Soloff, Robert S. 1964 "Sonic Drying", *The Journal of the Acoustical Society of America*, 38(5):961:965.

Swamy, R.M. and K.L. Narayana 1980 "Design of an Acoustic Stem-Jet Whistle", *PROC. ICEU-80*, New Delhi, India, 66-71.

Swamy, K.M. 1983 "Acoustic Aids Dewatering", *Ultrasonics*, 21(6):280-281.

United States Patent Number 5,198,122 1993 "Method of Detoxification of Substances by Utilization of Ultrasonic Energy".

United States Patent Number 5,098,538 1992 "Electroacoustical Soil Decontamination".

United States Patent Number 5,032,042 1991 "Method and Apparatus for Eliminating Non-Naturally Occurring Subsurface Liquid Toxic Contaminants from Soil".

White, J.E. 1965 Seismic Waves: Radiation, Transmission and Attenuation, International Series in the Earth Science, McGraw-Hill Book Company, New York, New York.

Wood, A.B. 1937 A Textbook of Sound, The Macmillan Company, New York, New York.